NONLINEAR OPTICS IN NOVEL PERIODIC MEDIA

by

Ravi Sadananda Hegde

A dissertation submitted in partial fulfillment
of the requirements for the degree of
Doctor of Philosophy
(Electrical Engineering)
in The University of Michigan
2008

Doctoral Committee:

Professor Herbert G. Winful, Chair
Professor Almantas Galvanauskas
Professor Paul R. Berman
Professor Peter D. Miller
Assistant Professor Tal E. Carmon

This thesis is dedicated to my advisor, Professor Herbert Winful.

ACKNOWLEDGEMENTS

I gratefully acknowledge the constant support, encouragement and training provided by my advisor Dr. Herbert Winful. I have benefited a lot from observing his approach to problem definition and solution. The wide array of problems encountered during my graduate study has certainly been instrumental in sharpening my problem solving skills.

I wish to acknowledge my gratitude to my co-advisor Dr. Galvanauskas. Dr. Galvanauskas brings a lot of energy and enthusiasm for fiber lasers and it is very contagious. The weekly brainstorming sessions with Dr. Winful and Dr. Galvanauskas were an integral part of my training as a researcher.

I wish to acknowledge the support of my doctoral committee. Professors Paul Berman, Tal Carmon and Peter Miller. Professor Carmon's own interest in stimulated Brillouin scattering made our discussions more fruitful to me. Discussions with Natasha Litchinister were especially helpful during the work on metamaterials. I wish to thank Peter Dragic at UIUC for helpful comments and suggestions for the work on SBS. Prof. Rand with his biting wit has always been a joy.

I acknowledge the support of many people at the optical science laboratory. My fellow graduate students Chi hung Liu, Tsie-wei, Hsienkie Hsiao have been supportive during all these years. The wonderful staff members have been very helpful and friendly.

The university of Michigan community has contributed a lot to broadening my

cultural horizons and it has been a wonderful stay during these years.

I wish to thank Chaya Aravind for her help with the editing and prrofreading of the document. I finally acknowledge the support of my family and friends.

TABLE OF CONTENTS

LIST OF FIGURES

Figure

ABSTRACT

NONLINEAR OPTICS IN NOVEL PERIODIC MEDIA

by

Ravi Sadananda Hegde

Chair: Herbert G. Winful

The major focus of the work in this thesis is on the solution of the electromagnetic wave equations in novel structures that exhibit nonlinearity in their response to the incident field. These structures are further characterized by the presence of a spatial periodicity in their dielectric permittivity. The presence of spatial periodicity results in a number of coherent scattering phenomena when the light wavelength is comparable to the period of this spatial perturbation. Here we use a combination of analytical and numerical methods to gain insight into these phenomena. Two different problems each involving a different nonlinear phenomenon have been considered.

First, we take the classical problem of hysteretic switching response exhibited by a nonlinear periodic structure. This problem is reexamined in the context of the presence of a negative refractive index (left-handed electromagnetic structure). We theoretically predict an exotic behavior that involves an omnidirectional response quite distinct from the well known behavior. We examine the field distribution in detail and propose the existence of a spatial soliton called the zero-n gap soliton. Next, we investigate the practical problem of output power scaling in fiber lasers. Self

scattering nonlinearities currently set the limit on power scalability. In particular, for narrow linewidth systems, Stimulated Brillouin scattering (SBS) is known to be the limiting nonlinearity. This scattering phenomenon is a result of Bragg reflection from a periodic index modulation induced by an acoustic wave. Several novel schemes are proposed and analyzed in terms of their ability to suppress SBS and enhance power scalability.

CHAPTER 1

Introduction

The presence of a spatial periodicity in electromagnetic structures leads to many interesting phenomena such as the occurrence of forbidden frequency bands in photonic bandgap structures and the diffraction of light from the periodic strain accompanying a sound wave. A general theory of electromagnetics in periodic media in the linear regime can be found in reference [1].

In this thesis, we are primarily concerned with nonlinear optical interactions in a periodic structure. First, nonlinearity can be non-propagating and be a property of the dielectric function of the structure and transmission can be investigated through such a structure as a function of the input field intensity. In 1979, Winful et al. [2] investigated nonlinear transmission near the stop band and predicted a hysteretic switching behavior. This behavior was attributed to the presence of a stable electromagnetic spatial soliton called the gap soliton [3]. We reexamine this problem in a structure containing an electromagnetic metamaterial. Second, the nonlinearity can be propagating in nature and can arise from a self scattering process as in the case of a Stimulated Brillouin scattering in a fiber laser.

1.1 Switching behavior in mixed index (negative-positive) superlattices

We briefly introduce the concept of electromagnetic metamaterial in this chapter.

1.1.1 Metamaterials and negative refraction

A Metamaterial is a material which gains its properties from its structure rather than directly from its composition. The term was coined in 1999 by Rodger M. Walser of the University of Texas at Austin and he defines them as macroscopic composites having a manmade, three-dimensional, periodic cellular architecture designed to produce an optimized combination, not available in nature, of two or more responses to specific excitation [4]. In order for its structure to affect electromagnetic waves, a Metamaterial must have structural features smaller than the wavelength of the electromagnetic radiation it interacts with. We consider photonic crystals distinct from metamaterials as their features are of similar size to the wavelength at which they function, and thus cannot be approximated as a homogeneous material.

1.1.2 Negative refraction

The optical properties of a medium can be characterized by its refractive index n that is obtained by $n = \pm\sqrt{\epsilon\mu}$. All naturally occurring media have both ϵ and μ positive or at most one of them negative. However, some engineered metamaterials have $\epsilon < 0$ and $\mu < 0$. Vesalago's seminal work proved transparency of these materials and established that this phenomenon can exist only for a band of frequencies [5].

Metamaterials with negative N have numerous counterintuitive properties in comparison with the naturally occurring electromagnetic media,

- Snell's law ($n_1 \sin(\theta_1) = n_2 \sin(\theta_2)$) still applies, but as n_2 is negative, the rays

will be refracted on the same side of the normal on entering the material.

- The Doppler shift is reversed: that is, a light source moving toward an observer appears to reduce its frequency.
- Cherenkov radiation points the opposite way.
- The time-averaged Poynting vector is antiparallel to phase velocity. This means that unlike a normal right-handed material, the wave fronts are moving in the opposite direction to the flow of energy.

For plane waves propagating in such metamaterials, the electric field, magnetic field and wave vector follow a left-hand rule, thus giving rise to the name left-handed metamaterials. Metamaterials are very promising to electromagnetics and optics researchers as they offer the possibility for new types of beam steerers, modulators, band-pass filters, lenses, microwave couplers, and antenna radomes. In particular, the Metamaterial has been claimed to be able to produce the so called super lens, a lens with resolution below the diffraction limit [6].

Many classical electromagnetic problems have been revisited in the context of left handedness. This warranted the investigation of the phenomenon of hysteretic switching in the context of negative refraction. We discuss this in detail in chapter 2.

1.2 Introduction to fiber lasers

The second kind of nonlinearity in periodic structures occurs in the case of self-scattering. An intense pump can interact with stray acoustic vibrations and with positive feedback induce self scattering. To understand the practical implications of this problem we introduce next the concept of a fiber laser.

Rare earth doped fibers are emerging as promising alternatives to currently preva-

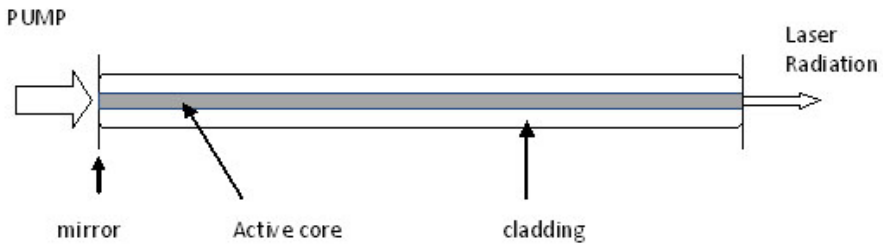

Figure 1.1: Simplified schematic of a fiber laser

lent solid-state laser systems due to their many advantages [7, 8]. A schematic of the fiber laser is shown in figure 1.1. It simply consists of a fiber whose core is doped with rare-earth ions. Pump radiation launched into this core is converted into laser radiation. The cavity of a fiber laser can be formed by butt-coupled mirrors, as shown in reference [9] or fiber-integrated mirrors such as Bragg-gratings or loop mirrors.

Fiber lasers provide many advantages such as [9],

- Immunity against thermo-optical problems typical of solid state laser systems. This is because of their excellent heat dissipation facilitated by large surface to active-volume ratio.
- Very high gain and low pump threshold values because of better confinement of laser and pump radiation.
- Compact and longer term stability due to the integrated optical nature.
- Optical-to-optical efficiencies well above 80% and consequent low induced thermal load in ytterbium-doped glass fibers [10].

However, due to the large product of intensity and interaction length inside the fiber core, nonlinearity can be observed at very low power levels and basically limits the performance of rare-earth-doped fiber systems before limitations due to thermo-optical issues or fracture of the fiber are reached. Due to this relatively low nonlinear

threshold, power scalability of fiber lasers has been significantly limited by optical nonlinearities to a couple of watts until the emergence of Large-Mode-Area (LMA) fibers, which have much larger modal areas and thus weaker nonlinear effects than conventional Single-Mode (SM) fibers. By using LMA fibers to reduce nonlinear effects [11, 12, 8], the diffraction-limited output power from fiber lasers has been rapidly increased from -100W to -3 kilo-watts in the past few years, as shown in figure 1.2.

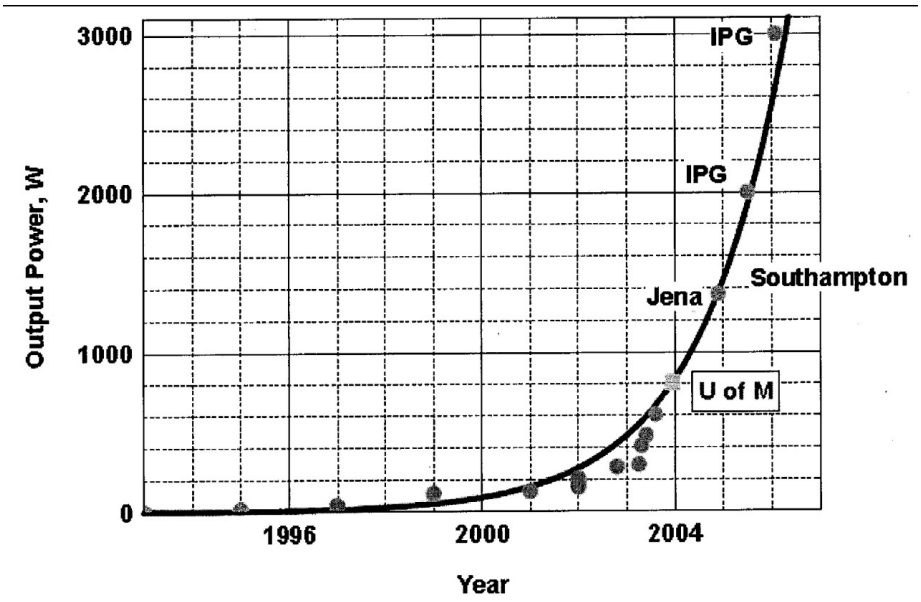

Figure 1.2: Rising power output levels of fiber lasers.

The trade-off, however, of using LMA fibers is the loss of the robust SM performance due to either multiple modes guided in the core, or the extremely poor modal guidance. To overcome this trade-off and maintain the beam quality of LMA fibers, external mode management techniques are needed to guide only one mode or to filter all higher-order modes in LMA fibers. In other words, with such mode management LMA fiber lasers can have both high nonlinear threshold and single-mode diffraction-limited output beam quality.

To further increase power scalability of fiber lasers and allow monolithic LMA

technology for $30\mu m$-core fibers, new fibers with both large modal areas and negligible inter-modal scattering are needed, and apparently none of conventional SM and MMILMA fibers are suitable. The concept of Effectively Single-Mode (E-SM) fibers possessing large modal areas ($V >> 2.405$) and allowing the propagation of the fundamental mode have been proposed to deal with this problem [11]. This is achieved by introducing relatively large modal losses of all higher-order modes, which suppress every mode except for the fundamental LP_{Ol} mode even when higher order modes are excited at the incident end. Unlike those higher-order modes, the fundamental LP_{Ol} mode has negligible loss, and thus becomes the only mode propagating in E-SM fibers. The advantage of E-SM fibers is those fibers could provide diffraction-limited beam quality with large mode areas, relying on no external mode management techniques. Moreover, large higher order mode losses prevent power scattering into those modes, and hence suppress inter-modal scattering when the fiber is perturbed. Such an advantage of scattering suppression is expected to significantly improve the robustness and reliability of LMA E-SM fibers and to enable monolithic fiber technology with very large modal areas, which is currently limited to $< 25\mu m$ core diameters.

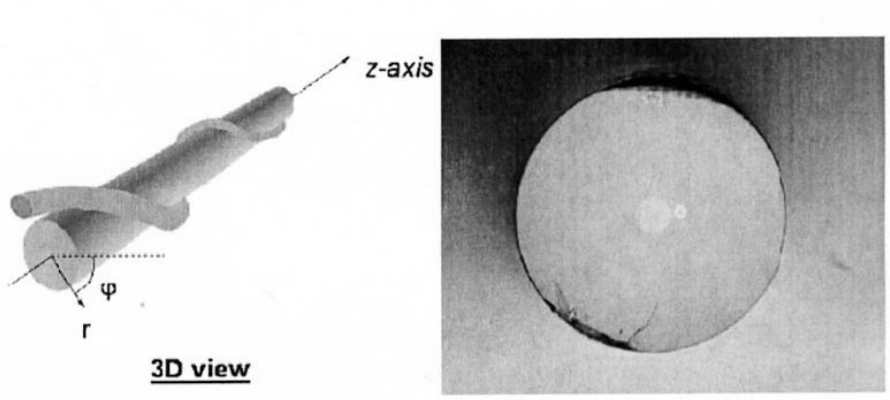

Figure 1.3: The CCC fiber

Practically the concept of E-SM fibers has been realized by a new fiber design called the Chirally-Coupled-Core fiber [11]. The CCC fiber contains a central main core and several helical side cores (see figure 1.3), in which the curvature-induced loss and mode-selective interaction between the cores provide strong loss to all higher order modes in the main core. As a result, the higher order modes in the main core leak through helical side cores and become cladding modes within short lengths, typically a few tens of centimeters. The fundamental LP_{0l} mode in the main core, on the contrary, has little interaction with helical side cores, and thus propagates in the main core with negligible leakage through the side cores (see figure 1.4).

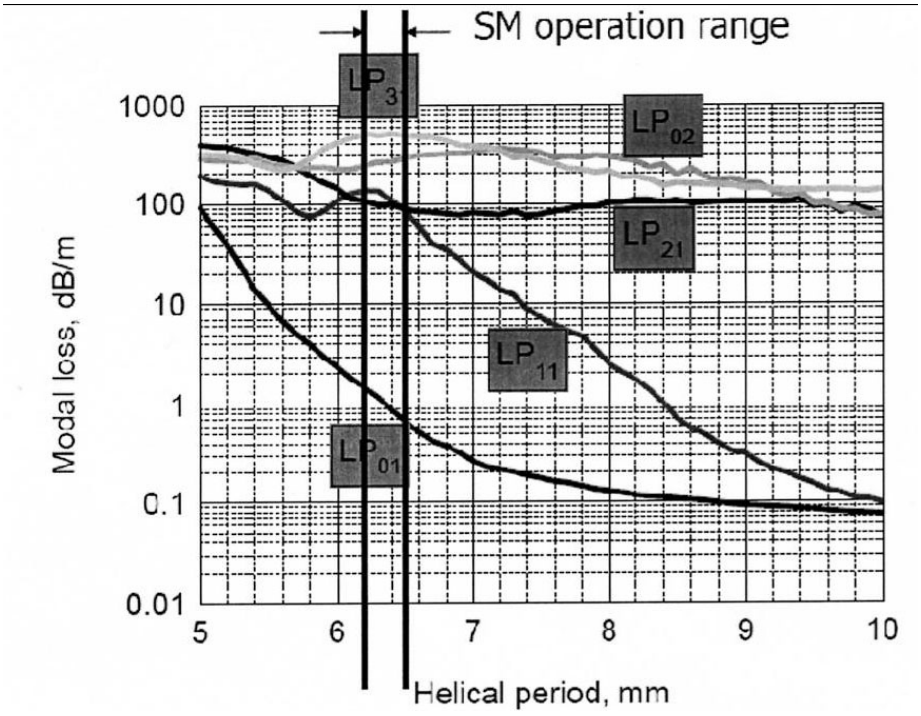

Figure 1.4: Modal losses of the CCC fiber

We refer the interested reader to [11] to further their understanding of the CCC fiber. For the purposes of this thesis it is important to note that the mechanism that provides for the modal losses can be used to separate two differing polarization states. This will be crucial when we present the ideas of chapter 5.

We will conclude our introduction to fiber lasers by discussing the idea of beam combining. It is desirable to increase the system power levels beyond what is possible with a single fiber laser. One promising technology that is being studied to achieve this is to combine a large number of relatively lower power beams into a single high-power beam. Wavelength beam combining (WBC) is one such technology which uses an N-element array where each element is operated at a different wavelength. The near-field and far-field beams are then overlapped with a dispersive element such as a diffraction grating. In this case, the source aperture and far-field solid angle both remain constant as the number of elements is increased so the radiance is proportional to the power, which scales as N. Much progress has been made in wavelength beam combining primarily because of the less demanding design requirements for building such systems compared to those that require mutual coherence among the elements [13]. From these considerations thus far, we can conclude that with narrow linewidth fiber laser output and WBC, power levels of 100 kW range can be envisaged for fiber laser systems. In this thesis, we thus focus on techniques that will allow power scaling with the narrow linewidth requirement.

1.2.1 Introduction to Stimulated Brillouin Scattering

We start initially with the concept of light scattering in optical propagation, a detailed account of which can be found in reference [14].

Raman and Brillouin scattering are scattering processes involving optical and acoustical phonons respectively. Rayleigh scattering is scattering from non-propagating density fluctuations. Rayleigh wing scattering is scattering from fluctuations in the orientation of anisotropic molecules. The typical parameters for these scattering processes are listed in [14]. On consideration of the peak gain and the bandwidth we should chiefly be interested in Brillouin and the Raman processes. Furthermore

in narrow-linewidth systems, stimulated Brillouin scattering (SBS) has much higher gain than SRS, has a lower threshold, and is thus the dominant process. Unlike SRS that has rather wide spectral shift (-13.2THz) and can be removed by spectral filters [11], SBS has very small frequency offset (-10 to 100 MHz) from the signal and consequently cannot be removed using similar spectral techniques. Thus we will further limit our consideration chiefly to SBS suppression in this work. We wish to mention that the work on distributed Stokes suppression (chapter 4) is general enough to be valid for SRS as well.

As discussed earlier, Stimulated Brillouin scattering (SBS) is a nonlinear process that can occur in optical fibers at input power levels much lower than those needed for stimulated Raman scattering (SRS). It manifests through the generation of a backward-propagating Stokes wave that carries most of the input energy, once the Brillouin threshold is reached. SBS can be detrimental for optical communication systems. At the same time, it can be useful through fiber-Brillouin lasers and amplifiers and for sensing applications [15].

The process of SBS can be described classically as a parametric interaction among the pump wave, the Stokes wave and an acoustic wave. The pump wave generates acoustical waves through the process of electrostriction which in turn causes a periodic modulation of the refractive index. The pump-induced index grating scatters the pump light through Bragg diffraction. The scattered light is downshifted in frequency because of the Doppler shift associated with a grating moving at the acoustic velocity v_A . The same scattering process can be viewed quantum-mechanically as if the annihilation of a pump photon creates instantaneously a Stokes photon and an acoustic phonon. Since both the energy and the momentum must be conserved during such scattering event, the frequency and the wave-vectors of the three waves

are related by

$$\omega_A = \omega_P - \omega_S, k_A = k_P + k_S, \tag{1.1}$$

where ω_P and ω_S are the frequencies and k_P and k_S are the wave vectors of the pump and Stokes waves respectively. The frequency ω_A and the wave vector k_A of the acoustic wave satisfy the dispersion relation

$$\omega_A = |k_A| v_A = 2 v_A k_P \sin(\theta/2), \tag{1.2}$$

where θ is the angle between the pump and Stokes waves. Equation (1.2) shows that the frequency shift of the Stokes wave depends on the scattering angle. In particular, it is maximum in the backward direction ($\theta = \pi$) and vanishes in the forward direction ($\theta = 0$). The frequency shift ν_B in the backward direction is given by

$$\nu_B = \frac{\omega_A}{2\pi} = \frac{2nv_A}{\lambda_P}, \tag{1.3}$$

where n is the refractive index and λ_P is the pump wavelength.

Before proceeding further, we should mention that in an optic fiber the guided nature of acoustic waves can lead to a relaxation of the wave-vector selection rule and as a result a small amount of forward propagating stokes can be generated. This phenomenon is called Guided-Acoustic-Wave Brillouin Scattering (GAWBS). We do not further consider this because of its extremely weak nature [15]. Similar to the case of SRS, the growth of the Stokes wave is characterized by the Brillouin-gain coefficient $g_B(\nu)$ whose peak value occurs at $\nu = \nu_B$. However, in contrast with the SRS case, the spectral width ν_B of the Brillouin-gain spectrum is very small (10 MHz instead of 5 THz). The spectral width is related to the damping time of acoustic waves or the phonon lifetime T_B. In fact, if the acoustic waves are assumed to decay

as $exp(-t/T_B)$, the Brillouin gain has a Lorentzian spectral profile given by

$$g_B(\nu) = g_B(\nu_B)\frac{(\Delta\nu_B/2)^2}{(\nu-\nu_B)^2+(\Delta\nu_B/2)^2}, \tag{1.4}$$

where $\Delta\nu_B$ is the full width at half maximum and is related to the phonon lifetime by $\Delta\nu_B = (\pi T_B)^-1$

The peak value of the Brillouin-gain coefficient occurring at $\nu = \nu_B$ is given by

$$g_B(\nu_B) = \frac{2\pi n^7 p_{12}^2}{c\lambda_p^2 \rho_0 \nu_B \Delta\nu_B}, \tag{1.5}$$

where p_{12} is the longitudinal elasto-optic coefficient, ρ_0 is the material density. The Brillouin-gain spectrum for silica fibers can differ significantly from that observed in bulk silica because of the guided nature of optical modes and the presence of dopants in the fiber core. An example of the measured gain spectrum that is typically observed can be found in [15].

In chapter 3, we will describe a method for numerically calculating the Brillouin gain spectrum in the case when the acoustic guidance properties of the fiber are altered in the cross sectional plane by doping. In chapter 4, the SBS process in the case where an elastic grating is inscribed in the propagating medium is discussed. Both these methods are shown to be useful in the reduction in local value of Brillouin gain at peak frequency. Similar to the SRS case, the development of SBS in optical fibers requires the consideration of mutual interaction between the pump and Stokes waves. Under steady-state conditions, applicable for a cw or quasi-cw pump, such an interaction is governed by the coupled-intensity equations. For the case of nearly equal loss for the pump and the Stokes waves we have,

$$\begin{aligned} \frac{dI_P}{dz} &= -g_B(\nu) I_P I_S - \alpha I_P \\ \frac{dI_S}{dz} &= -g_B(\nu) I_P I_S + \alpha I_S, \end{aligned} \tag{1.6}$$

where the subscripts on the I term identify the pump and the Stokes waves respectively and g_B is the Brillouin-gain coefficient. Under the no-pump depletion approximation, the equations considerably simplify to show a Stokes wave growing exponentially in the backward direction as given by

$$I_S(z) = I_S(0)exp(g_B I_{P0} L_{eff} - \alpha L), \tag{1.7}$$

with A_{eff} denoting the effective core area and an effective interaction length given by

$$L_{eff} = \frac{1}{\alpha}\left[1 - exp(-\alpha L)\right]. \tag{1.8}$$

By following a method shown in [16], the Brillouin threshold is found to occur at a critical pump power given by

$$g_B P_0^{cr} L_{eff}/A_{eff} = 21. \tag{1.9}$$

This formula is only approximate as it makes assumptions about the exact parameters of the Brillouin gain spectrum [17, 18]. It also depends in general on the evolution of the polarization states of both the pump and the Stokes. In the case of complete polarization scrambling the threshold will increase by a factor of 2. In chapter 5., we revisit this now classical threshold derivation for the general case of a distributed Stokes loss and revise the above formula. In chapter 5, the distributed Stokes loss occurring in a circularly dichroic medium is considered and SBS equations are re-derived for this special case.

1.2.2 Survey on currently available methods for suppressing SBS

In this section we review the methods that have been proposed to suppress SBS in optical fibers. SBS is a three wave process involving the pump, the Stokes and the acoustic waves. We can thus classify the available methods as:

- Modification of pump wave parameters.
- Modification of fiber acoustic environment.
- Modification of the Stokes wave.

Modification of the Pump wave parameters

The simplest method to suppress SBS is to broaden the laser spectrum so that the signal's effective linewidth is greater than that of the Brillouin gain spectrum [19, 20, 21]. Indeed, SBS is caused by nonlinear interaction between acoustic phonons and photons and is inherently a narrow-linewidth process. For example, the Brillouin linewidth in bulk silica is 23 MHz [15]. Assuming Lorentzian spectra, the Brillouin gain coefficient g_B scales with signal bandwidth according to

$$\hat{g_B} = \frac{\Delta\nu_L}{\Delta\nu_L + \Delta\nu_B}, \tag{1.10}$$

where $\Delta\nu_L$ is the laser linewidth, $\Delta\nu_B$ is the Brillouin linewidth and g_B is the Brillouin gain for a signal spectrum. When $\Delta\nu_L > \Delta\nu_B$, SBS is effectively suppressed and other nonlinear effects, such as stimulated Raman scattering (SRS) with a significantly higher threshold than SBS, set the power limit. However, this SBS suppression method is not suitable when a very narrow linewidth signal is required from a fiber laser or amplifier (or a fiber system in general).

Modification of the fiber acoustic environment

Modification of the fiber acoustic environment can again be achieved in two ways. First, the acoustic parameters of the fiber can be varied in the longitudinal direction. This by itself does not change the peak gain or the linewidth by much locally, although it does have a strong effect on the Brillouin frequency shift. The effect of this is that the total gain for any length of the fiber undergoes an effective drop in peak

gain with the consequent increase in gain bandwidth. We next briefly discuss these methods. For example, a fiber with a varying core size in an acoustic guiding fiber chirps the Brillouin gain spectrum and reduces the peak Brillouin gain constant [22]. Varying the index of refraction and inducing stresses in the fiber have a similar effect of broadening the Brillouin gain spectrum. However, to achieve a large degree of SBS suppression these techniques require one to induce a very large non-uniformity along the fiber length. This is both difficult and expensive to implement, and can negatively influence optical mode properties and introduce large optical losses.

To determine the Brillouin-gain spectrum when the acoustic parameters are varied slowly along the length of the fiber, we can write for the total gain as in reference [23]

$$G(\nu) = \int_0^L g_B(\nu, z)\, dz, \tag{1.11}$$

which can be further simplified to

$$G(\nu) = g_0 \int_0^L \frac{1}{1 + ((\nu - \nu_B(z/L))/(\Delta\nu_B/2))^2}\, dz, \tag{1.12}$$

where ν_B is the frequency downshift as a function of z and we assume a lorentzian lineshape locally with a FWHM of $\Delta\nu_B$. This formulation is true for lengths of fiber less than 100m [22]. The increase in threshold is then given by

$$P_i nc = -10 \log \int_0^1 \frac{1}{1 + ((\nu - \nu_B(l))/(\Delta\nu_B/2))^2}\, dl. \tag{1.13}$$

Thus, under the short fiber length approximation ($z < 100m$), we see that the threshold increase is dependent only on the distribution of the Brillouin frequency shift.

The typical dependence of Brillouin frequency downshift on tensile strain and temperature are shown in reference [24]. These can be used in conjunction with

an actual distribution of temperature/strain and equation to obtain the increase in threshold obtainable as a result of imposing nonuniformity along the length of the fiber.

Liu [25] has developed a more detailed model for the SBS process and threshold enhancement effects in a fiber with gain and temperature and core non-uniformities and has shown a 7dB suppression. Reference [26] specifically considers temperature gradient induced by pump absorption. Reference [27] discusses the SBS threshold increase obtainable by application of strain distribution and reports up to 8dB for a 580m DSF.

From this discussion we can conclude that although variation of acoustic parameters in the longitudinal direction is a feasible method, its potential seems limited to around 10 dB increase in threshold. We therefore investigated the effect of varying the properties in the cross sectional plane. It should be apparent from eq. 1.14, that a combination of the two approaches can be used for furthering the threshold enhancements.

Dragic introduced the idea of an acoustic ring guide as a method of decreasing the local value of peak Brillouin gain [28]. This idea has since been extended to include design of arbitrary doping profiles for SBS suppression [29]. In Chapter 3, we develop a model to carefully consider SBS suppression effects and propose a doping profile design for SBS suppression.

A natural extension of the idea of acoustic guidance control is the use of specialized band-gap structures that can inhibit/enhance acoustic phonons [30, 31]. the authors in [30] suggest designs that could completely suppress SBS. Reference [32] provides experimental work that characterizes SBS in these structures. These structures have been primarily modeled through finite-element simulations. To gain insight into the

nature of SBS in bandgap structures, in chapter 4, we study SBS in a 1D elastic grating and relate the suppression to the metrics of the bandgap structure.

Modification of the Stokes wave

Most of the methods proposed for suppression of SBS consider variation of the acoustic environment. While this is certainly a useful approach, most workers have ignored the possibility of modifying the optical environment for the backscattered Stokes wave as a possible means for SBS suppression. Lee et al [33] were the first researchers to propose using a fiber Bragg grating designed particularly to filter out the Stokes wave for SBS suppression. This method has been criticized for its problems, chief among them being the requirement of writing a fine grating along the length of the fiber and secondly, the possibility of affecting pump propagation. The authors have suggested some schemes for mitigating these difficulties namely the writing of gratings in periods.

In this work, we propose a radically simpler alternative method for achieving distributed Stokes suppression. Our method relies on using circular polarized light and a fiber design that provides for circular dichroism. Our method uses currently available manufacturing technology and in addition has the advantage of nonlinearity saturation with length.

In chapter 5, we analyze the SBS process in the presence of distributed stokes loss and show the saturating nonlinearity effect. In Chapter 6, the SBS process is analyzed for circularly polarized pump in a circularly dichroic fiber with residual linear birefringence. We also briefly discuss design concepts for achieving circular dichroism in an optical fiber.

It is hoped that with the simpler alternative schemes for SBS suppression proposed and expounded upon in this dissertation, high-power single transverse beam output

in the 10kW range become feasible. These in combination with coherent WBC schemes could potentially soon lead to fiber laser sources with output power in the MW range.

CHAPTER 2

Omnidirectional optical switching in mixed negative/positive index periodic structures

2.1 Introduction

Most well known optical phenomena undergo interesting twists when studied in the presence of negative index media (first proposed by the Russian physicist Veselago [5]). It is our interest in this chapter to study the nonlinear optical effect of hysteretic transmission in the presence of a periodic negative refractive index.

Periodic dielectric structures have stop bands in frequency within which an electromagnetic wave undergoes coherent Bragg scattering and is totally reflected by the structure. In 1979, Winful et al. showed that the inclusion of an intensity-dependent refractive index makes it possible to tune the stop band and thus switch the structure from a highly reflecting state to a totally transmitting state [34, 35]. In the totally transmitting state, the structure exhibits a nonlinear resonance with a field distribution that peaks at the center [2]. This nonlinear resonance structure associated with the Bragg gap is known as a gap soliton [3] and has been the subject of intense studies [36].

Recently, a completely new kind of bandgap was discovered in structures where the average refractive index vanishes at certain frequencies [37, 38, 39, 40]. One way to achieve such a zero-n gap is to create a periodic structure with alternating layers

of positive index materials and negative-index materials (also termed left-handed materials by Veselago [5]). For mixed positive-negative-index periodic structures, it has been shown that inclusion of a single nonlinear defect layer results in tunable transmission and bistability [41, 42, 43]. That structure however is essentially a Fabry-Perot resonator with linear distributed-feedback reflectors enclosing a nonlinear lumped element.

This zero-n gap has very unusual properties in that it is robust to scaling and disorder [44]. This gap exhibits an omnidirectional feature [39], which makes it of great interest for applications requiring a wide field of view. These properties of the zero-n gap are quite different from those of the usual Bragg gap of positive index structures.

It is therefore of interest to investigate whether these novel properties of the zero-n gap persist in the presence of a periodic nonlinearity in the refractive index. We thus investigated the nonlinear transmission of a positive-negative periodic structure with inherent periodic nonlinearity.

We find that the zero-n gap exhibits a hysteretic response which is relatively insensitive to input angle, in contrast to the behavior of the Bragg gap. We show that a novel kind of gap soliton associated with the zero-n gap exists in periodic structures with alternating positive- and negative index layers. We call this the zero-n gap soliton and show that it is relatively insensitive to input angle, unlike the usual Bragg gap soliton. This raises the intriguing possibility of an omnidirectional gap soliton that is also robust in the presence of disorder and loss.

2.2 Theory

2.2.1 Specification of the structure

Here we consider the case where the periodic structure itself is inherently nonlinear. The positive index layers exhibit Kerr-type nonlinearity while the negative index medium is taken to be linear, although nonlinearity in its electric and magnetic susceptibilities can be easily included.

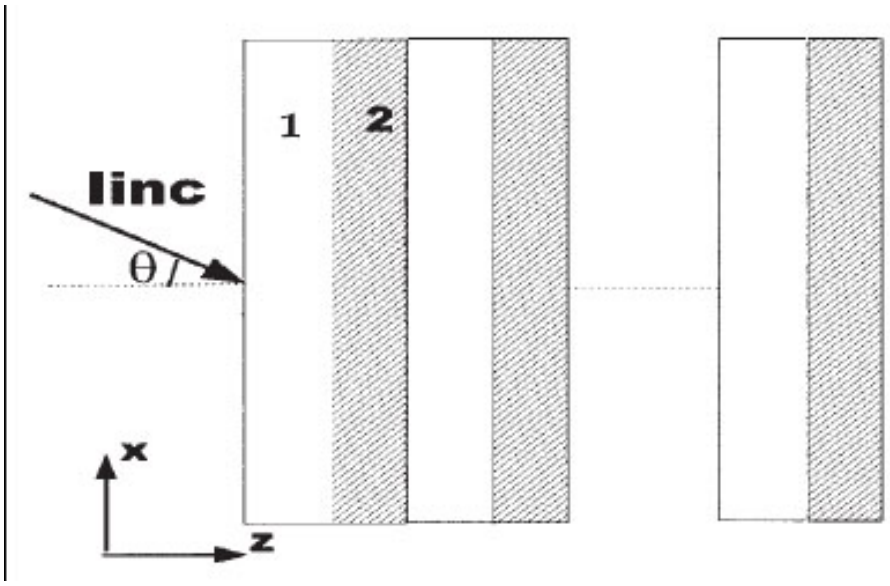

Figure 2.1: Schematic of the nonlinear periodic structure

The periodic structure (shown in figure 2.1) consists of N unit cells occupying the region $0 < z < D$ translationally invariant in the $x - y$ plane and bounded on both sides by free space. Each cell is formed of two films, film 1 and film 2, with respective thicknesses $d1$ and $d2$. Film 1 is a positive-index material with an intensity-dependent permittivity described by

$$\epsilon_1(\omega, z) = \epsilon_1^{'}(\omega, z) + \epsilon_{NL}(|\mathbf{E}|^{\mathbf{2}}). \tag{2.1}$$

Film 2 is a negative-index or left-handed material. Its relative permittivity and

permeability variations are taken to be of the following forms, respectively:

$$\epsilon_2(f) = 1.6 + \frac{40}{0.81 - f^2 - \iota f L} \qquad (2.2)$$
$$\mu_2(f) = 1 + \frac{25}{0.814 - f^2 - \iota f L},$$

where f is the frequency in GHz and L represents the effect of loss. The implicit assumption in this formulation is that the negative index layer permits the use of an effective index for the frequency range of interest. The particular form of these expressions is so chosen to exhibit negative refraction in the GHz range, a frequency range where currently negative refraction has been demonstrated.

2.2.2 Solution of the electric field distribution in the structure

We solve for TE-polarized fields in this structure of the form

$$\mathbf{E(z,t)} = \mathbf{E(z)e^{\iota k_0(\beta x - ct)}}, \qquad (2.3)$$

where $k_0 = \omega/c, \beta = \sin(\theta) and \theta$ is the angle which the incident wave vector makes with the z axis. The spatial evolution of the electric field is governed by the wave equation (similar to [45])

$$\frac{d^2E}{d\zeta^2} + p^2E + \mu_i \epsilon i N L(|E|^2) = 0, (i = 1, 2), \qquad (2.4)$$

where $p^2 = \mu_i \epsilon_i^{'}(\omega, z) - \beta^2$ and $\zeta = k_0 z$.

The solutions for the most general case have to be obtained by numerical integration of equation (2.4). To obtain the transmission of the structure, we specify the E-field and its derivative at the output face and successively integrate equation (2.4) all the way to the input end. At the interfaces between two films, we apply the

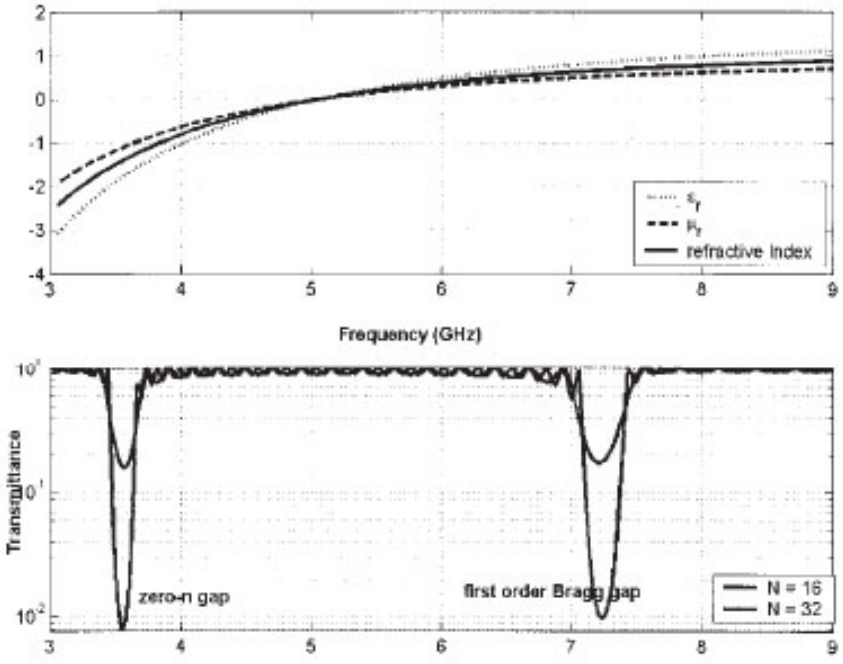

Figure 2.2: Material parameters of the negative layer and the transmittance of the structure as a function of frequency at normal incidence ($N = 16, 32$)

following boundary conditions:

$$E_i = E_j \tag{2.5}$$
$$\mu_j \frac{dE}{d\zeta}_i = \mu_i \frac{dE}{d\zeta}_j .$$

In the linear films, we use the following transmission matrix to propagate the fields:

$$\begin{bmatrix} \cos(p_i k d_i) & -(1/p_i)\cos(p_i k d_i) \\ p_i \sin(p_i k d_i) & \cos(p_i k d_i). \end{bmatrix}, \tag{2.6}$$

where the subscript refers to the film number in the unit cell. In a left-handed medium, the Poynting vector and the propagation vector are antiparallel Thus, if the film is a negative-index type, then a negative value of p is used.

2.2.3 Transmission spectrum with the nonlinearity turned off

We choose $d1 = d2 = 10mm$. Film 1 is a positive index material with $\epsilon^{'} = 2, \mu = 1$. The positive layer exhibits a Kerr-type nonlinearity modeled by γL. The dispersion relations and the linear transmission spectrum (for $N = 16, 32$) are shown in figure 2.2. The zero-n gap occurs at a frequency at which the following condition is satisfied:

$$\sqrt{\epsilon_1(f)\mu_1(f)}d_1 = \sqrt{\epsilon_1(f)\mu_1(f)}d_2. \tag{2.7}$$

For the parameters used here, the zero-n gap occurs at 3.55 GHz. This gap for an infinite structure is expected to show omnidirectionality. However, in a finite structure, the gap center does vary slightly with the incident angle and the number of layers. This can be attributed to the fact that in a finite structure the end reflections influence the overall transmission.

2.3 Bistable Transmission

The intensity-dependent refractive index makes it possible to tune the properties of the periodic structure, resulting in optical switching, hysteresis, and bistability. Figure 2.3 shows the intensity-dependent transmission for an input signal tuned inside the 1st-order Bragg gap. At this frequency, both media in the periodic structure have a positive refractive index. For an input at normal incidence, the transmission displays a large bistable region as the incident intensity is varied. The bistable response is, however, very sensitive to the incident angle. For the same input frequency, bistability is strongly degraded at an angle of 5^o and disappears completely at an incident angle of 10^o.

This sensitivity to incident angles is in marked contrast to the nonlinear behavior of the zero-n gap. Figure 2.4 shows the bistable response of the structure for an

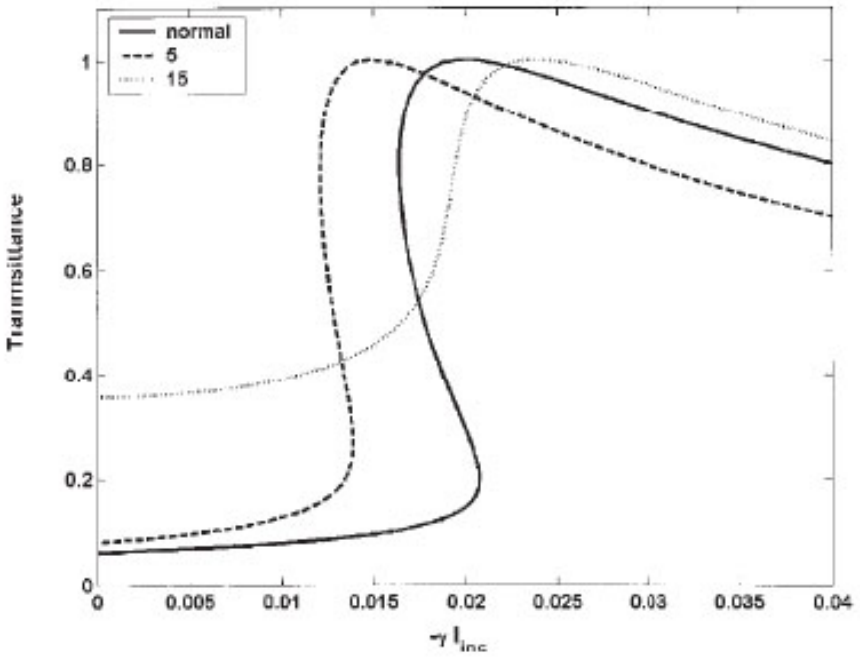

Figure 2.3: Hysteresis behavior of transmittance as a function of a defocusing γI_{inc} for detuning near the 1st-order Bragg gap ($f = 7.15GHz, N = 32$) for incident angles $0^o, 5^o$ (note that for 15^o, hysteresis is not observed)

input frequency tuned inside the zero-n gap.

In contrast with the Bragg gap case, for detuning near the zero-gap center (f near 3.55 GHz), the hysteresis curves (Figures 2.5 and 2.4) for a wider range of incidence angles are seen to follow each other closely. Bistability persists for angles as large as 45^o. This is the result of the omnidirectionality feature that is present in the linear response of the zero-n gap. Because of the asymmetric nature of the dispersion about the center frequency of this gap, the detailed nature of the nonlinear transmission curves depend on whether the input is detuned slightly to the left or to the right of the gap center. Figure 2.5 shows the bistability curves for an input frequency slightly to the right of the zero-n gap center. The intensity required for bistability is somewhat higher in this case, but the transmission curves still follow each other closely as the incident angle is varied.

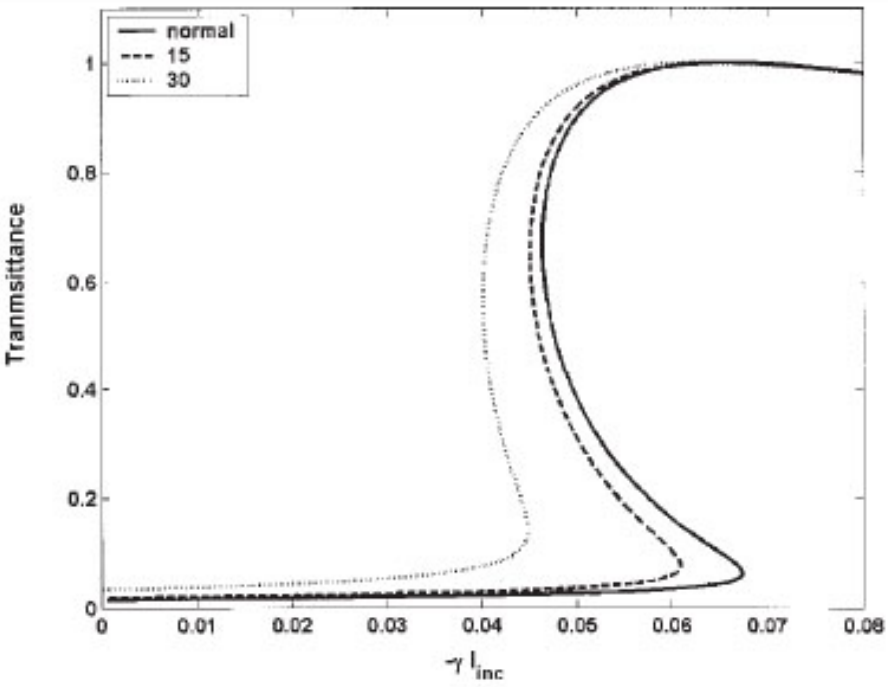

Figure 2.4: Bistable response for detuning to the left of the zero-n gap.

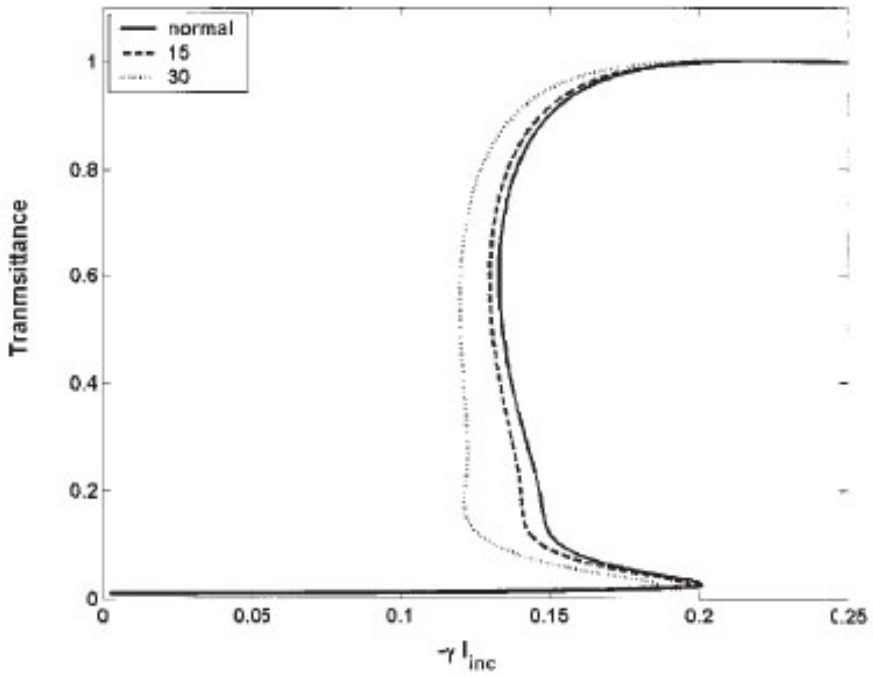

Figure 2.5: Bistable response for detuning to the right of the zero-n gap.

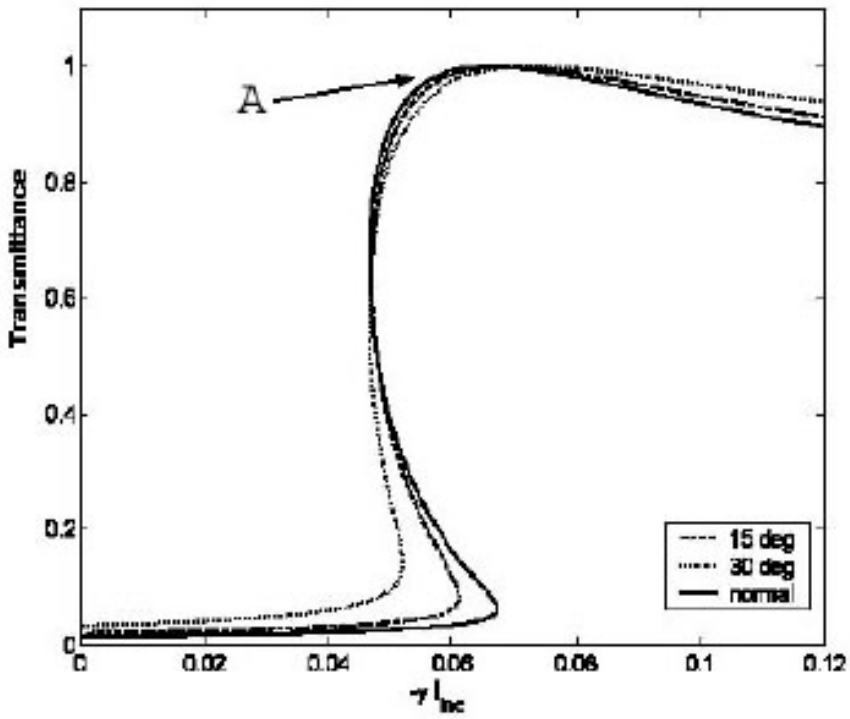

Figure 2.6: Hysteresis behavior of transmittance as a function of a defocusing γI_{inc} for detuning to the left of the zero-n gap ($f = 3.51GHz, N = 32$) for incident angles $u = 0^o, 15^o, and 30^o$.

2.4 The Zero-n gap soliton

The transmission is multivalued, leading to hysteresis and bistability. Also notice that the hysteresis curves for different incident angles almost overlap at the high transmittance point. At the point marked A in figure 2.6 the transmission is nearly unity, signifying a transmission resonance. The spatial distribution of the magnitude of the E field associated with this transmission resonance is shown in figure 2.7.

This is the zero-n gap soliton. In the figure, the soliton is overlaid upon the periodic structure, with shaded regions representing the negative index material. For the zero-n gap soliton the local maxima and minima of the field distribution occur at the interfaces between the layers. Also, it can be seen that the minima of this soliton distribution do not go all the way to zero. A look at the phase variation of the E field inside the structure (Figure 2.8) helps us understand this behavior.

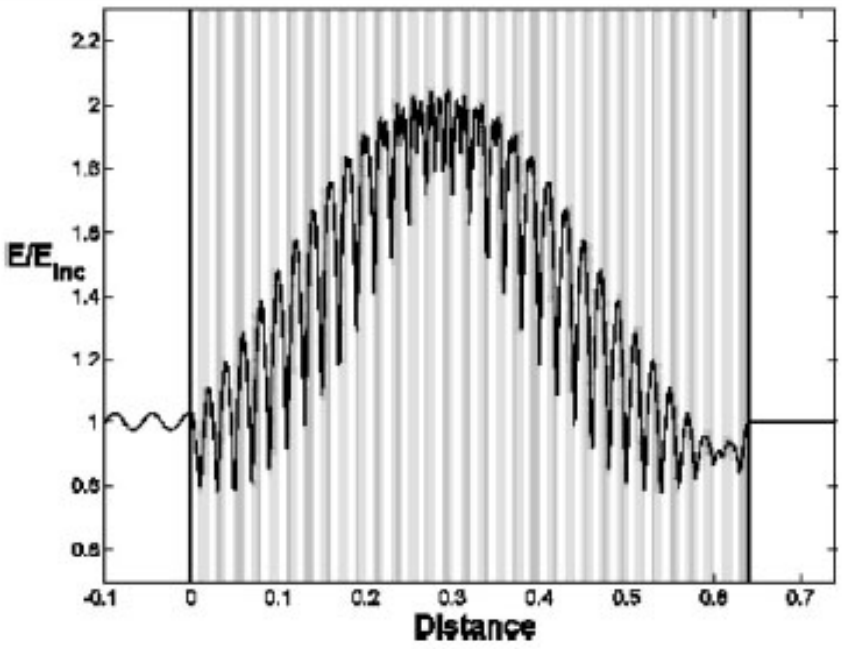

Figure 2.7: Zero-n gap soliton: spatial distribution of the E field magnitude (normalized by E_{inc}) when a defocusing $\gamma I_{inc} = 0.064$ results in a near-unity transmittance ($f = 3.51GHz, N = 32$) at normal incidence

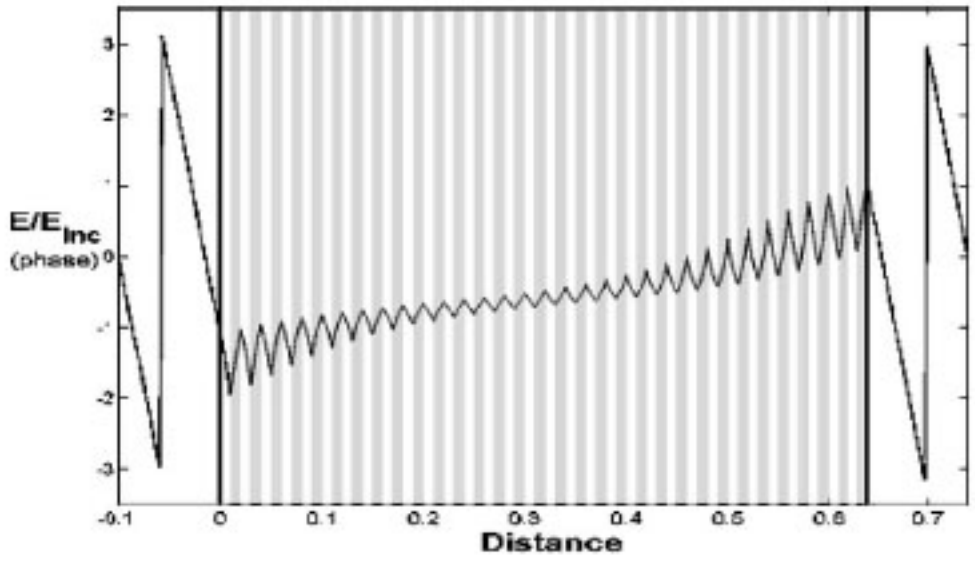

Figure 2.8: Spatial distribution of the phase of the E field for conditions as in figure 2.7

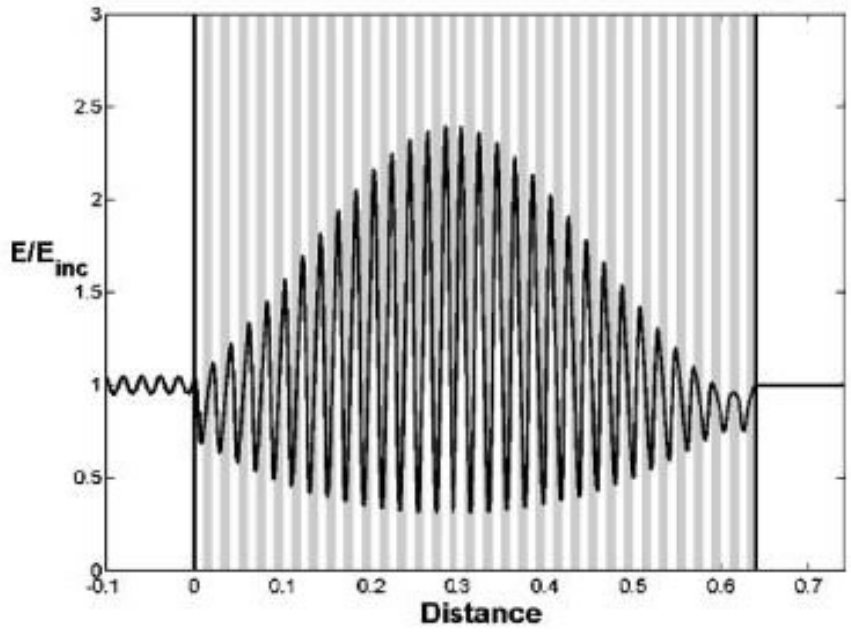

Figure 2.9: Bragg gap soliton observed when a defocusing $\gamma I_{inc} = 0.027$ is used ($f = 7.15$ GHz, $N = 32$)
at normal incidence

The phase does not build up to π across a layer. Because there is not a *pi* phase shift, complete destructive interference does not occur between layers. It is also seen that at the interface between a positive-index and a negative-index layer there is a change in the sign of the slope of the electric field. This is a result of the sign change in magnetic permeability as one crosses from a positive index to a negative-index medium.

For comparison the gap soliton associated with the Bragg gap soliton is shown in figure 2.9. The frequency is chosen to lie in the Bragg gap. It is seen that the minima of the field pattern are nearly zero for the Bragg gap soliton. This is because the evolution of the phase across a bilayer is continuous and goes all the way to π.

2.4.1 Properties of the zero-n gap soliton

It is of interest to see whether the zero-n gap soliton exhibits some of the interesting features, such as omnidirectionality and robustness, of the linear zero-n gap

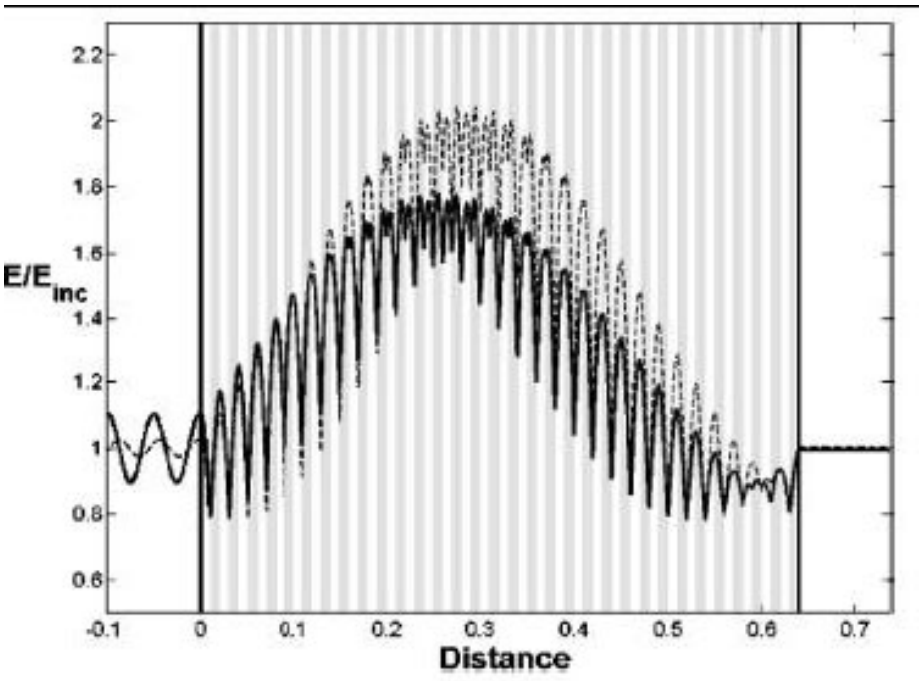

Figure 2.10: Zero-n gap soliton for an incident angle of 30^o (solid curve) as compared to the one at normal incidence (dotted curve). $\gamma I_{inc} = 0.064$ for both cases and other conditions as in figure 2.7

itself. The dependence of the zero-n gap soliton on incidence angle is shown in Figure 2.10.

For the same input intensity it persists for angular detuning as large as 30^o from the normal. Thus the robust nature of the zero-n gap with respect to input angle persists in the presence of nonlinearity. The Bragg gap soliton disappears for detuning as small as 5^o. The reason the Bragg gap soliton exhibits a sensitive dependence on input angle is simply its sensitivity to lattice scaling. To achieve a Bragg gap soliton at the new angle, one would have to change the incident frequency and increase the input intensity. Beyond a certain input angle, no Bragg gap soliton exists.

Finally we consider the effect of loss on the existence of the zero-n gap soliton. Figure 2.11 shows the variation of the gap soliton as the loss is increased. The soliton shape is preserved even at relatively high losses.

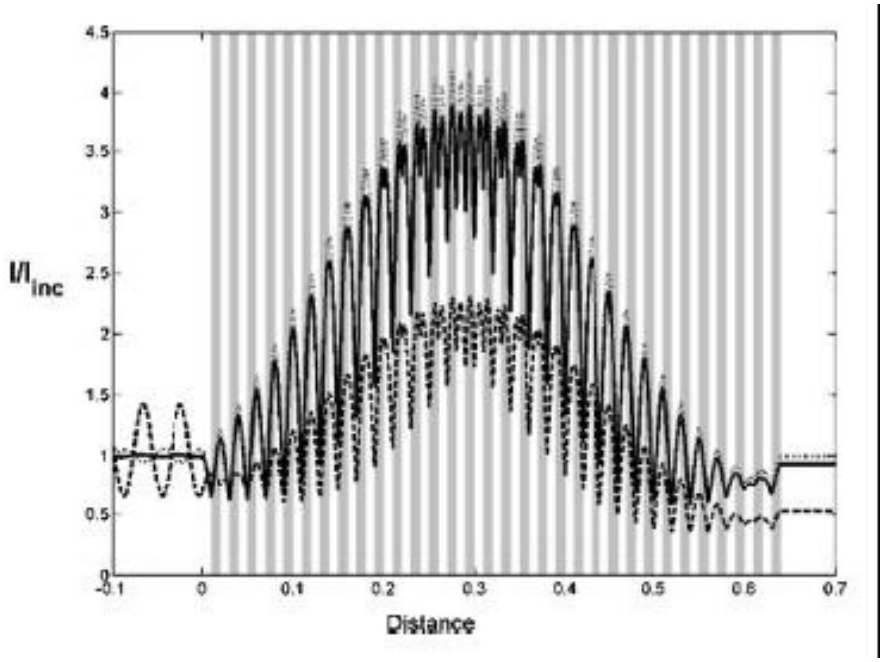

Figure 2.11: Zero-n gap soliton for an incident angle of 0^o for a lossy structure at two different values of the loss term ($L = 0.01, 0.001$) as compared to a lossless structure (solid curve). The amplitude decreases as the loss term increases.

2.5 Conclusion

Although the zero-n gap soliton can exist in any frequency range where negative refraction exists, in this work we have considered materials in which the negative refraction occurs at microwave frequencies. This is because the experimental demonstrations of left-handed materials have been at those frequencies, although there is much active research aimed at realizing negative refraction at optical frequencies. Since the gap soliton requires a Kerr nonlinearity, it is natural to ask what values of the nonlinear coefficient are achievable at microwave frequencies. Measurements at 94 GHz have revealed an n_2 as large as $2.63x10^{-4}cm^2/W$ in liquid suspensions of elongated microparticles [46, 47]. Such materials have been used to demonstrate phase conjugation through degenerate four-wave mixing at those frequencies.

In summary, we have studied the nonlinear transmission of a periodic structure

containing alternating layers of positive-index and negative-index materials. The gap associated with a zero-average refractive index exhibits a bistable response that is relatively insensitive to input angles, in contrast to the behavior of the usual Bragg gap. We have introduced the concept of the zero-n gap soliton associated with these structures. Such zero-n gap solitons retain the exotic features associated with the linear zero-n bandgap.

This would make possible the operation of all-optical switches that have a wide field of view. The phenomenon of negative refraction is always accompanied by dispersion [5] and, hence, plays a key role in nonlinear gap tuning. By changing the dispersion in the negative-index material, the gap tuning and hysteresis behavior can be controlled.

CHAPTER 3

Acoustic waveguide engineering for suppressing SBS in optic fibers

3.1 Introduction

SBS involves the interaction of pump, the backward scattered Stokes waves and a co-propagating acoustic wave. Most of the traditional approaches to SBS threshold enhancement in an optic fiber have involved methods aimed at broadening the SBS gain spectrum. For example, a fiber with a varying core size in an acoustic guiding fiber chirps the Brillouin gain spectrum and reduces the peak Brillouin gain constant [22]. Varying the index of refraction [48], inducing stresses in the fiber [49] and applying temperature gradients [24, 25, 23] have a similar effect of broadening the Brillouin gain spectrum. However, to achieve a large degree of SBS suppression these techniques require one to induce a very large non-uniformity along the fiber length. This is both difficult and expensive to implement, and can negatively influence optical mode properties and introduce large optical losses.

An alternative approach involves the alteration of the acoustic waveguiding properties of the fiber in the fiber cross plane to reduce the peak gain locally. This technique can then be used in conjunction with the methods already discussed to extend the levels of threshold enhancement that can be achieved by altering the acoustic environment of the fiber (see [7, 29]).

In this chapter, we discuss the modeling aspects for determining the threshold enhancement possible by altering the acoustic properties in the cross sectional plane of the fiber. In particular, the acoustic ring method and the acoustic ramp profile are considered. We also investigate the effect of core size scaling and discuss the implications for fiber design.

The chapter is organized as follows. We start with an introduction to acoustic guidance in optic fibers and the approach to quantify SBS parameters in a waveguide. We then introduce aspects related to modeling the SBS process for the particular designs of interest namely the ring and the ramp profiles. We classify the possible acoustic modes in these profiles and describe the procedure for solving for these modes. The procedure for constructing the spontaneous Brillouin gain spectrum is then described. The chapter then focuses on application of the theory to example profiles. These profiles have been chosen to reflect actual experimental fiber parameters. We finally discuss the implications of these results and derive a set of design guidelines that should be helpful in designing fiber lasers with a desired level of SBS suppression and ease of manufacture.

3.2 Theory

3.2.1 Acoustic guidance in optic fibers

The study of elastic waves in rods and other cylindrical structures has been the subject of active study since the early 1940's. The general solution for the acoustic modes even in the case of a core embedded in an infinite cladding are fairly complex [50] and do not decouple in the general case into pure longitudinal or shear waves. However the modes that do contribute to light scattering will have the ϕ component of their displacement vector $\mathbf{u}_\phi = 0$.

3.2.2 Gain of the SBS process

The mechanism or acousto-optic scattering is the elasto-optic effect in which the acoustic strain fields interact with the incident electric field via the elasto-optic tensor p_{klmn}. The scattering of light resulting from the strain fields in an optical fiber has been treated in [50].

The incident electric field E_i scatters into the scattered field E_s and we have $E_s = DE_i$, where D is the tensor amplitude of the scattered field and is given by

$$D = D_0 \left[\int_{core} \mathbf{E}_i^* \cdot \delta \cdot \mathbf{E}_s \, dV + \int_{cladding} \mathbf{E}_i^* \cdot \delta \cdot \mathbf{E}_s \, dV \right]. \tag{3.1}$$

The relevant dielectric perturbations $\delta\epsilon$ are functions of the acoustic strain fields $(S_{p,q})$ and are expressed as

$$\begin{aligned}
\delta\epsilon_{rr} &= -\epsilon_0 n^4 \left(p_{11} S_{rr} + p_{12} S_{\phi\phi} + p_{12} S_{zz} \right), \\
\delta\epsilon_{\phi\phi} &= -\epsilon_0 n^4 \left(p_{11} S_{\phi\phi} + p_{12} S_{rr} + p_{12} S_{zz} \right), \\
\delta\epsilon_{\phi r} &= -\epsilon_0 n^4 \left(2 p_{44} S_{\phi r} \right).
\end{aligned}$$

The photoelastic constants, p, are provided in [51] for vitreous silica at $\lambda = 632.8nm$ as $p_{11} = 0.121, p_{12} = 0.271 and p_{44} = -0.075$. The strain fields are calculated as in reference [50] as

$$\begin{aligned}
S_{rr} &= \frac{\partial u_r}{\partial r}, \\
S_{\phi\phi} &= \frac{u_r}{r} + \frac{1}{r}\frac{\partial u_\phi}{\partial \phi}, \\
S_{zz} &= \frac{\partial u_z}{\partial z}, \\
S_{\phi\phi} &= \frac{1}{2}\left(\frac{1}{r}\frac{\partial u_r}{\partial \phi} + \frac{\partial u_\phi}{\partial r} - \frac{u_\phi}{r} \right),
\end{aligned}$$

where u is the acoustic displacement vector.

The scattering amplitude tensor D is further broken into components as

$$D_{p,q} = \int_{vol} \bar{E}_p^* \delta\hat{\epsilon}_{p,q} \bar{E}_q \, dV, \tag{3.2}$$

where $p, q = r, \phi, z$ are the cylindrical coordinates.

Taking E_z to be zero in the fiber, the non-zero contributions to the scattering amplitude are $D_{rr}, D_{\phi\phi}$ and $D_{r\phi}(= D_{\phi r})$ as shown in reference [50]. Physically this can be explained by the fact that a grating perpendicular to the traveling optical waves is most effective. Furthermore, the analysis in [50] showed that D_{rr} is the dominant scattering amplitude, followed by D_{zz} with an overall contribution of a few percent to the total scattering amplitude.

Much like optical fibers are weakly guiding for optical waves, they can also be weakly guiding for acoustic waves. To satisfy this condition, the acoustic velocities in the core and cladding should satisfy $V_a^{core} < V_a^{cladding}$. This is usually the case for typical fibers with P_2O_5 and/or GeO_2-doped cores and pure silica claddings (see [52]). When the shear and longitudinal acoustic waves are decoupled, and we assume that the shear velocity and mass density are constant in the radial direction $V_{core}^s \approx V_{cladding}^s$ and $\rho_{core} \approx \rho_{cladding}$). This leads to a set of solutions for u known as 'Leaky' modes, designated L_{nm}. These are the most significant acoustic modes in the SBS process in a typical optical fiber. Interestingly, these modes have a dispersion relationship identical to that of the optical mode in the fiber [28]. Furthermore reference [51] establishes that the backward Brillouin scattering of the fundamental optical mode can occur only for the modes L_{0m}. Additionally, the fundamental leaky mode, L_{01}, has been shown to dominate SBS in a typical single clad fiber.

In some cases where the fiber core is substantially acoustically multimode, several acoustic modes can be excited in the SBS interaction. This was suggested in [52] and observed empirically in reference [53]. However, in all cases, the L_{01} mode dominated

the Brillouin spectra. This is expected since the L_{01} acoustic mode is mathematically identical to the $LP_{01}(HE_{11})$ optical mode, and thus the spatial overlap integral is very high.

Implications for our modeling work

The implications of this for modeling work are that a full vectorial solution for the elastic waves is rarely necessary. In this work, the elastic waves are assumed to satisfy the scalar wave equation (meaning that their displacement has predominantly a z component). However, a full vectorial simulation was also carried out and its results were found not to differ significantly from a scalar simulation. In particular, the changes in the value of the peak gain were found to be not numerically significant. For reasons of computational efficiency, we thus chose to stick with the scalar assumption. The framework is general enough to accommodate full vectorial solutions. Such solutions can be now easily obtained using commercial FEM software like COMSOL if further accuracy is needed.

3.3 Acoustic waveguide structures and solving for acoustic modes

A step index acoustic waveguide can be classified as either acoustic guiding or acoustic antiguiding depending on the relative values of the longitudinal acoustic velocity in the core and the cladding ($V_a^{core}, V_a^{cladding}$ respectively). We have $V_a^{core} < V_a^{cladding}$ for acoustic guiding and $V_a^{core} < V_a^{cladding}$ for acoustic anti-guiding. The acoustic antiguiding fiber is found to result in a peak Brillouin gain that can be less than a guiding acoustic fiber of comparable radius. However acoustic anti-guising fiber needs specialized doping methods.

Before we investigate novel overlap reducing structures, we study the acoustic

Fiber	$V1(m/s)$	$V2(m/s)$	$V3(m/s)$	$a(\mu m)$	$b(\mu m)$	NA
548	5890	5756	5933	4.3	13.5	0.15
727	6073	5322	5933	2.2	6.0	0.165

Table 3.1: Basic fiber data for the experimental low-SBS fibers.

modes of these two step index structures. We then modify the simple step index by adding a guiding acoustic ring layer around the core. Doping diffusion effects can result in a non step like radial distribution of acoustic velocities. We then finally investigate the acoustic guidance of the so-called ramp profile. To gain further insight and to help obtain design guidelines, we choose two fiber configurations that are drawn from currently available SBS suppression fibers.

Fiber 548 is acoustic guiding and fiber 727 is acoustic anti-guiding. The optical mode is the standard scalar wave equation solution for a step index fiber. Instead of the standard Gaussian wave, we express it in terms of Bessel functions. The pump has the free space wavelength λ_0 and the effective mode index n_{eff} for the primary mode is determined by solving for the characteristic equation resulting from the matching of the wavefunction and its derivative at the step boundary.

We can then define the mode effective area as

$$A_{eff} = \frac{\langle I \rangle^2}{\langle I^2 \rangle}, \tag{3.3}$$

where $I = I(x, y)$ is the local optical intensity and $\langle - \rangle$ denotes the integration in the transverse plane. The propagation constants for the optical and acoustical waves then become

$$\beta_{opt} = \frac{2\pi n_{eff}}{\lambda_0}, \beta_{acc} = 2\beta_{opt}. \tag{3.4}$$

The acoustical waves are assumed to be solutions of the scalar wave equation

$$(\nabla^2 + \beta^2(r))\phi = 0, r \geq 0, \tag{3.5}$$

where ϕ denotes the acoustical wave function in the transverse plane. When we assume longitudinal acoustic waves, it can stand for the displacement in the z direction or the local density fluctuation. To obtain the eigenvelocity of the mode, continuity of ϕ and its derivative$\frac{\partial \phi}{\partial r}$ is assumed across any transition boundary. Also the derivative is assumed zero at the outer boundary if traction free surface exists or ϕ is assumed to be zero if the surface is clamped.

The acoustic modes are solved and should be compared to the optical mode profile for understanding the gain contribution of the particular mode. In solving for the acoustic modes, we are interested in two things: the eigenvelocity of the mode and its modeshape. The eigenvelocities are determined by solving for the characteristic determinant of each particular mode. These are essential to calculate the Brillouin frequency shifts associated with the particular optical mode. The acoustic modeshapes are normalized so that each acoustic mode has equal acoustic power. We defer discussion of the normalization procedures when we discuss procedure for simulating the gain spectrum. However, it is to be noted that the plots of modeshapes in the following pages involve such normalizations.

3.3.1 Acoustic guiding fiber

The acoustic guiding fiber has the general velocity profile shown in figure 3.1. The example calculations will be performed on fiber 548 whose index profile is shown in figure 3.2. The optical mode for fiber 548 is shown in figure 3.3. The fiber supports guided acoustic modes and the bulk (or cladding) modes which we discuss below.

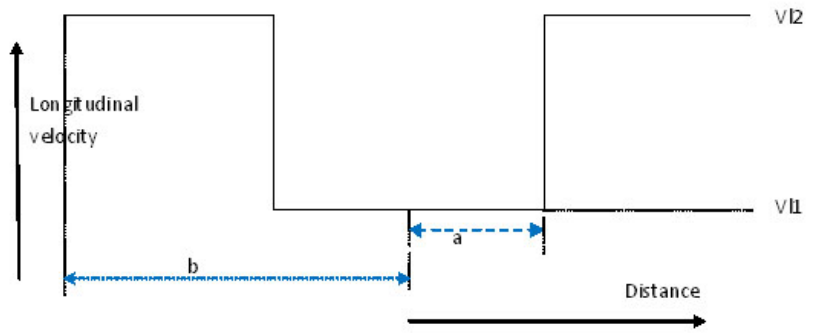

Figure 3.1: Acoustic guiding fiber index profile

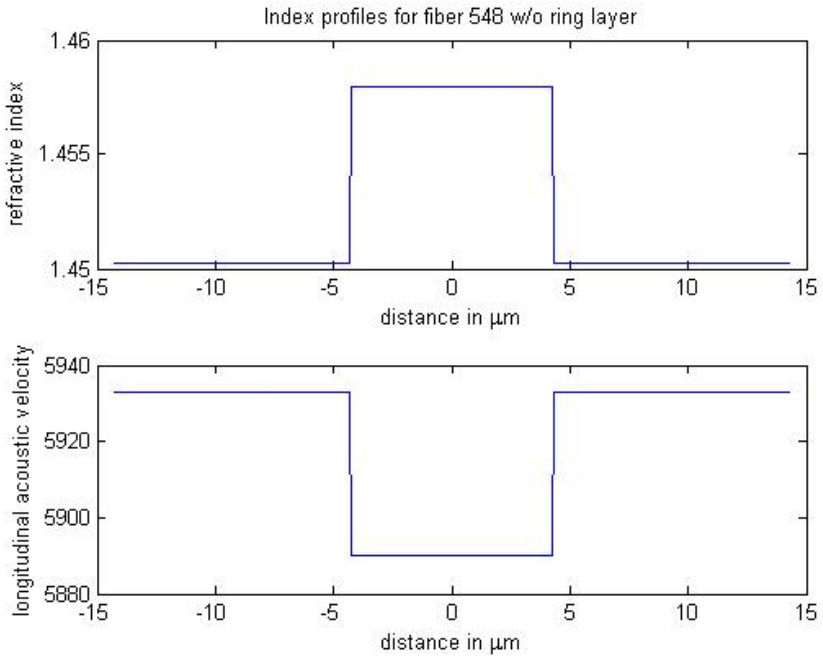

Figure 3.2: Index profile of fiber 548 without the guiding ring.

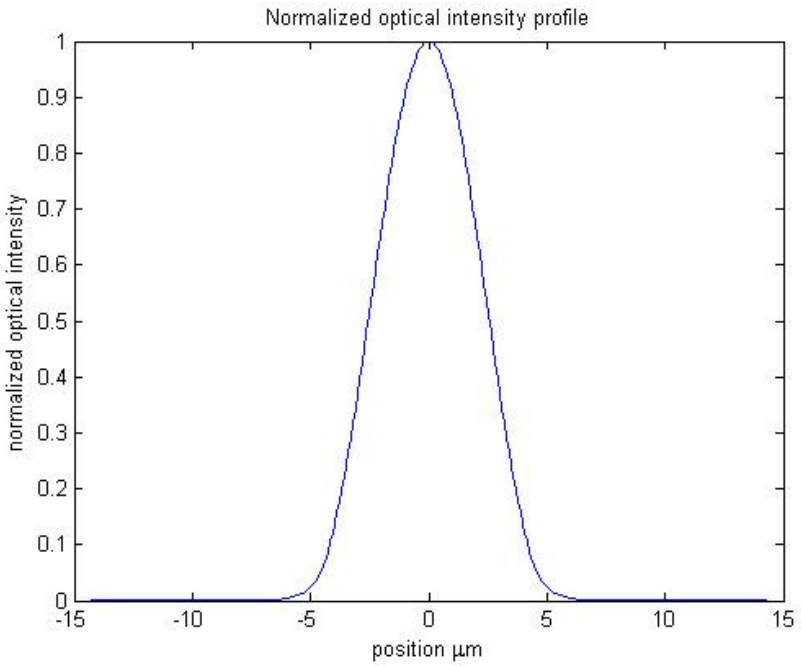

Figure 3.3: Optical mode profile for fiber 548 and its ringed counterpart.

Modes guided in layer 1

These modes have effective velocity that satisfies $V_{l1} < V_{eff} < V_{l2}$ and the wave-function is given by $\phi(r) = \begin{cases} AJ_0(h_1 r) & 0 \leq r \leq a, \\ BK_0(\tilde{h}_2 r) & a < r \leq b, \end{cases}$ where the constants are defined as

$$h_1 = \beta_{acc}\frac{\sqrt{V^2 - V_{l1}^2}}{V_{l1}}, \tilde{h}_2 = \beta_{acc}\frac{\sqrt{V_{l2}^2 - V^2}}{V_{l2}}.$$

The characteristic determinant for finding the eigenvelocities is then given by

$$\begin{vmatrix} J_0(h_1 a) & -K_0(\tilde{h}_2 a) \\ -h_1 J_1(h_1 a) & \tilde{h}_2 K_1(\tilde{h}_2 a) \end{vmatrix} = 0.$$

As an example, this determinant is plotted as a function of velocities for fiber 548. We also show how the modes are picked from such a graph and the corresponding modes have been plotted in figure 3.5

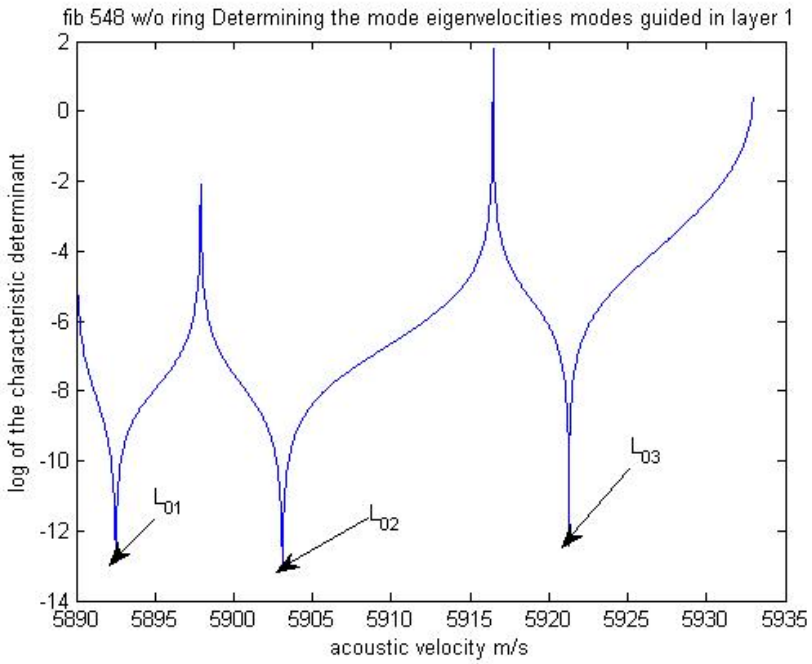

Figure 3.4: Plotting the characteristic determinant for determination of mode eigenvelocities for the guided modes.

Modes guided in layer 1 and 2

These modes have effective velocity that satisfies $V_{l1} < V_{l2} < V_{eff}$ and the wave-function is given by

$$\phi(r) = \begin{cases} AJ_0(h_1 r) & 0 \le r \le a, \\ BJ_0(h_2 r) + CY_0(h_2 r) & a < r \le b, \end{cases}$$

where the constants are defined by

$$h_1 = \beta_{acc}\frac{\sqrt{V^2 - V_{l1}^2}}{V_{l1}}, h_2 = \beta_{acc}\frac{\sqrt{V^2 - V_{l2}^2}}{V_{l2}}.$$

The characteristic determinant for finding the eigenvelocities is then given by

$$\begin{vmatrix} J_0(h_1 a) & -J_0(h_2 a) & -Y_0(h_2 a) \\ -h_1 J_1(h_1 a) & -h_2 J_1(h_2 a) & -h_2 Y_1(h_2 a) \\ 0 & -J_1(h_2 b) & -Y_1(h_2 b) \end{vmatrix} = 0.$$

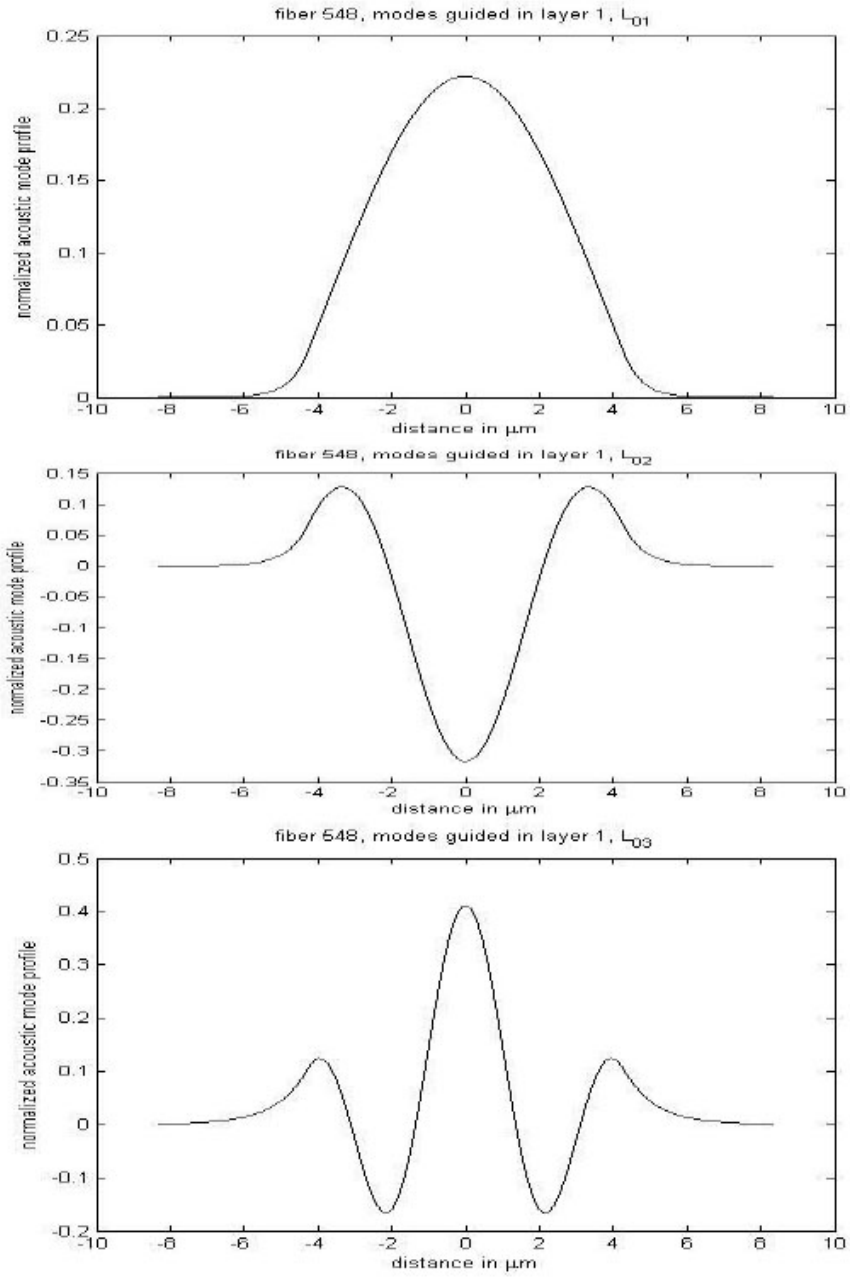

Figure 3.5: Modeshapes for the guided modes for fiber 548 w/o ring.

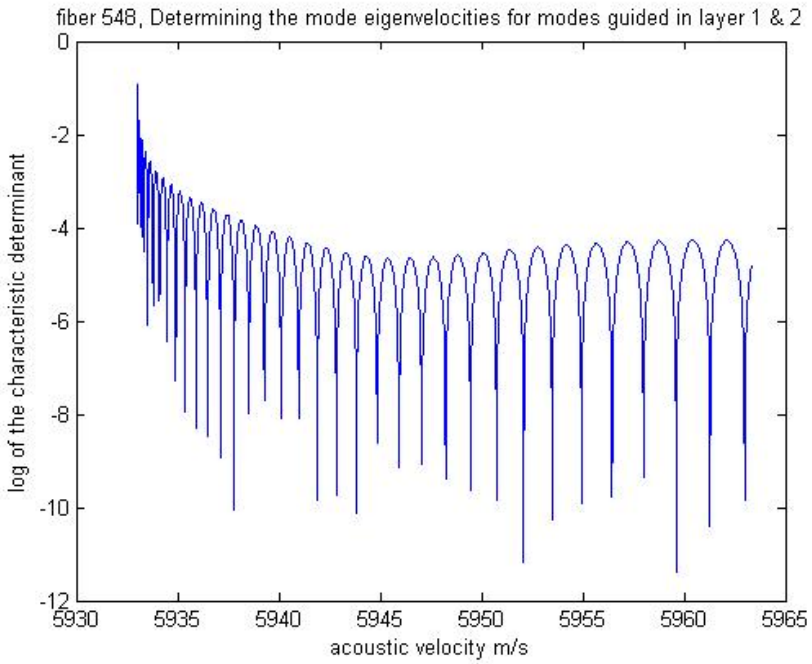

Figure 3.6: Determining the mode eigenvelocities for the bulk guided (cladding) modes.

The mode picking plots are shown in figure 3.7 for fiber 548 and the modeshapes for the first five cladding modes are plotted in figure 3.8.

3.3.2 Acoustic guiding fiber with acoustic guiding ring

The acoustic guiding fiber with the addition of a guiding ring layer has the velocity profile shown in figure 3.9. We choose fiber 548 with a ring for illustration of this case. (figure 3.10). The fiber supports guided acoustic modes and the bulk (or cladding) modes as before, but in addition the guiding ring now supports modes of its own.

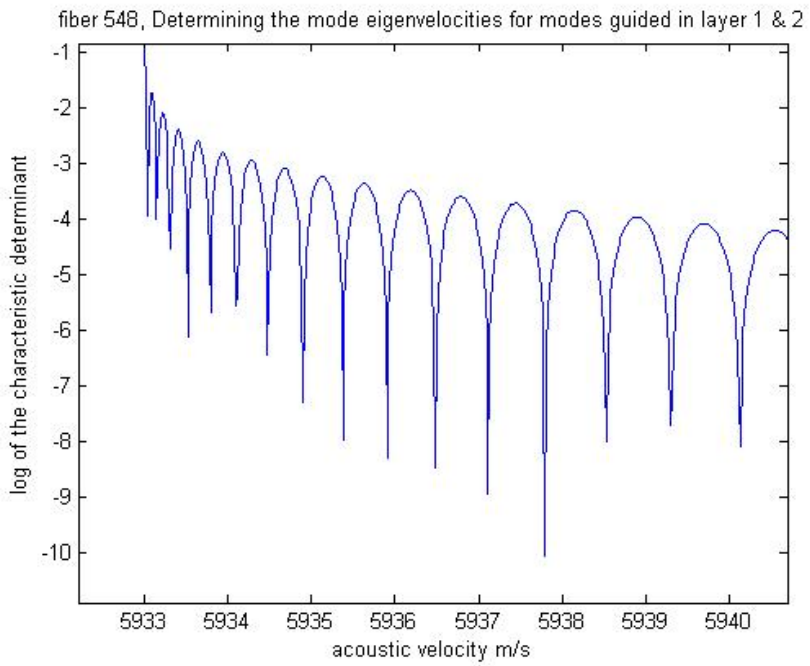

Figure 3.7: We zoom in on the modes that have the maximum contribution.

Modes guided in the ring

These modes have effective velocity that satisfies $V_{l2} < V_{eff} < V_{l1} < V_{13}$ and the wavefunction is given by

$$\phi(r) = \begin{cases} AI_0(\tilde{h_1}r) & 0 \leq r \leq a, \\ BJ_0(h_2 r) + CY_0(h_2 r) & a < r \leq a1, \\ DK_0(\tilde{h_3}r) & a1 < r \leq b, \end{cases}$$

where the constants are defined as

$$\tilde{h_1} = \beta_{acc}\frac{\sqrt{V_{l1}^2 - V^2}}{V_{l1}}, h_2 = \beta_{acc}\frac{\sqrt{V^2 - V_{l2}^2}}{V_{l2}}, \tilde{h_3} = \beta_{acc}\frac{\sqrt{V_{l3}^2 - V_{l1}^2}}{V_{l3}}. \tag{3.6}$$

The characteristic determinant for finding the eigenvelocities is then given by

$$\begin{vmatrix} I_0(\tilde{h_1}a) & -J_0(h_2 a) & -Y_0(h_2 a) & 0 \\ \tilde{h_1}I_1(\tilde{h_1}a) & -h_2 J_1(h_2 a) & -h_2 Y_1(h_2 a) & 0 \\ 0 & J_0(h_2 a_1) & Y_0(h_2 a_1 & -K_0(\tilde{h_3}a_1) \\ 0 & -h_2 J_1(h_2 a_1 & -h_2 Y_1(h_2 a_1 & \tilde{h_3}K_1(\tilde{h_3}a_1) \end{vmatrix} = 0.$$

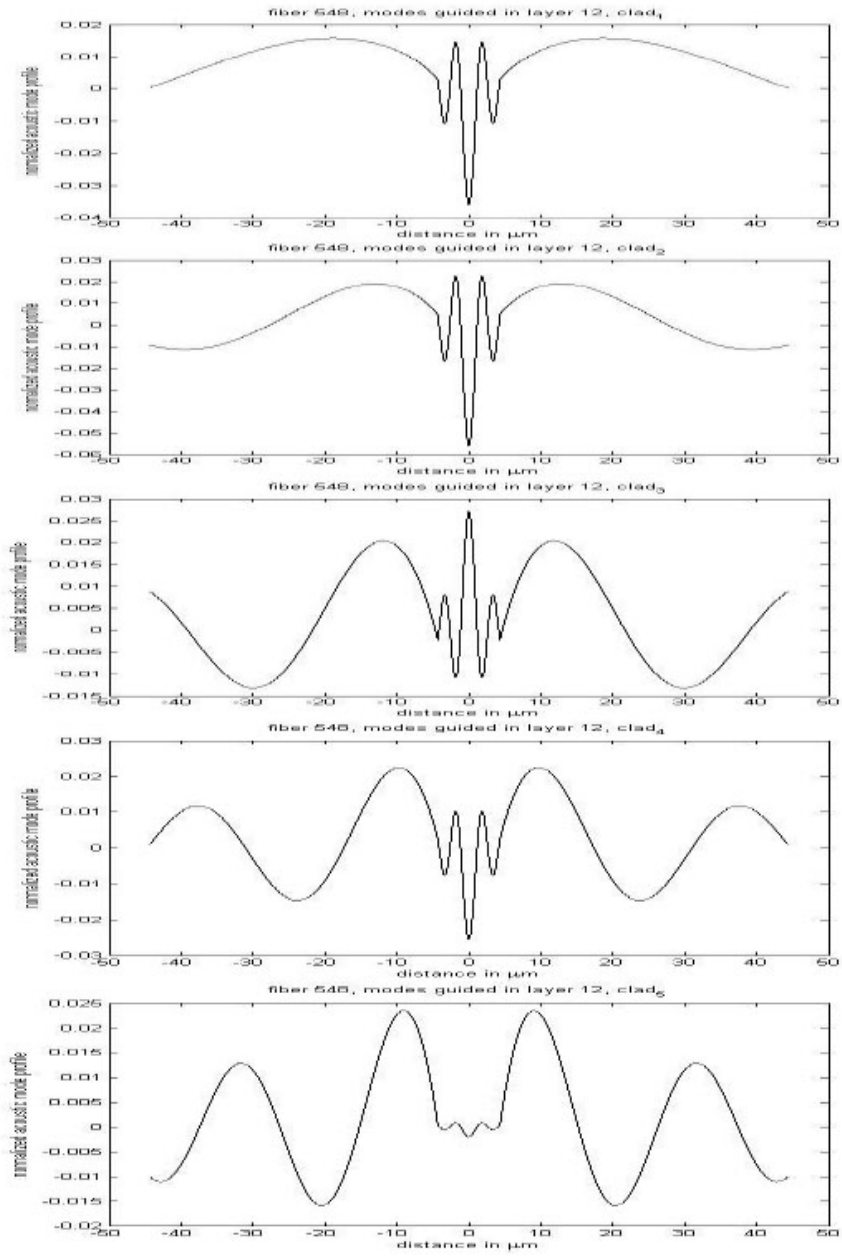

Figure 3.8: Modeshapes for the first five cladding modes.

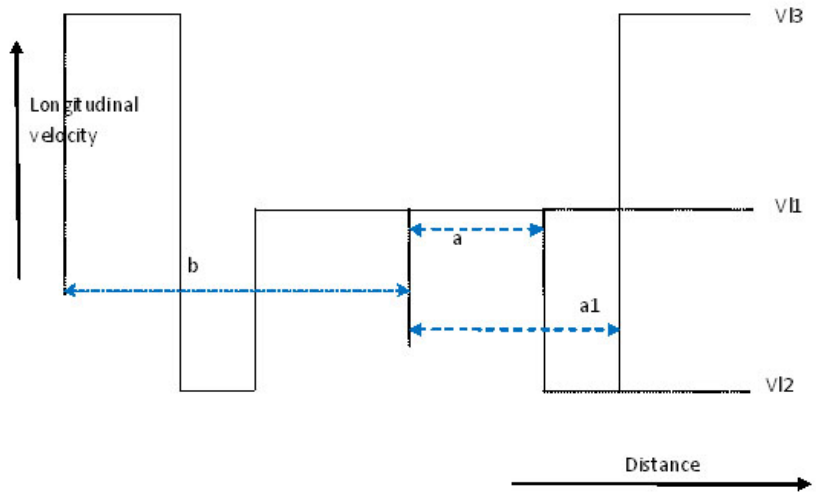

Figure 3.9: Acoustic guiding fiber with ring

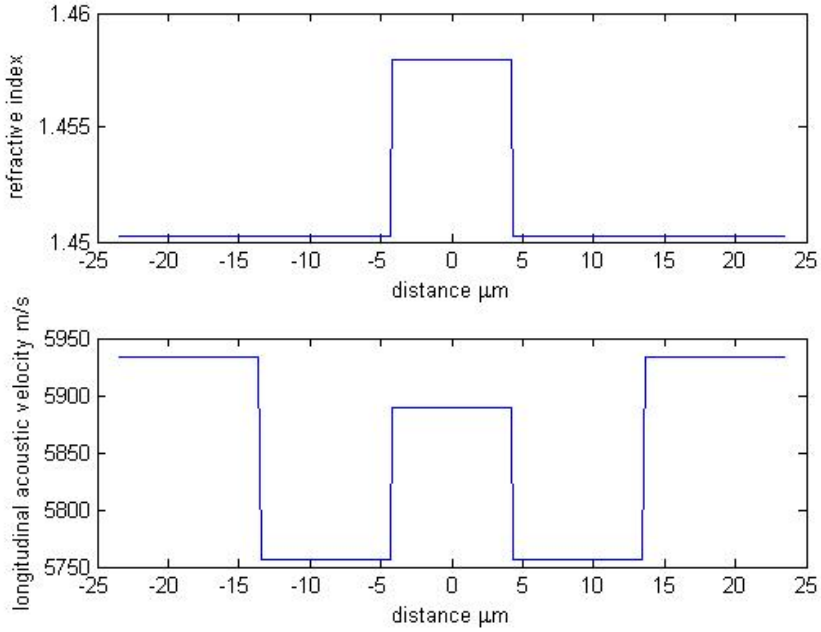

Figure 3.10: Index profile for fiber 548 with ring.

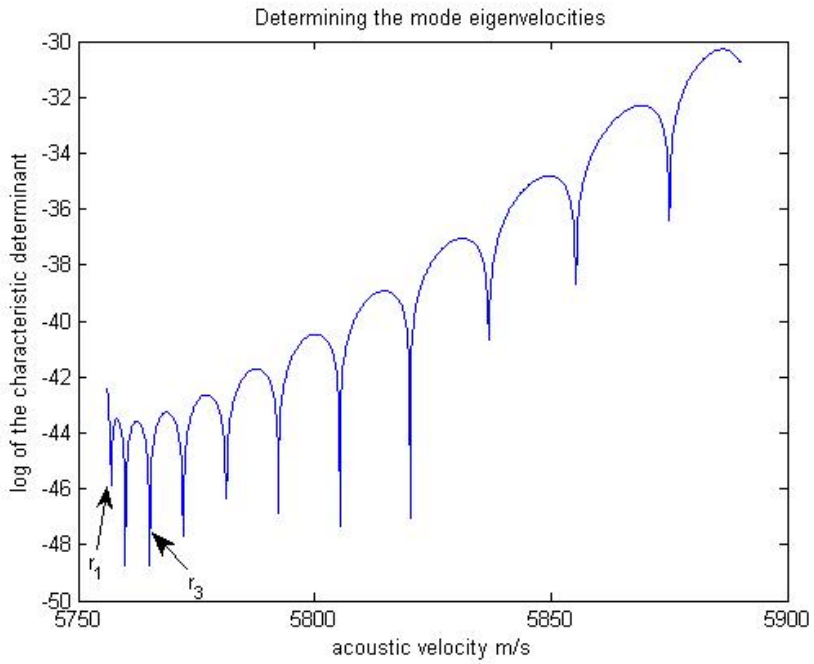

Figure 3.11: Plot for determining the eigenvelocities of the ring guided modes for fiber 548.

The plot of the characteristic determinant for picking the ring mode eigenvelocities is shown in figure 3.11 for fiber 548. The corresponding modeshapes for the ring modes are shown in figure 3.12

Modes guided in the inner layers

These modes have effective velocity that satisfies $V_{l2} < V_{l1} < V_{eff} < V_{13}$.

The wavefunction is given by

$$\phi(r) = \begin{cases} AJ_0(h_1 r) & 0 \leq r \leq a, \\ BJ_0(h_2 r) + CY_0(h_2 r) & a < r \leq a1, \\ DK_0(\tilde{h_3} r). & a1 < r \leq b, \end{cases}$$

where the constants are defined as

$$h_1 = \beta_{acc}\frac{\sqrt{V^2 - V_{l1}^2}}{V_{l1}}, h_2 = \beta_{acc}\frac{\sqrt{V^2 - V_{l2}^2}}{V_{l2}}, \tilde{h_3} = \beta_{acc}\frac{\sqrt{V_{l3}^2 - V_{l1}^2}}{V_{l3}}. \tag{3.7}$$

The characteristic determinant for finding the eigenvelocities is then given by

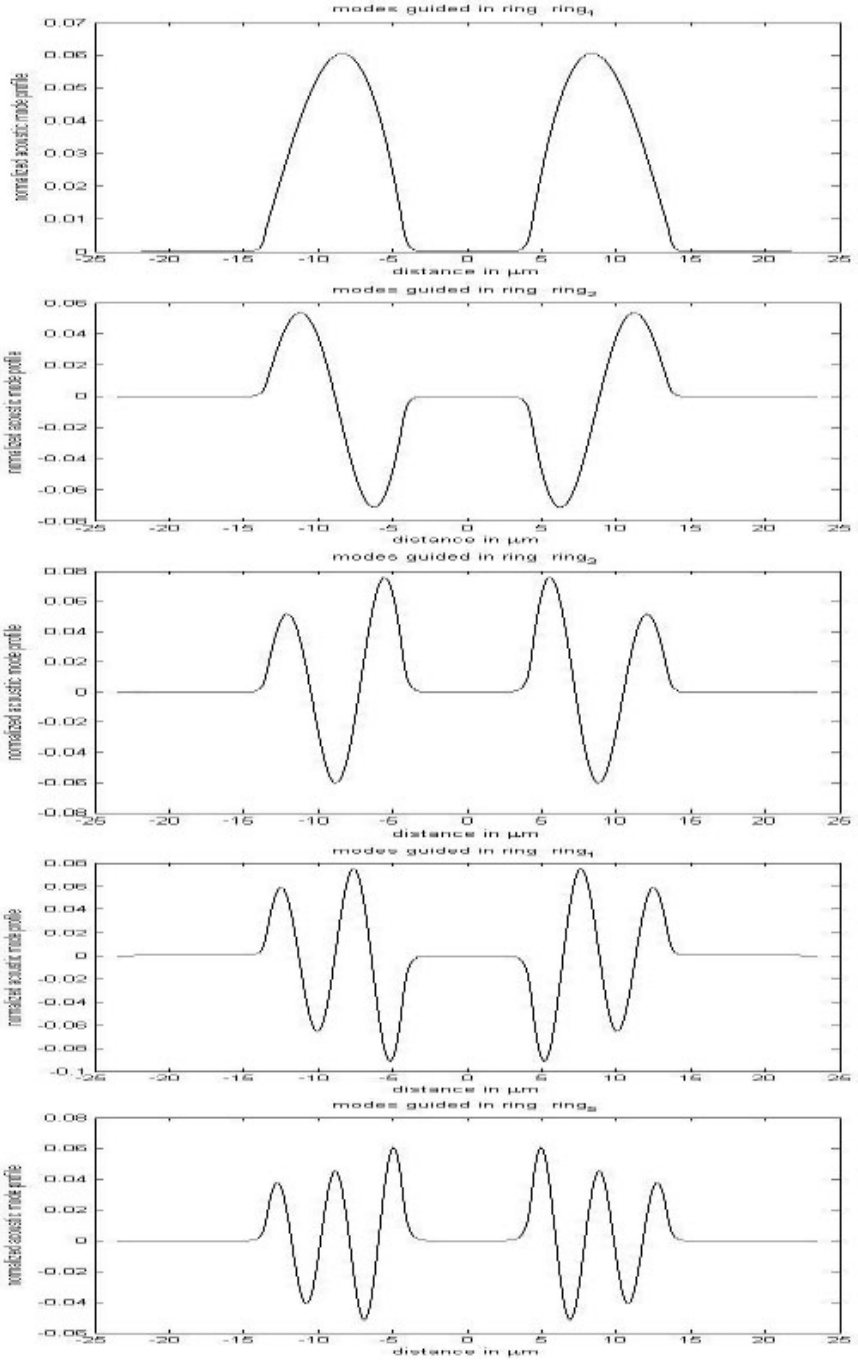

Figure 3.12: Modeshapes for the ring guided modes.

$$\begin{vmatrix} J_0(h_1a) & -J_0(h_2a) & -Y_0(h_2a) & 0 \\ -h_1J_1(h_1a) & h_2J_1(h_2a) & h_2Y_1(h_2a) & 0 \\ 0 & J_0(h_2a_1) & Y_0(h_2a_1 & -K_0(\tilde{h_3}a_1) \\ 0 & -h_2J_1(h_2a_1 & -h_2Y_1(h_2a_1 & \tilde{h_3}K_1(\tilde{h_3}a_1)) \end{vmatrix} = 0.$$

The characteristic determinant for fiber 548 is plotted in figure 3.13 and mode-shapes for the inner guided modes in figure 3.14.

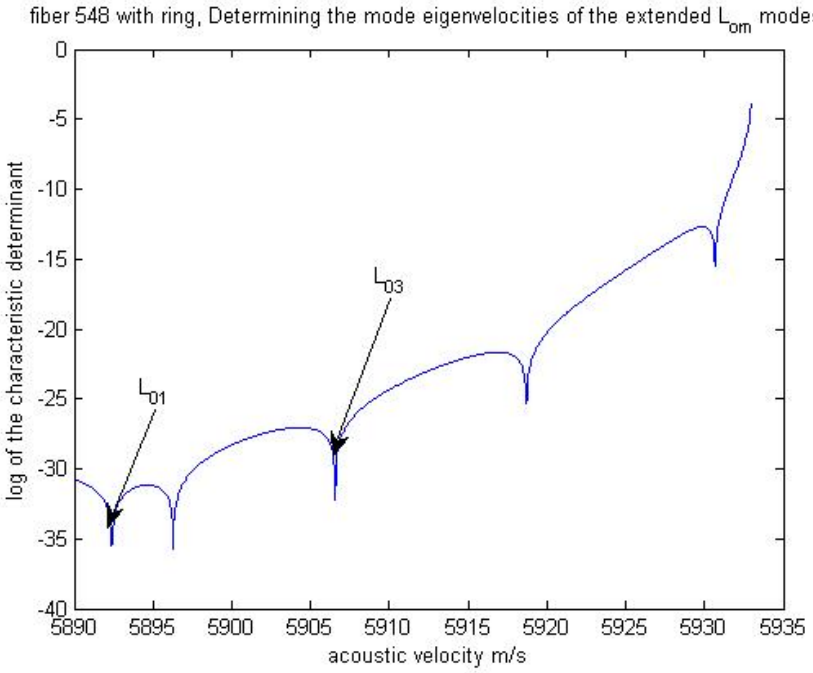

Figure 3.13: Plot for determining the eigenvelocities of the inner layer guided modes for fiber 548.

Modes guided in the cladding

These modes have effective velocity that satisfies $V_{l2} < V_{l1} < V_{13} < V_{eff}$.

The wavefunction is given by

$$\phi(r) = \begin{cases} AJ_0(h_1r) & 0 \le r \le a, \\ BJ_0(h_2r) + CY_0(h_2r) & a < r \le a1, \\ DJ_0(h_2r) + EY_0(h_2r) & a1 < r \le b, \end{cases}$$

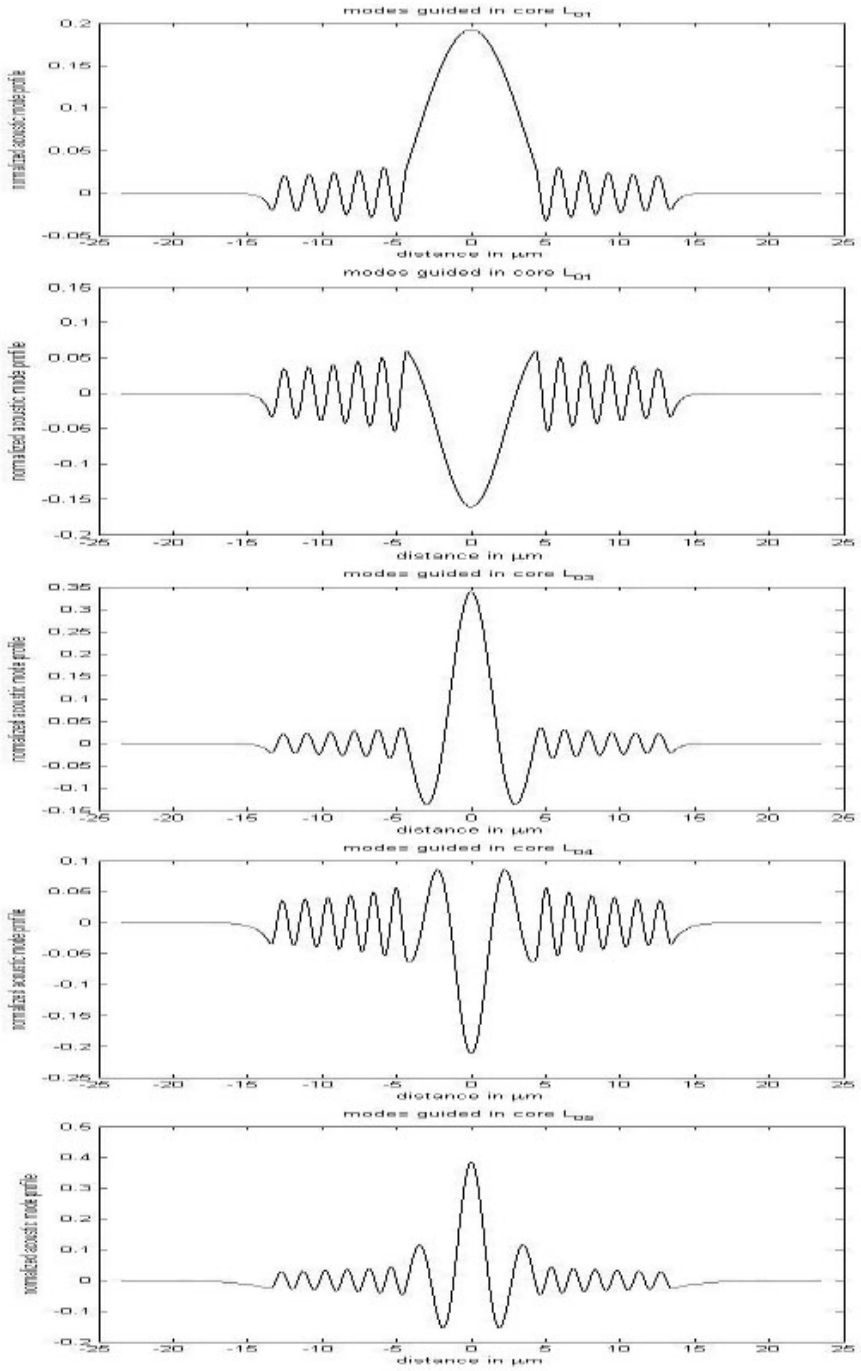

Figure 3.14: Modeshapes for the innerlayer guided modes.

where the constants are defined as

$$h_1 = \beta_{acc}\frac{\sqrt{V^2 - V_{l1}^2}}{V_{l1}}, h_2 = \beta_{acc}\frac{\sqrt{V^2 - V_{l2}^2}}{V_{l2}}, h_3 = \beta_{acc}\frac{\sqrt{V^2 - V_{l3}^2}}{V_{l3}}. \tag{3.8}$$

The characteristic determinant for finding the eigenvelocities is then given by

$$\begin{vmatrix} J_0(h_1a) & -J_0(h_2a) & -Y_0(h_2a) & 0 & 0 \\ -h_1J_1(h_1a) & h_2J_1(h_2a) & h_2Y_1(h_2a) & 0 & 0 \\ 0 & J_0(h_2a_1) & Y_0(h_2a_1 & -J_0(h_3a_1) & -Y_0(h_3a_1) \\ 0 & -h_2J_1(h_2a_1 & -h_2Y_1(h_2a_1 & h_3J_1(h_3a_1) & h_3Y_1(h_3a_1) \\ 0 & 0 & 0 & J_1(h_3b) & Y_1(h_3b) \end{vmatrix} = 0.$$

These modes are similar to the corresponding modes in the ringless case. Also, in the guided case and hence we will not plot them here.

3.3.3 Acoustic anti-guiding fiber

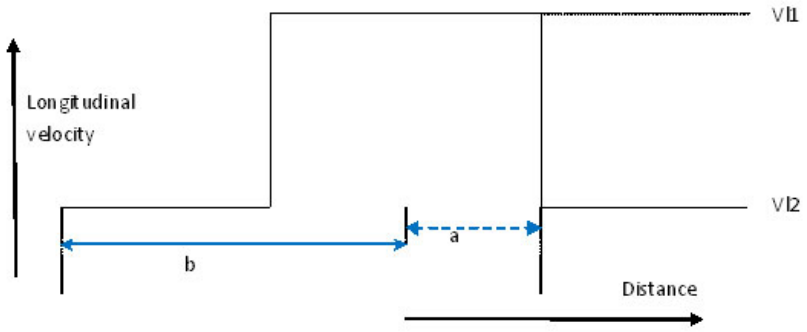

Figure 3.15: Acoustic anti guiding velocity profile

The acoustic anti-guiding fiber has the velocity profile shown in figure 3.15. We choose fiber 727 for illustration of this case. (figure 3.16 for the index profile and 3.23 for the optical mode-profile).

Radiation modes

These modes have effective velocity that satisfies, $V_{l2} < V_{eff} < V_{l1}$

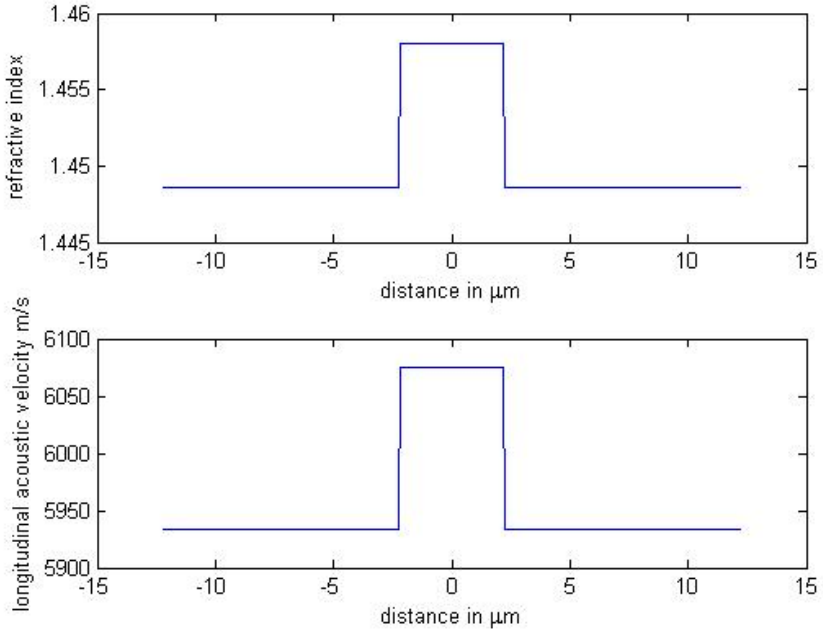

Figure 3.16: Fiber 727 index profile

The wavefunction is given by

$$\phi(r) = \begin{cases} AI_0(\tilde{h}_2 r) & 0 \leq r \leq a, \\ BJ_0(h_2 r) + CY_0(h_2 r) & a < r \leq b, \end{cases}$$

where the constants are defined as

$$\tilde{h}_1 = \beta_{acc}\frac{\sqrt{V_{l1}^2 - V^2}}{V_{l1}}, h_2 = \beta_{acc}\frac{\sqrt{V^2 - V_{l2}^2}}{V_{l2}}.$$

The characteristic determinant for finding the eigenvelocities is then given by

$$\begin{vmatrix} I_0(\tilde{h}_1 a) & -J_0(h_2 a) & -Y_0(h_2 a) \\ \tilde{h}_1 I_1(\tilde{h}_1 a) & h_2 J_1(h_2 a) & h_2 Y_1(h_2 a) \\ 0 & -J_1(h_2 b) & -Y_1(h_2 b) \end{vmatrix} = 0.$$

The characteristic function for determining the eigenvelocities of the radiation modes is shown in figure 3.17. We then plot the first few modeshapes for the radiation modes in figure 3.18.

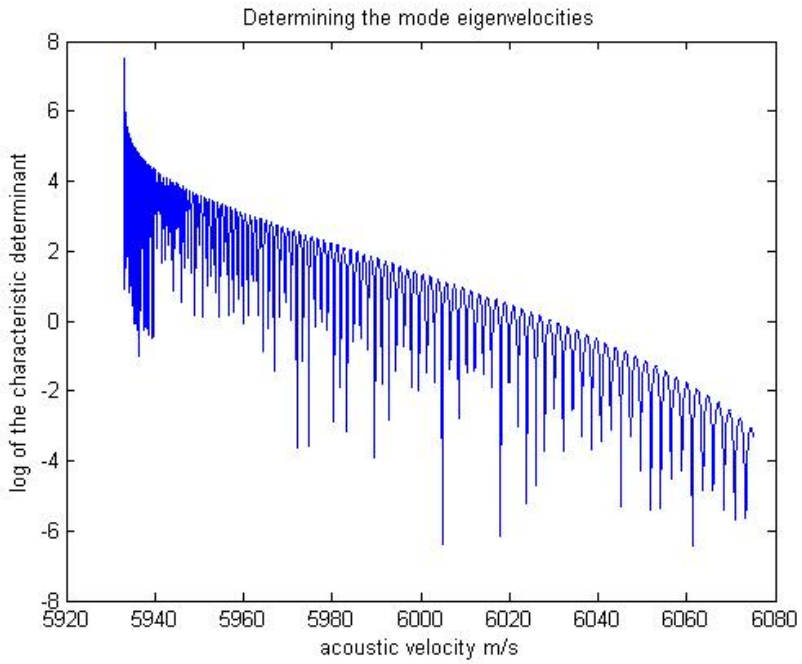

Figure 3.17: Determining the eigenvelocities of the radiating modes.

Bulk modes

The equations are similar to the case for guided fibers. We plot the characteristic determinant in figure 3.19 and typical modeshape of the bulk modes in figure 3.20

3.3.4 Acoustic anti-guiding fiber with acoustic guiding ring

The acoustic anti-guiding fiber with the addition of a guiding ring has the velocity profile shown in figure 3.21 . We choose fiber 727 for illustration of this case. (figure 3.22 for the index profile and 3.23 for the optical mode-profile).

Ring guided and bulk guided modes

The equations are very similar to the cases previously discussed and will not be reproduced. However, since the cladding modes are significant because of their contribution to the Brillouin gain, we plot the characteristic determinant in figure 3.24 and the modeshape in figure 3.25).

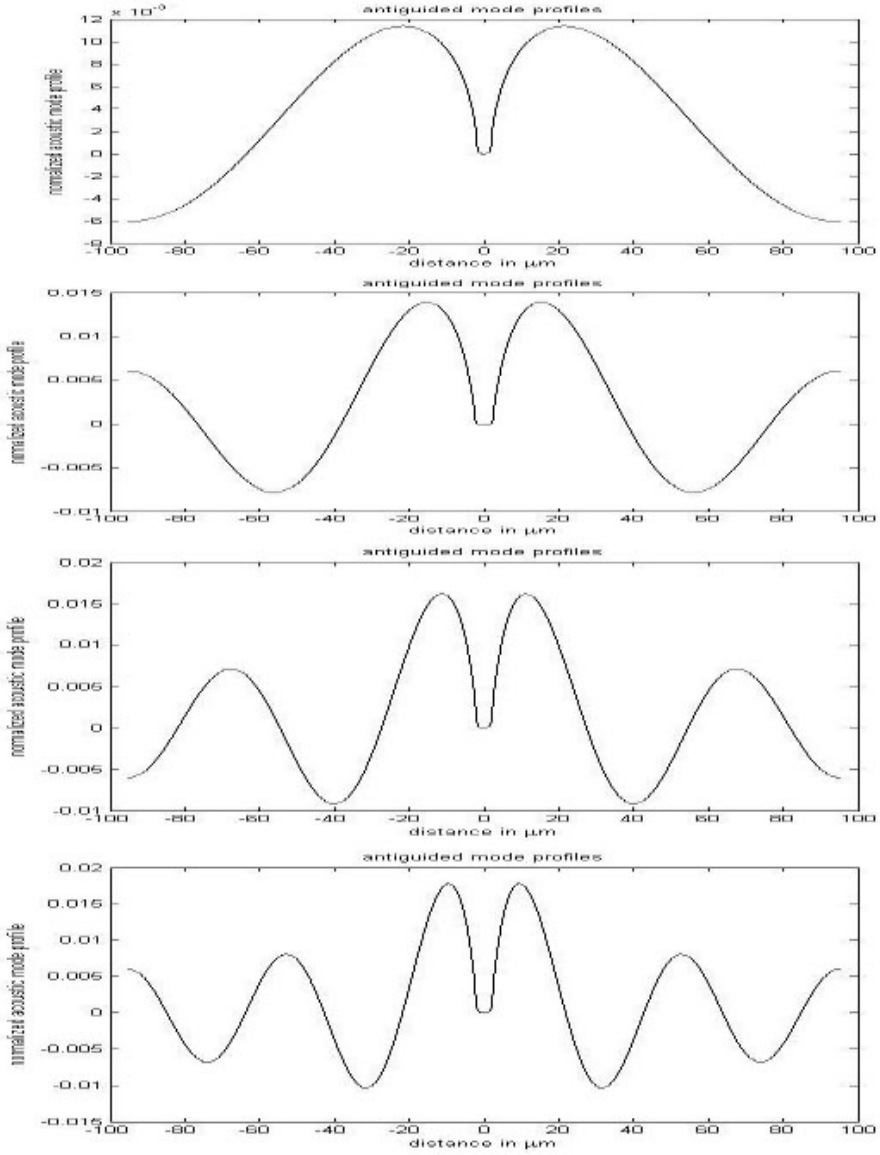

Figure 3.18: Radiation modes of the anti-guiding fiber.

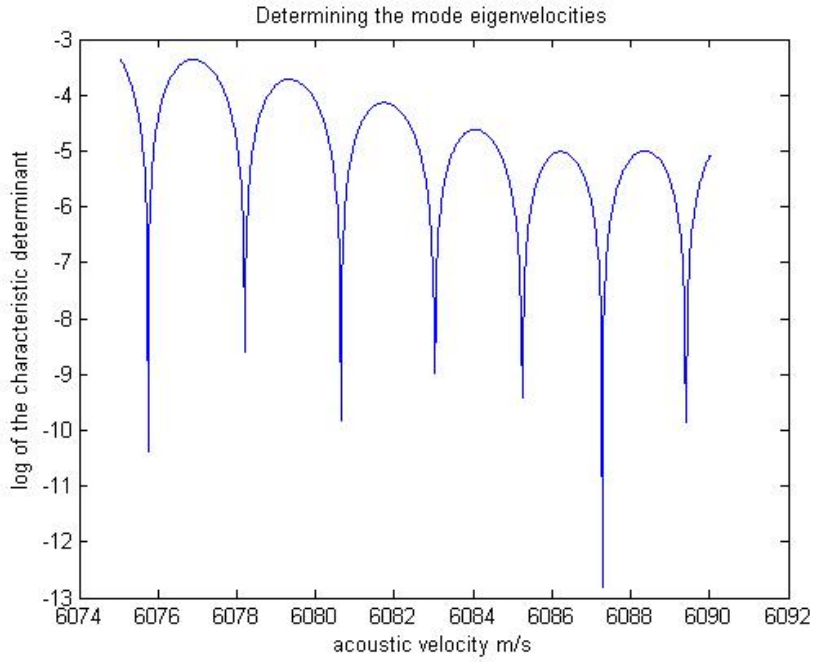

Figure 3.19: Determining the eigenvelocities of the bulk modes.

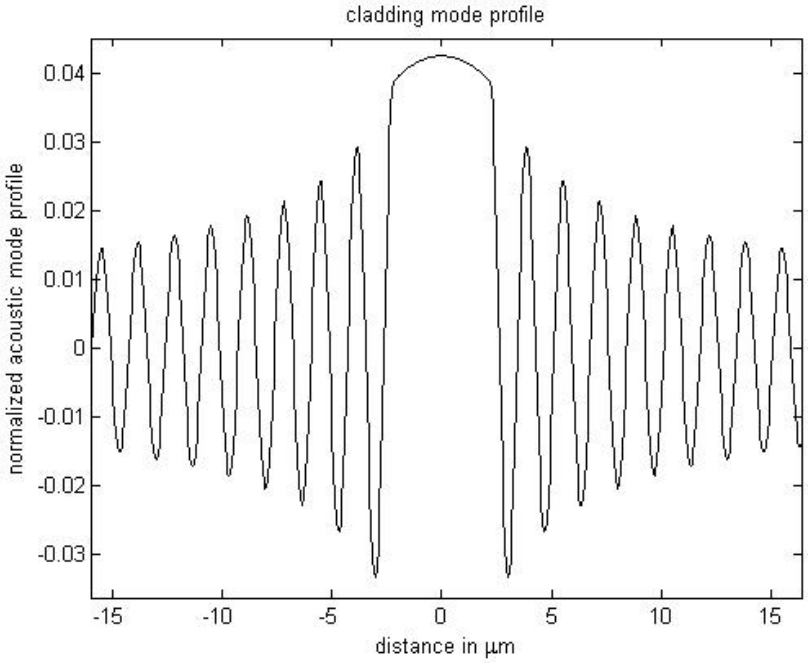

Figure 3.20: Typical modeshape of the bulk modes for the antiguiding fiber.

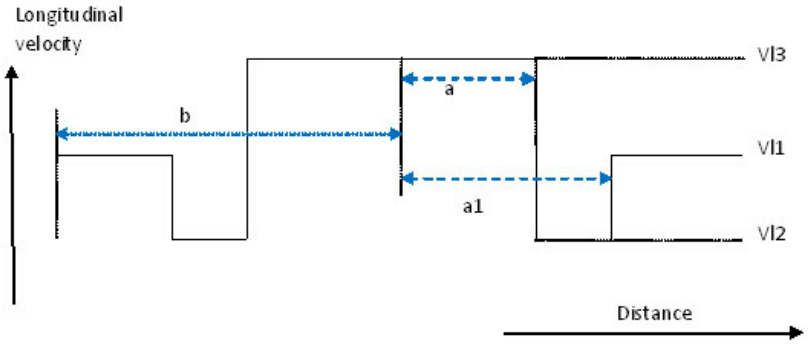

Figure 3.21: Acoustic anti-guiding with ring

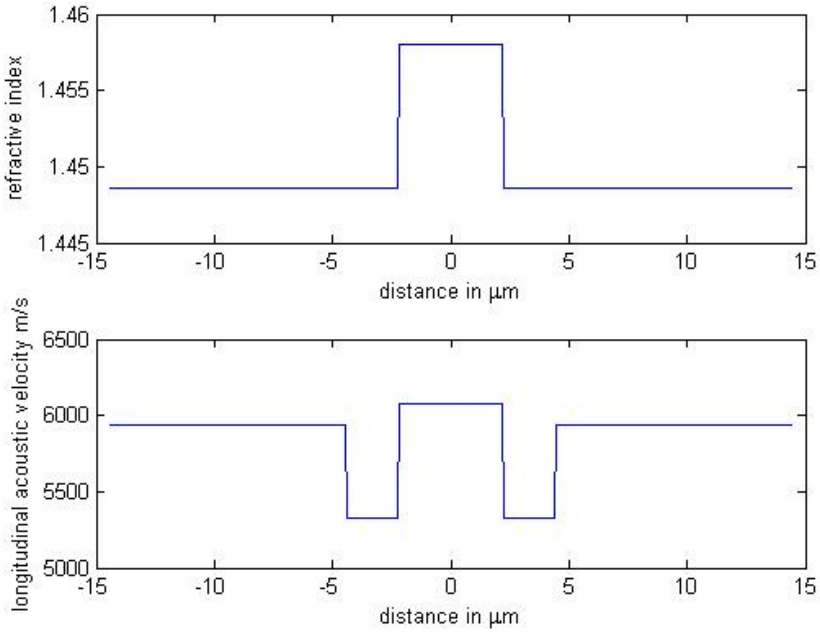

Figure 3.22: Index profile for fiber 727 with ring.

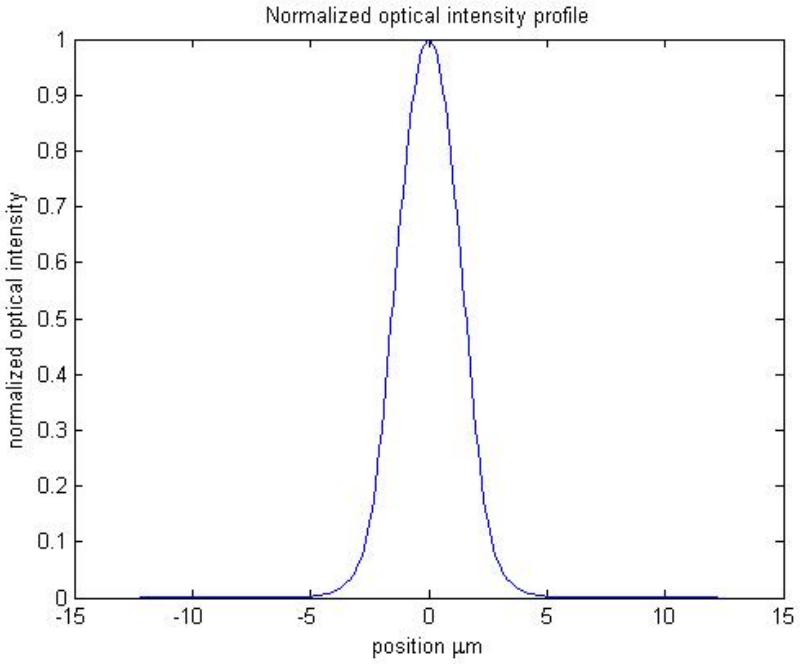

Figure 3.23: Optical mode profile for fiber 727

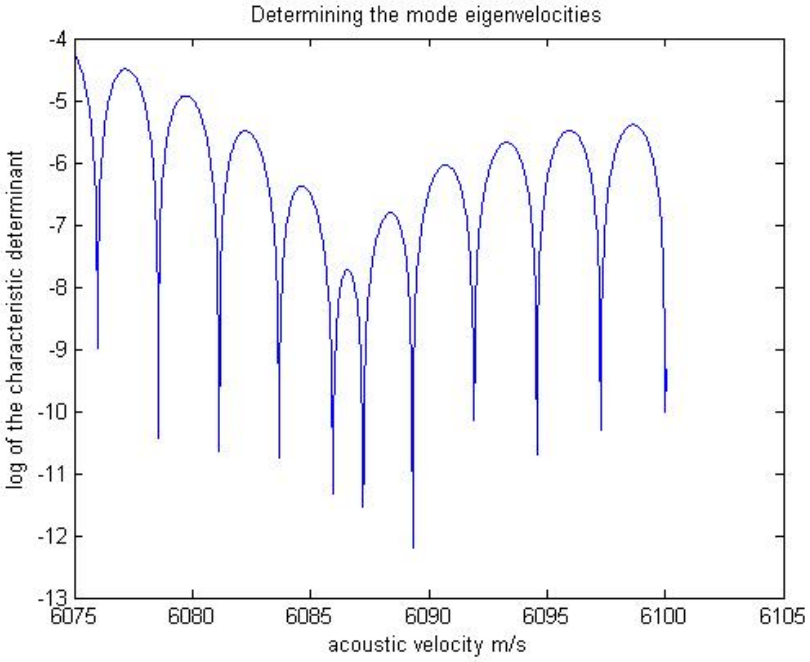

Figure 3.24: Determining eigenvelocities of the primary bulk guided modes.

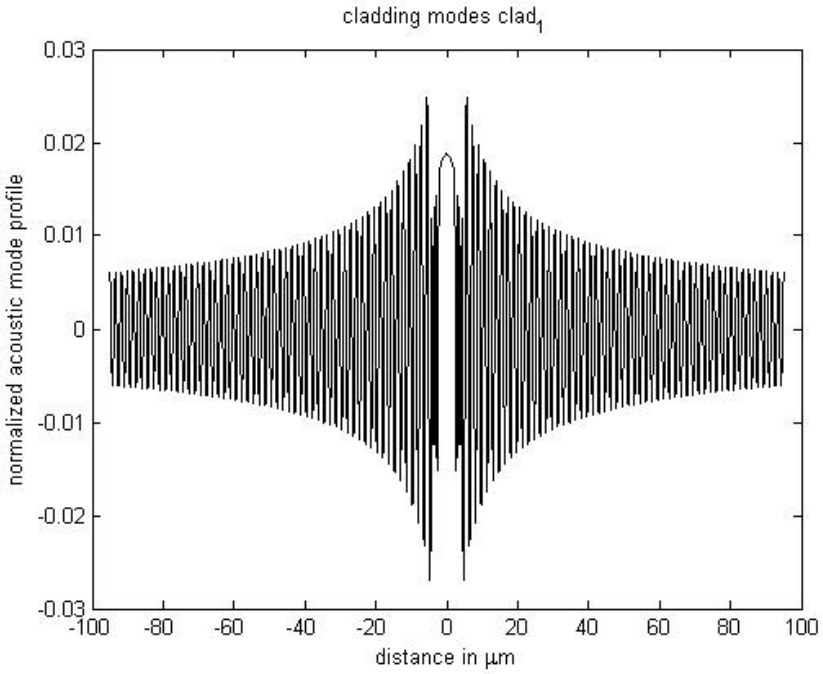

Figure 3.25: First bulk mode for fiber 727 with ring.

Modes guided in the cladding

These modes have effective velocity that satisfies, $V_{l3} < V_{l2} < V_{eff} < V_{l1}$.

The wavefunction is given by,

$$\phi(r) = \begin{cases} AI_0(\tilde{h}_1 r) & 0 \leq r \leq a, \\ BJ_0(h_2 r) + CY_0(h_2 r) & a < r \leq a1, \\ DJ_0(h_2 r) + EY_0(h_2 r) & a1 < r \leq b, \end{cases}$$

where the constants are defined as

$$\tilde{h}_1 = \beta_{acc}\frac{\sqrt{V_{l1}^2 - V^2}}{V_{l1}}, h_2 = \beta_{acc}\frac{\sqrt{V^2 - V_{l2}^2}}{V_{l2}}, h_3 = \beta_{acc}\frac{\sqrt{V^2 - V_{l3}^2}}{V_{l3}}. \tag{3.9}$$

The characteristic determinant for finding the eigenvelocities is then given by

$$\begin{vmatrix} I_0(\tilde{h}_1 a) & -J_0(h_2 a) & -Y_0(h_2 a) & 0 & 0 \\ +\tilde{h}_1 J_1(\tilde{h}_1 a) & h_2 J_1(h_2 a) & h_2 Y_1(h_2 a) & 0 & 0 \\ 0 & J_0(h_2 a_1) & Y_0(h_2 a_1 & -J_0(h_3 a_1) & -Y_0(h_3 a_1) \\ 0 & -h_2 J_1(h_2 a_1 & -h_2 Y_1(h_2 a_1 & h_3 J_1(h_3 a_1) & h_3 Y_1(h_3 a_1) \\ 0 & 0 & 0 & J_1(h_3 b) & Y_1(h_3 b) \end{vmatrix} = 0.$$

The plot of characteristic determinant is given in figure 3.26 and a typical mode-shape for these modes is given in figure 3.27

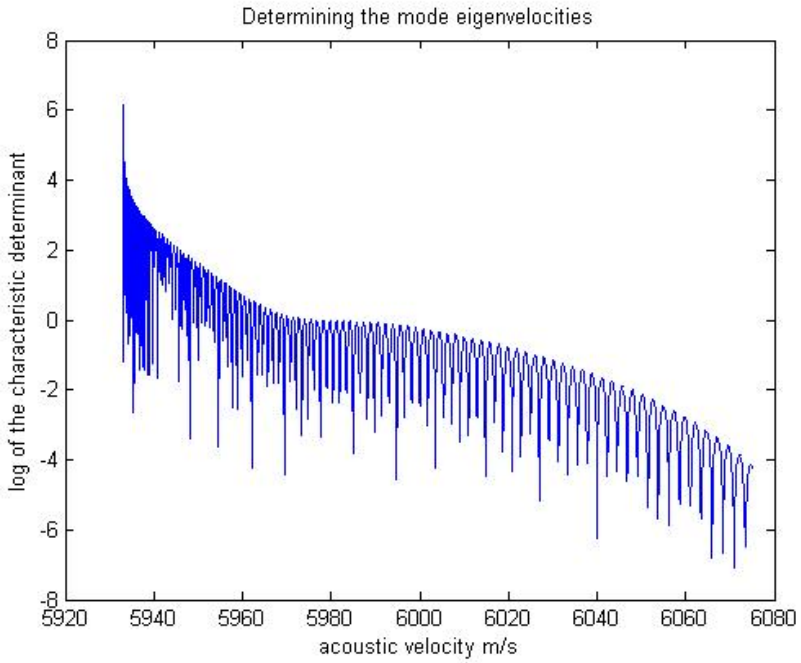

Figure 3.26: Determining the radiation mode eigenvelocities.

3.3.5 Acoustic anti-guiding Ramp profile

The step like boundaries we have chosen for the acoustic index profiles are an idealization. Due to dopant diffusion effects we would expect to have a profile more like the one shown in figure 3.28. We discuss the solution of acoustic modes in a generalized profile of this form. The solution proceeds by breaking the generalized

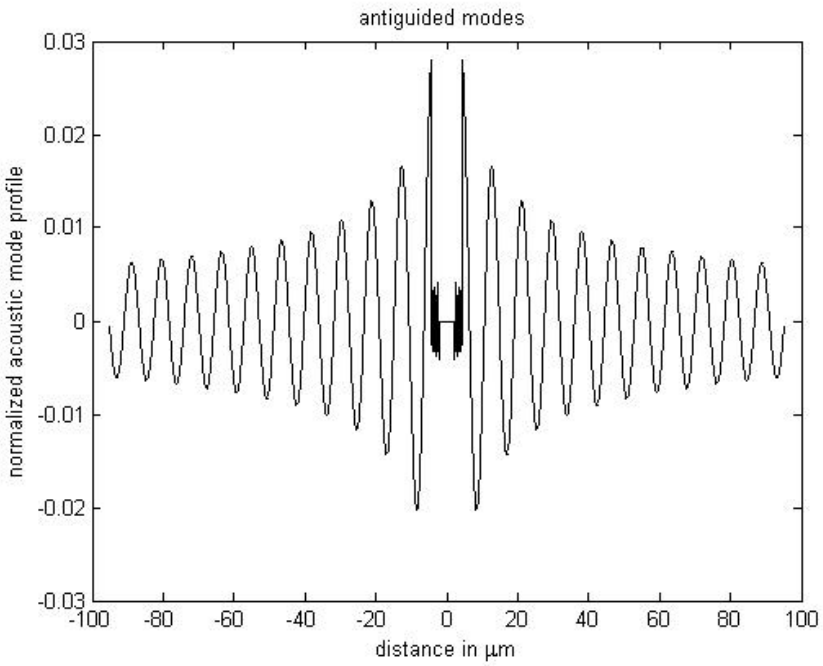

Figure 3.27: Typical modeshape for a radiation mode of fiber 727 with ring.

profile into strips of constant acoustic velocity. As an example we have written a program that breaks the generalized profile into five layers. This approach is more general and thus any profile can be broken down into strips depending on the desired accuracy of the Brillouin spectrum.

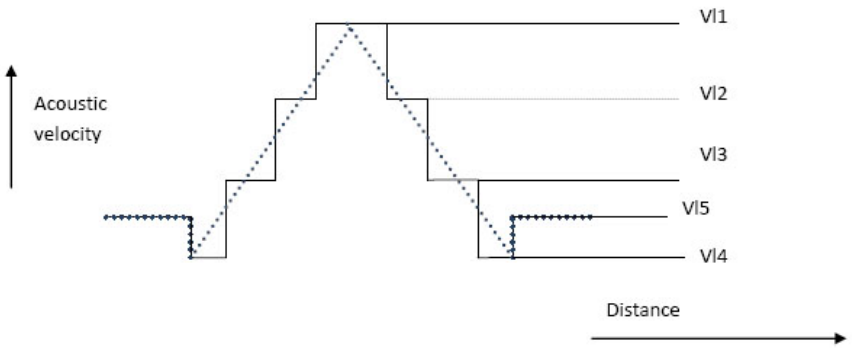

Figure 3.28: Generalized anti-guiding ring profile or the ramp profile and its 5 layer approximation.

We discuss now the procedure for solving the acoustic modes in the five layer structure. The ordering of velocities is given by $V_{l1} > V_{l2} > V_{l3} > V_{l5} > V_{l4}$. The

structure thus supports

- ring guided modes that satisfy $V_{l1} > V_{l2} > V_{l3} > V_{l5} > V_{eff} > V_{l4}$
- Radiation modes that satisfy $V_{l1} > V_{eff} > V_{l5}$
- Bulk guided modes that satisfy $V_{eff} > V_{l1}$.

The procedure for finding the eigenvelocities is similar to the cases already discussed. Suffice it to say that we are now looking at larger determinants that involve matching the wavefunction and its derivative at each of the layer boundaries.

3.4 Procedure for simulating spontaneous Brillouin spectrum

The procedure for obtaining the Brillouin gain spectrum is similar to that in reference [54], where we solve for the acoustic modes, obtain the Brillouin gain for each mode and then stitch a spectrum by assuming a lorentzian lineshape. As in reference [29], we can thus express this as

$$S(\nu) = \sum_{i=0}^{N} g_B \frac{A_{eff}}{A_{ao}^i} L(\nu) \tag{3.10}$$

where $S(\nu)$ denotes the spectrum computed over all the N acoustic modes, g_B is the Brillouin gain coefficient of the medium and w is the FWHM of the spectrum, $L(\nu)$ denotes the lorentzian lineshape

$$L(\nu) = \frac{(w/2)^2}{(\nu - \nu_B)^2 + (w/2)^2}, \tag{3.11}$$

where ν_B is the eigenfrequency of the particular acoustic mode. It is related to the mode eigenvelocity through

$$\nu_B = \frac{V_A^m 2 n_{eff}}{\lambda_0}. \tag{3.12}$$

We also define the acousto-optic mode area [29] as

$$A_m^{ao} = \left[\frac{\langle f^2(r)\rangle}{\zeta_m(r) f^2(r)}\right]^2 \left\langle \zeta_m^2(r)\right\rangle, \tag{3.13}$$

where f stands for the optical field and ζ denotes the acoustical field. The acoustical field is thus normalized by calculating acoustical power through $\langle\zeta_m^2(r)\rangle$. The triangle braces denote integration over the cross sectional plane.

3.5 Results and Discussion

The numerical procedure above was validated against the results shown in [54].

3.5.1 Acoustic guiding fiber(fiber 548)

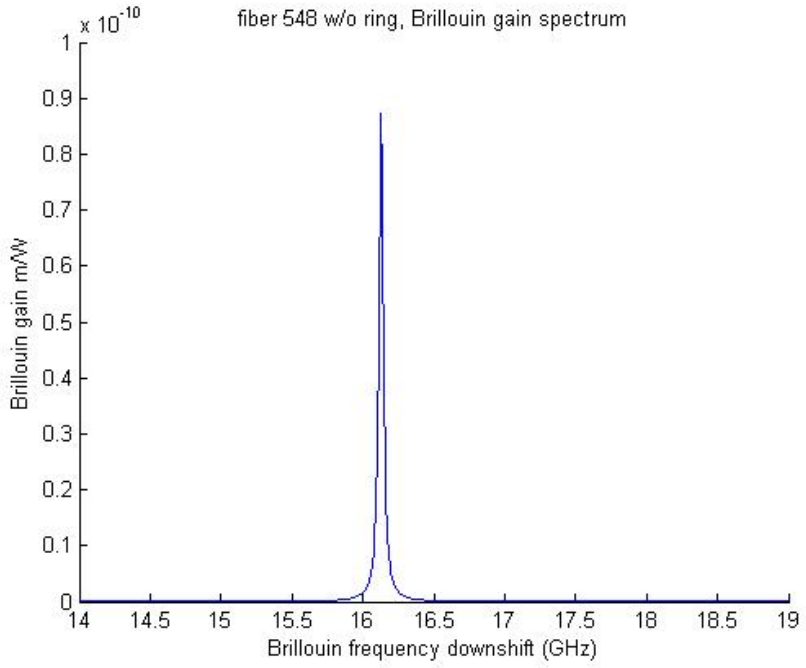

Figure 3.29: Brillouin gain spectrum of fiber 548 without ring.

The Brillouin gain spectrum is seen to consist of only one peak and the contribution is from the guided modes. The reason becomes clear when we plot the modeshapes of the guided and the cladding modes in figure 3.29. For the guiding

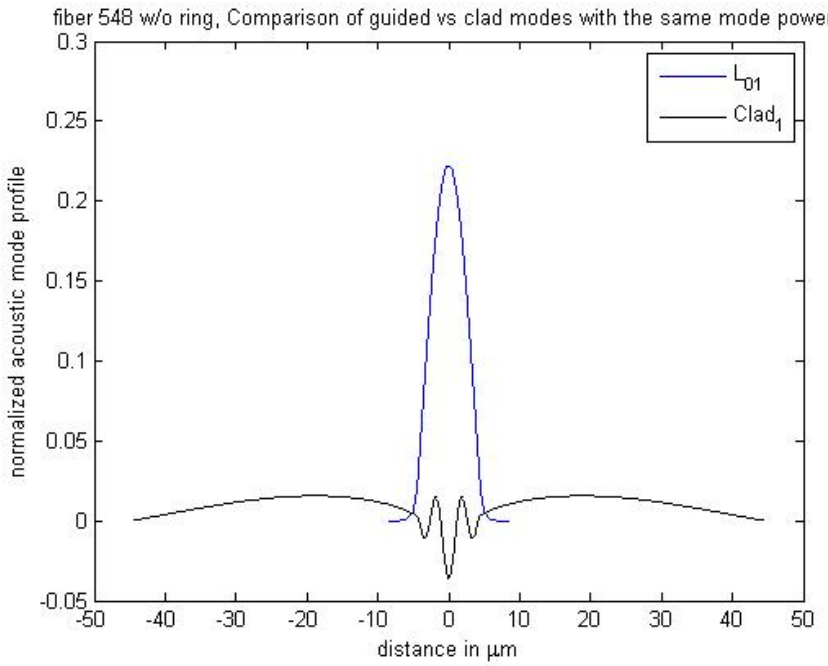

Figure 3.30: Comparison of guided and cladding modes of equal power.

fiber, we thus need to sum the contributions of the guided modes for calculating the threshold. Such a procedure has been performed in [29].

We then simulated the guiding fiber with a ring to see if any significant suppression can be obtained. Since we know that the contribution comes from the guided mode, we predict not to obtain much suppression in the peak gain. This can be clearly seen in the plotted spectrum of figure 3.31. The modeshapes of different kinds of modes are plotted in figure 3.32 and they further support our reasoning. We thus conclude that an acoustic ring layer is unsuitable for SBS suppression in an acoustic guiding fiber.

3.5.2 Case 2: Acoustic anti-guiding fiber 727

The Brillouin gain spectrum (figure 3.33) is seen to consist of two distinct peaks, one determined by the radiation modes and the other by the cladding modes. However, it is seen that the cladding modes have a larger contribution (see figure 3.34 for

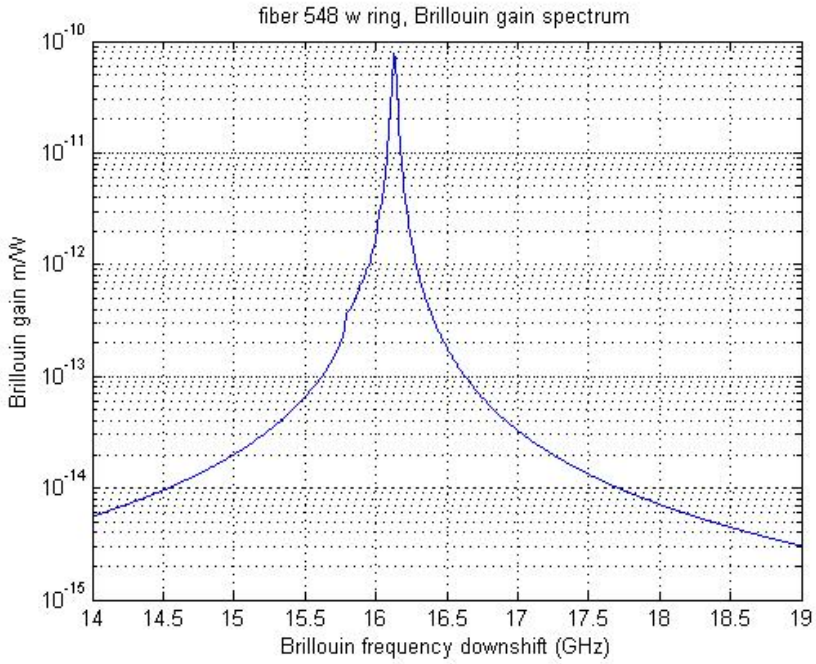

Figure 3.31: Brillouin gain spectrum for 548 with added ring.

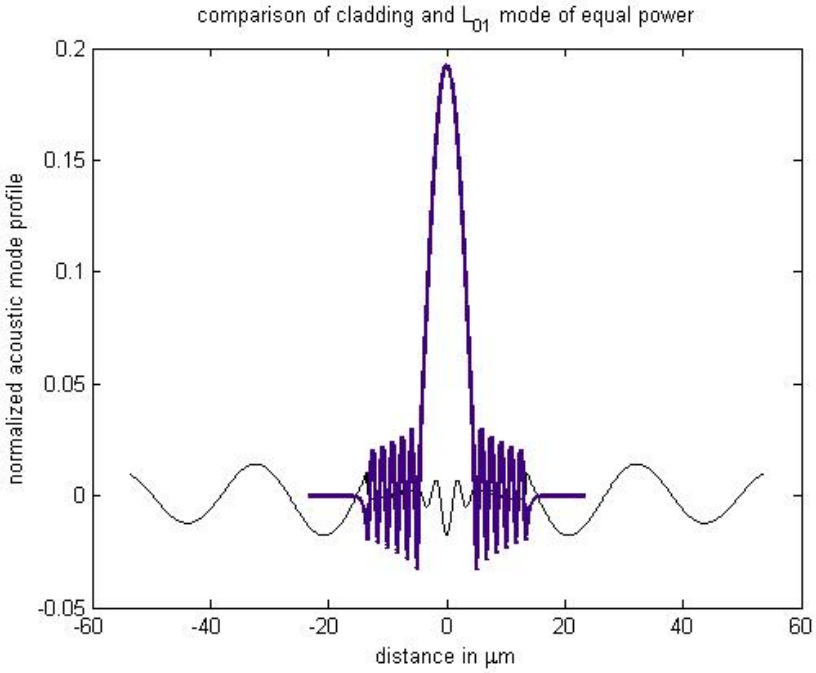

Figure 3.32: Comparison of modeshapes for different modes for 548 with ring.

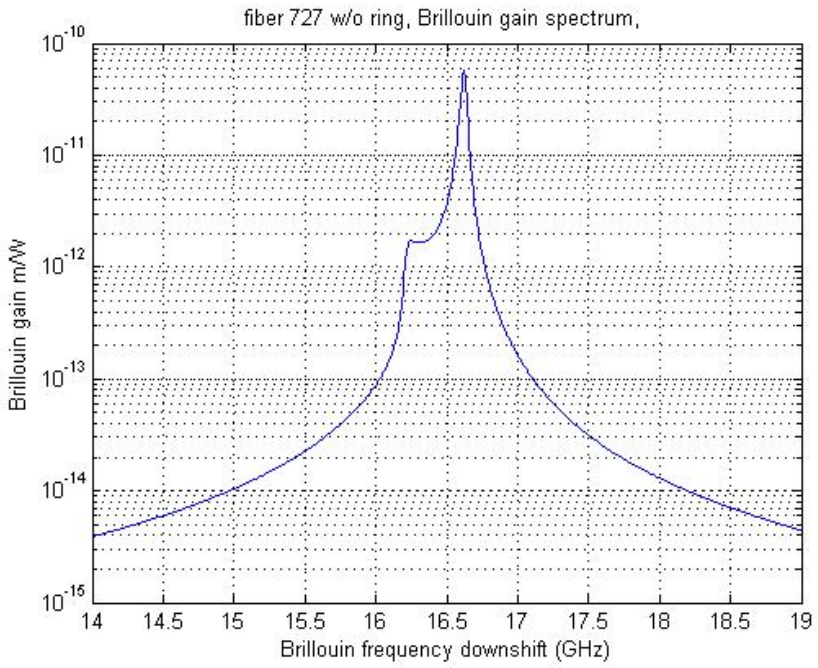

Figure 3.33: Brillouin gain spectrum for 727 without ring.

comparing modeshapes) and the threshold will thus be determined by the cladding or the bulk modes. Also the contribution to the peak was determined to be primarily due to the first few cladding modes.

The addition of a ring is seen to significantly alter the Brillouin gain spectrum by reducing the impact of the bulk modes but in addition imposing several new peaks contributed by the ring guided modes. The ring modes however do not contribute as much as the bulk modes and thus their effect on the threshold is not significant. For the case of a 2.2 micron wide ring suppression in SBS gain of close to 7 dB is shown.

We investigate the effect of scaling the ring size and find that a ring of 2.2 micron is the most optimal. In practice, the optimal ring size will depend on several factors including the effect of dopants on the Brillouin gain coefficient, the phonon decay lifetime and the diffusion effects.

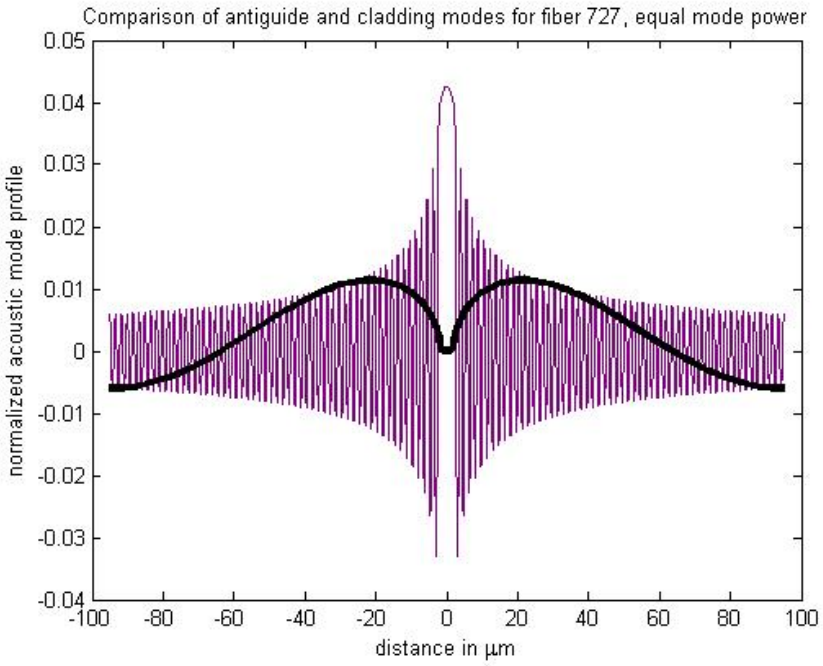

Figure 3.34: Comparison of modeshapes for different modes for 727 without ring.

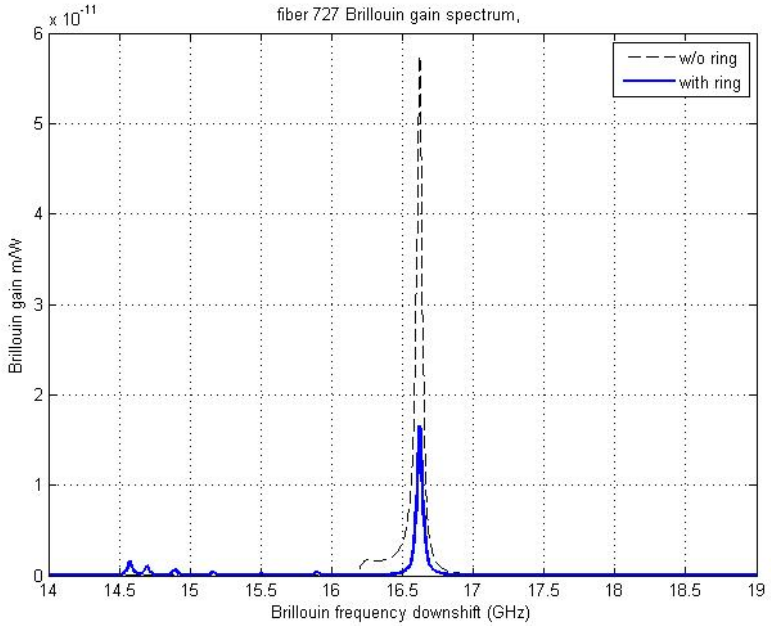

Figure 3.35: Brillouin gain spectrum for 727 with ring.

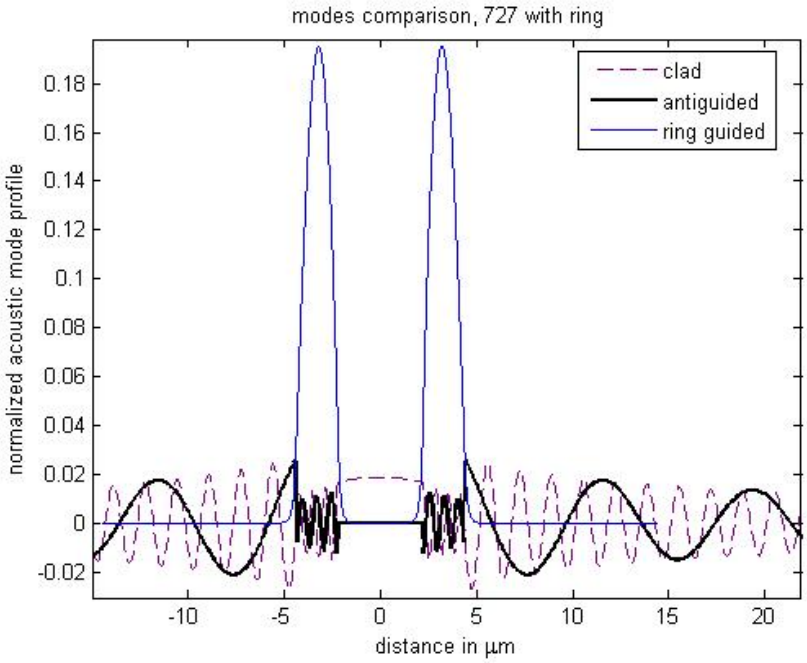

Figure 3.36: Comparison of modeshapes for different modes for 727 with ring.

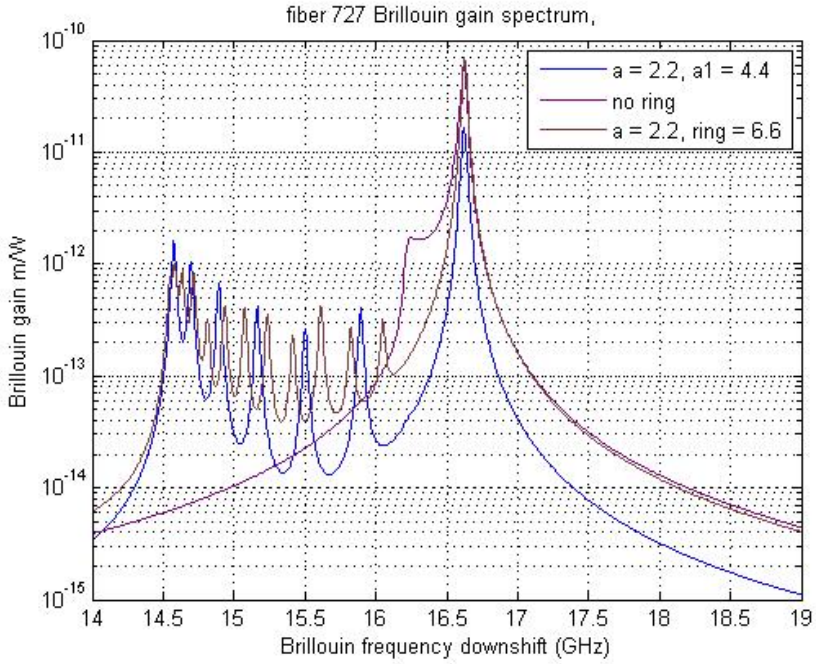

Figure 3.37: Effect of ring size scaling

Because the ring primarily alters the modeshapes outside the core, we expect the effectiveness of the ring method to drop down with scaling in the core size. We observe this effect in figure 3.37.

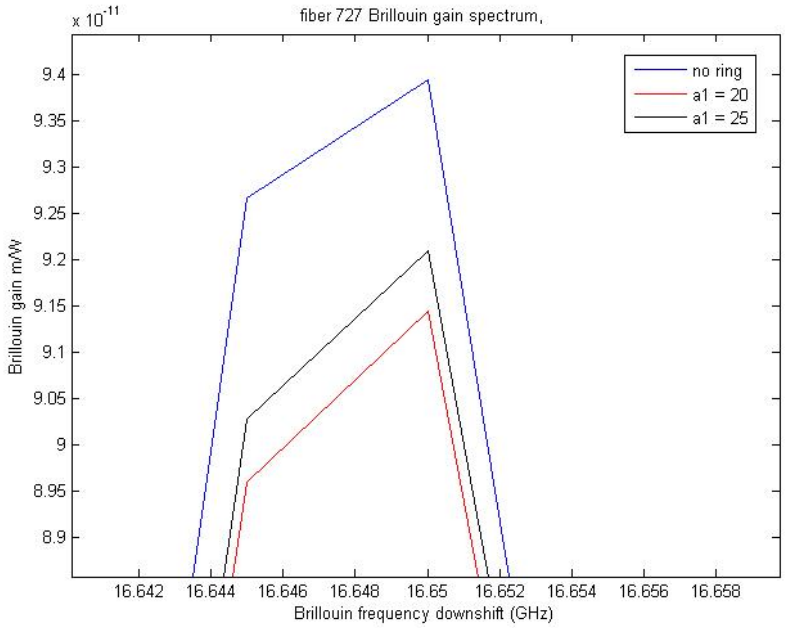

Figure 3.38: Gain spectrum for 33 micron core size.

To this effect we next investigate the Ramp profile. The ramp profile (see figure 3.39 aims to alter the overlap mainly in the core area.

The ramp profile is compared with a guiding type fiber. We plot the spectrum in figure 3.40 and see about 7 dB suppression.

We also investigated the effect of core size scaling on this particular design and find the corresponding drop in effectiveness when we scale to a 50 micron core size. (see figure 3.41)

3.6 Conclusions

A chief advantage of our waveguide is that SBS suppression can be achieved independently of the optical mode. An additional advantage is that SBS suppression

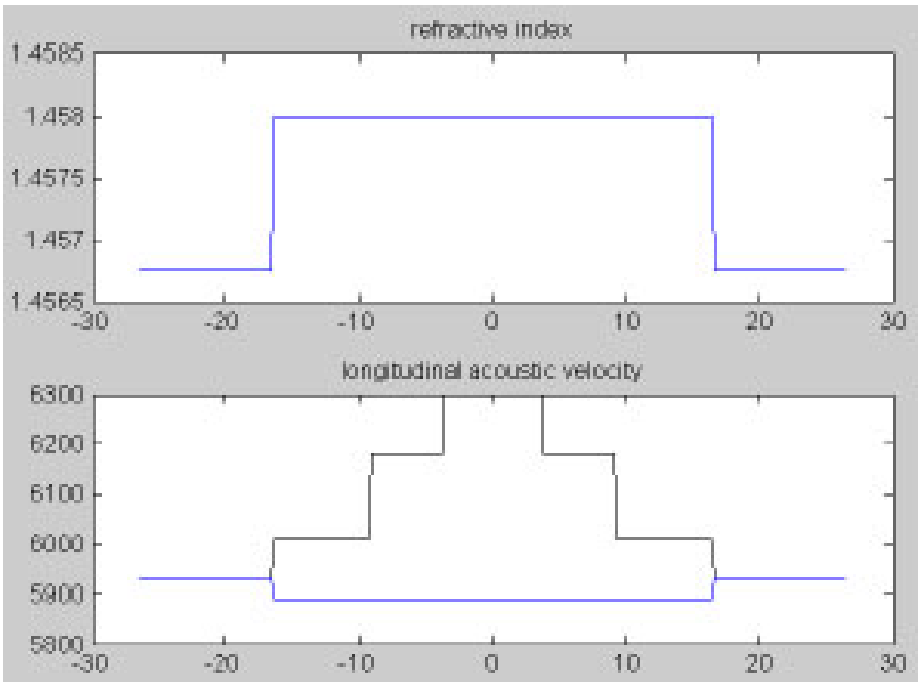

Figure 3.39: Ramp profile design for 33 micron core

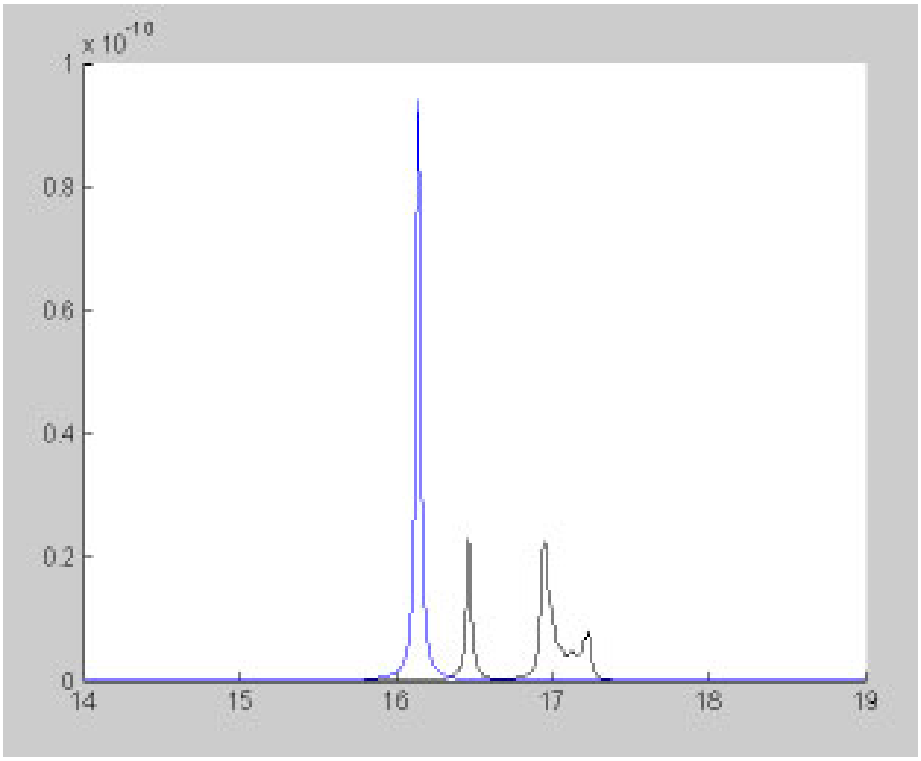

Figure 3.40: Gain spectrum for 33 micron core size.

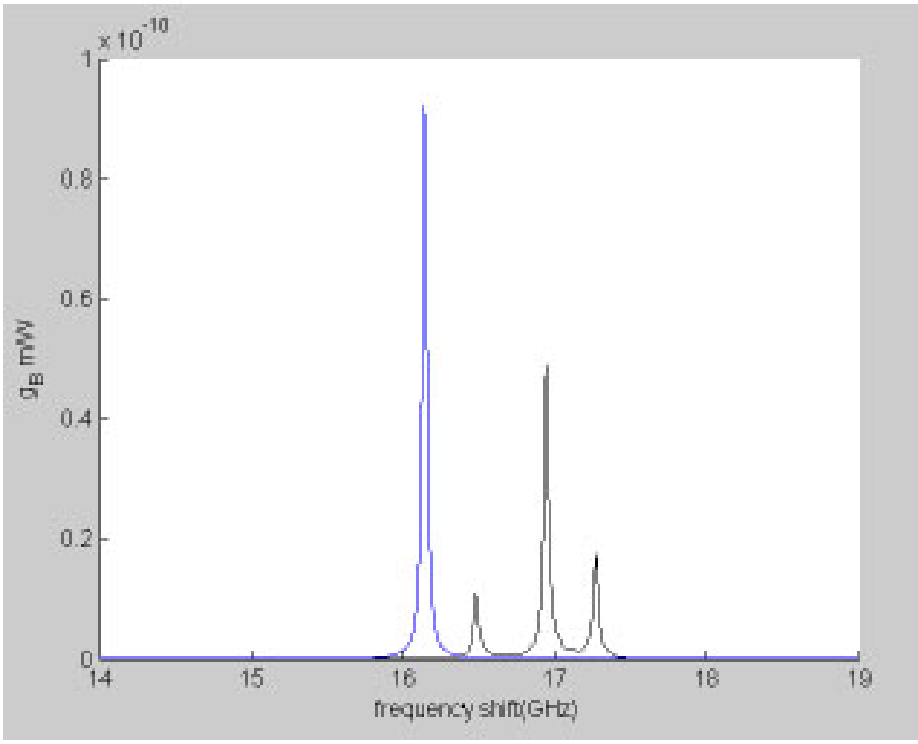

Figure 3.41: Gain spectrum for 50 micron core size.

is length-independent, and thus the technology can be applied to LMA laser fibers. However, we find that there is an inherent scaling issue with respect to core size. Further work in this area should be focused on other structures that particularly target the bulk modes.

CHAPTER 4

Analysis of Stimulated Brillouin scattering in a one-dimensional phononic bandgap structure

4.1 Introduction

Recently photonic/phononic crystal fiber structures have been proposed that can achieve simultaneous photonic-gap guidance of optical waves and phononic-bandgap inhibition of acoustic wave propagation, in which SBS effects can be mitigated (see [31]) without detrimentally affecting optical pump wave. The elastic bandgap in these hybrid bandgap fibers arises through a carefully engineered core nanostructure. These structures can be employed for both electro-optic modulation and SBS inhibition. Experimental work has been conducted on these structures to characterize their response (see [55]). They show a suppression of 6 dB (see [30]). However, it is unclear as to how sensitive the threshold suppression will be to manufacturing defects and their scalability with core size.

Another recently discussed method is the incorporation of a fiber optical grating that presents a stop band for the Stokes wave (see [33]). The grating enhances threshold by inhibiting the buildup of the Stokes wave. The authors are careful to mention the manufacturing defects of the grating and present suitable arguments to circumvent this issue. However, in silica fibers, the SBS induced Stokes wave is downshifted from the pump by only 13 GHz. This makes it very difficult to design

a grating that can suppress the Stokes wave and leave the pump unaffected. We believe that this is a major limitation of the above scheme.

We propose instead the incorporation of an elastic grating. Since the wavelength of the elastic waves is about twice that of the pump and the stokes, any residual optical grating created by the elastic grating will be far detuned from the pump and hence has negligible effect on pump propagation. This method preserves the simplicity and the easy core-size scalability of the approach in reference [33] relative to the hybrid nanostructure approach [31], while getting around problem of designing a grating with stringent cutoff requirements.

In this chapter, we show that the enhancement in Brillouin threshold obtainable in such a structure can be expressed in terms of the Brillouin gain spectrum characteristics and the modulation depth of the designed grating. The chapter is organized as follows, in section II, we discuss the theory and derive the threshold enhancement in the case of no-pump depletion approximation. In section III, we numerically integrate the equations relaxing the pump depletion approximation.

4.2 Theory of SBS in a 1D elastic grating

During SBS, the incident pump wave (wavelength λ_p) scatters from a forward traveling acoustic wave and excites a Stokes wave propagating in the backward direction. The Stokes and the pump can then amplify the forward traveling acoustic wave through electrostriction. A rigorous treatment of SBS would involve employing equations of linear elasticity to model the material displacement vector waves (see ref[15] in [29]). But in an optic fiber, the acoustic wave is predominantly longitudinal and hence we can neglect its transverse components (see refs. [14,16] in [29]).

This simplification leads us to adopt a scalar approximation to the equation de-

scribing the acousto-optic interaction in fiber structure with a longitudinal variation in elastic properties. We note that the scalar approximation is not valid for analysis of SBS in the more complicated photonic/Phononic crystal fiber where the full generality has to be taken into account.

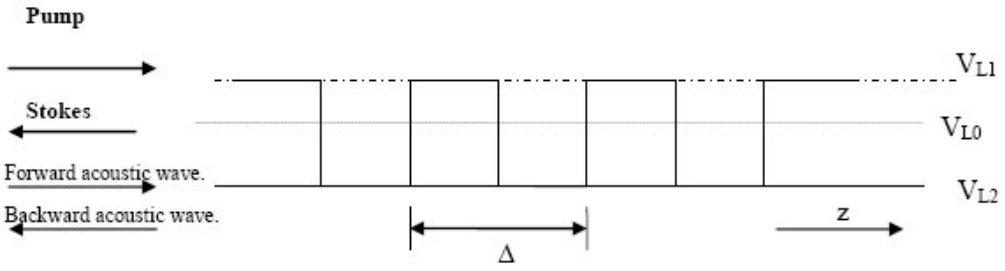

Figure 4.1: Schematic of the elastic grating structure being analyzed.

Figure 4.1 shows the schematic for our analysis. The elastic grating is shown to induce a square wave like variation of the longitudinal acoustic velocity, with a period Δ, along the direction of wave propagation z. By conservation of energy and momentum we have

$$\omega_A = \omega_P - \omega_S, k_A = k_P + k_S, \tag{4.1}$$

where the subscript A denotes the acoustic wave. Using $k_p \approx k_s = 2\pi/\lambda_p$, we get $k_A = 2k_p$. To ensure that the grating creates a stop band of interest, we choose $\Delta \approx \lambda_A/2 = \lambda_p/4$.

The equation for acousto-optic interaction [29] is given by

$$\frac{\partial^2 \rho}{\partial t^2} - \Gamma \frac{\partial^2}{\partial z^2}\frac{\partial \rho}{\partial t} - V_l^2(z)\frac{\partial^2 \rho}{\partial z^2} = -\frac{\gamma}{2}\nabla^2 \mathbf{E}^2, \tag{4.2}$$

where ρ is the amplitude of the pressure field variations around the mean value ρ_0, $\mathbf{E}$ is the amplitude of the electric field. Γ and γ are the damping factor for acoustic phonons and the electrostrictive constant in the material respectively. $V_l^2(z)$ is the squared longitudinal acoustic velocity along the fiber (as shown in figure 4.1) and

can be expressed in terms of a Fourier series. We drop the higher order terms for simplicity and finally get

$$V_l^2(z) = V_{l0}^2 \pm \frac{\iota \Delta V_l^2}{\pi} exp(\mp \iota \frac{2\pi}{\Delta} z) V_{l0}^2 = \frac{V_{l1}^2 + V_{l2}^2}{2} \Delta V_l^2 = V_{l1}^2 - V_{l2}^2, \tag{4.3}$$

Assuming a polarization preserving fiber, the electric field can be expressed as a sum of forward traveling pump and backward traveling Stokes waves

$$E(z,t) = \frac{1}{2} E_p exp(\iota(\omega_p t - \beta_p z)) + \frac{1}{2} E_s exp(\iota(\omega_s t + \beta_s z)) + c.c., \tag{4.4}$$

where, (E_p, E_s), (ω_p, ω_s) and (β_p, β_s) denote the amplitude, frequency and the wavevectors of pump and Stokes fields respectively and c.c. stands for the complex conjugate.

We can model the effect of the elastic grating by introducing a backward traveling acoustic wave in addition to the forward traveling electrostriction driven acoustic wave. The pressure field in equation 4.2 can be thus expressed as a sum of forward and backward traveling components as

$$\rho(z,t) = \frac{1}{2} \rho_f exp(\iota(\Omega t - qz)) + \frac{1}{2} \rho_b exp(\iota(\Omega t + qz)) + c.c.. \tag{4.5}$$

ρ_f , ρ_b are the amplitudes of the forward and the backward traveling acoustic waves. (Ω, q) denote the frequency and the wavevector of the acoustic waves respectively. We have $\Omega = \omega_p - \omega_s, q = \beta_p + \beta_s$

The electric field satisfies the wave equation

$$\nabla^2 E - \frac{\epsilon}{c^2} \frac{\partial^2 E}{\partial t^2} - \mu_0 \frac{\partial^2 P_{NL}}{\partial t^2}, \tag{4.6}$$

where ϵ_l is the linear part of the dielectric constant and P_{NL} is the nonlinear polarization induced by the forward traveling acoustic wave and is given by

$$\mathbf{P_{NL}} = \frac{\gamma}{\rho_\mathbf{0}} \rho \mathbf{E}, \tag{4.7}$$

where γ is the electrostrictive constant, ρ is the pressure variation around the mean value ρ_0 that couples with the electric field through electrostriction.

In solving for the evolution of the electric field amplitudes, we make the assumption, that the nonlinear polarization P_{NL} can be treated as a small perturbation, the optical field is quasi monochromatic and that the fiber is polarization maintaining. We neglect dispersion in the optical properties of the material as far as the pump and the Stokes fields are concerned. We substitute equations (4.4),(4.5) and (4.7) in (4.6), separate out terms with similar exponentials and impose the phase matching condition and obtain under the slowly varying envelope approximation

$$\begin{aligned} \frac{\partial E_p}{\partial z} + \frac{\alpha}{2}E_p + \frac{n}{c}\frac{\partial E_p}{\partial t} &= \frac{-\iota\omega\gamma\mu_0 c}{4\rho_0 n}\rho_f E_s \\ -\frac{\partial E_s}{\partial z} + \frac{\alpha}{2}E_p + \frac{n}{c}\frac{\partial E_s}{\partial t} &= \frac{-\iota\omega\gamma\mu_0 c}{4\rho_0 n}\rho_f^* E_p, \end{aligned} \tag{4.8}$$

where $\alpha_p \approx \alpha_s = \alpha$ and n are the loss coefficients and the refractive index for the pump and stokes waves, $\omega_p \approx \omega_s = \omega$ and p_{12} is the component of the electrostrictive tensor and is related to the electrostrictive coefficient γ by $\gamma = \dfrac{2n^5\omega\epsilon p_{12}}{cq}$

In the steady state limit, we thus express equation (4.8) as

$$\begin{aligned} \frac{\partial E_p}{\partial z} + \frac{\alpha}{2}E_p &= \frac{-\iota 2n^4\pi^2 p_{12}}{\lambda^2\rho_0 q}\rho_f E_s \\ -\frac{\partial E_s}{\partial z} + \frac{\alpha}{2}E_p &= \frac{-\iota 2n^4\pi^2 p_{12}}{\lambda^2\rho_0 q}\rho_f^* E_p. \end{aligned} \tag{4.9}$$

To obtain the evolution equations for the pressure waves, we write for the RHS of equation (4.2)

$$\nabla^2 E^2 \approx -\frac{1}{2}E_p E_s^* q^2 exp(\iota(\Omega t - qz)) + c.c. \tag{4.10}$$

Substituting equations (4.10) and (4.5) in equation (4.2) and applying the slowly varying approximation and grouping terms with similar exponentials we get

$$\begin{aligned} -\Omega^2\rho_f e^{-\iota qz} + \iota\Omega\Gamma q^2\rho_f e^{-\iota qz} - V_{lo}^2(-q^2\rho_f)e^{-\iota qz} \\ -V_{lo}^2(-2\iota q)\frac{\partial\rho_f}{\partial z}e^{-\iota qz} - q^2\frac{\Delta V_l^2}{\iota\pi}exp(\iota(2q-\frac{2\pi}{\Delta})z)\rho_b = -\frac{\gamma}{2}q^2E_pE_s^*. \\ -\Omega^2\rho_b e^{-\iota qz} + \iota\Omega\Gamma q^2\rho_b e^{-\iota qz} - V_{lo}^2(-q^2\rho_b)e^{-\iota qz} \\ -V_{lo}^2(+2\iota q)\frac{\partial\rho_b}{\partial z}e^{-\iota qz} - q^2\frac{\Delta V_l^2}{\iota\pi}exp(-\iota(2q-\frac{2\pi}{\Delta})z)\rho_b = 0. \end{aligned} \tag{4.11}$$

We can set the term $exp(i(2q-\frac{2\pi}{\Delta})z)$ to 1 by the phase matching condition and thus simplify to

$$\begin{aligned} \rho_f + \frac{2\iota qV_{lo}^2}{q^2V_{lo}^2-\Omega^2+\iota\Omega\Gamma q^2}\frac{\partial\rho_f}{\partial z} - \frac{q^2v_{lo}^2(\Delta V_l^2/V_{lo}^2)}{q^2V_{lo}^2-\Omega^2+\iota\Omega\Gamma q^2}\rho_b &= \frac{-\gamma q^2/2}{q^2V_{lo}^2-\Omega^2+\iota\Omega\Gamma q^2}E_pE_s^* \\ \rho_b - \frac{2\iota qV_{lo}^2}{q^2V_{lo}^2-\Omega^2+\iota\Omega\Gamma q^2}\frac{\partial\rho_b}{\partial z} + \frac{q^2v_{lo}^2(\Delta V_l^2/V_{lo}^2)}{q^2V_{lo}^2-\Omega^2+\iota\Omega\Gamma q^2}\rho_f &= 0. \end{aligned}$$

Let us define the Brillouin shift frequency (or the peak Brillouin frequency) $\Omega_B = 2\pi\nu_B$ and the FWHM of the gain spectrum around the peak frequency as $W_B = \Gamma q^2/2\pi$. We note that $\Omega_B = q^2V_{lo}^2$ and so at the peak gain frequency, equation (4.12) reduces to

$$\begin{aligned} \rho_f + \frac{V_{lo}}{\pi W_B}\frac{\partial\rho_f}{\partial z} + \frac{\nu_B}{\pi W_B}\frac{\Delta V_l^2}{V_{lo}^2}\rho_b = \frac{-\iota\gamma q^2}{8\pi^2\nu_B W_B}E_pE_s^* \\ \rho_b - \frac{V_{lo}}{\pi W_B}\frac{\partial\rho_f}{\partial z} - \frac{\nu_B}{\pi W_B}\frac{\Delta V_l^2}{V_{lo}^2}\rho_f = 0. \end{aligned} \tag{4.12}$$

The evolution equations derived so far will now be expressed in a normalized form, The electric field amplitudes are normalized with respect to the pump amplitude at the input as $A_p = E_p/E_p(0)$ and $A_s = E_s/E_p(0)$. The length is normalized to unity

so $z = z/L$. Let $I_0 = \frac{1}{2}c\epsilon n 2E_p E_p^*$ denote the input intensity and the Brillouin gain coefficient

$$g_B = \frac{4\pi^8 p_{12}^2}{\lambda_p^2 \rho_0 \nu_B W_B}.$$

We also define the parameters R and L_z as

$$\begin{aligned} L_z &= \frac{\nu_B}{\pi W_B} \\ R &= \frac{1}{\pi}\frac{\nu_B}{W_B}\frac{\Delta V_l^2}{V_{lo}^2}, \end{aligned}$$

where R denotes the degree of coupling achieved by the elastic grating at the peak acoustic frequency. It is related to the Brillouin gain spectrum characteristics and the modulation depth of the elastic grating. L_z signifies the length scale over which hypersonic phonons damp out in the material.

The pressure amplitudes are normalized so that the term $A_p A_s^*$ appears on the RHS of the evolution equation for equation (4.12). Thus the set of evolution equations for the wave amplitudes in the normalized form (similar to [56])

$$\begin{aligned} \frac{\partial A_p}{\partial z} &= -\frac{\alpha L}{2}A_p - \frac{g_B I_0 L}{2}\rho_f A_s \\ \frac{\partial A_s}{\partial z} &= +\frac{\alpha L}{2}A_s - \frac{g_B I_0 L}{2}\rho_f^* A_p \\ \rho_f + \frac{L_z}{L}\frac{\partial \rho_f}{\partial z} + R\rho_b &= A_p A_s * \\ \rho_f + \frac{L_z}{L}\frac{\partial \rho_f}{\partial z} + R\rho_b &= 0. \end{aligned} \tag{4.13}$$

In these equations Hypersonic phonons are damped out quickly over distances much smaller than those over which the source term on the right hand side of the pressure evolution equation varies significantly, hence we can drop the term containing $\frac{\partial \rho}{\partial z}$ in equation 4.13 similar to reference [14].

4.3 Results and discussion

For typical values in an optic fiber, $\nu_B = 11GHz$, $W_B = 12MHz$ and assuming an elastic grating created by doping with GeO_2 (.5% by weight, see [54]), $R = 2.1$. If $L_z/L << R$, ρ_f is approximately equal to $\frac{A_p A_s^*}{(1+R^2)}$. The equations (4.13) in that case are of a form very similar to the case without the presence of the grating. In the no - pump depletion approximation, the threshold power is then seen to scale by a factor of $1/(1 + R^2)$. We thus conclude that the threshold enhancement obtainable by the elastic grating can be related in a simple way to the parameter R by the factor $(1/1 + R^2)$. Using a fourth order Runge-Kutta method and boundary conditions similar to [56], the equations (13) are solved without the pump depletion approximation. In figure 4.2, we plot the variation of pump and Stokes intensity for a case (above threshold) with and without the presence of elastic grating. In figure 4.3, we plot the conversion efficiency (with and without grating). The effect of the grating in suppression can be seen to obey the $(1/1 + R^2)$ relation.

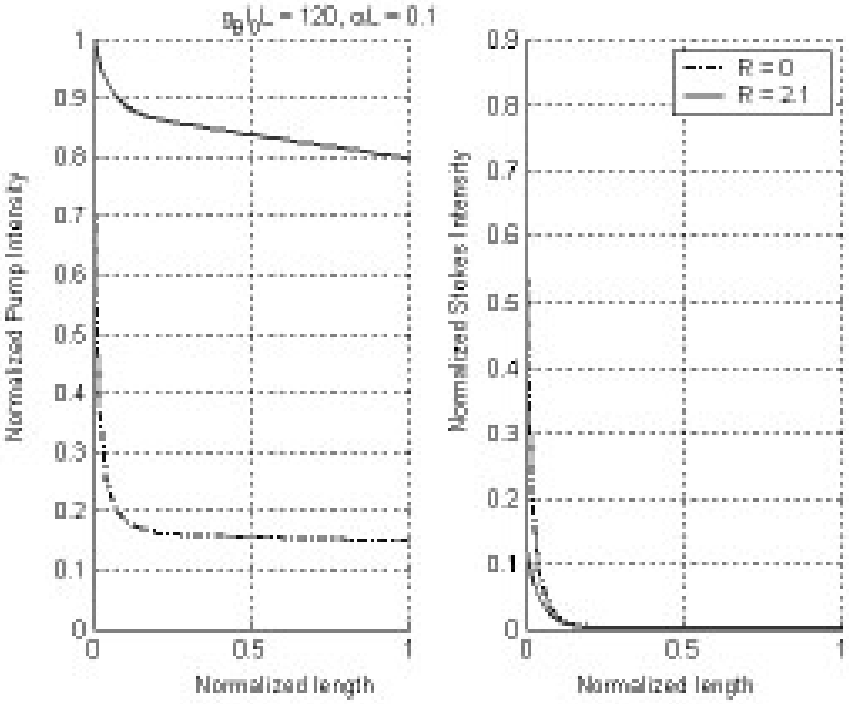

Figure 4.2: Pump and Stokes intensity against fiber length

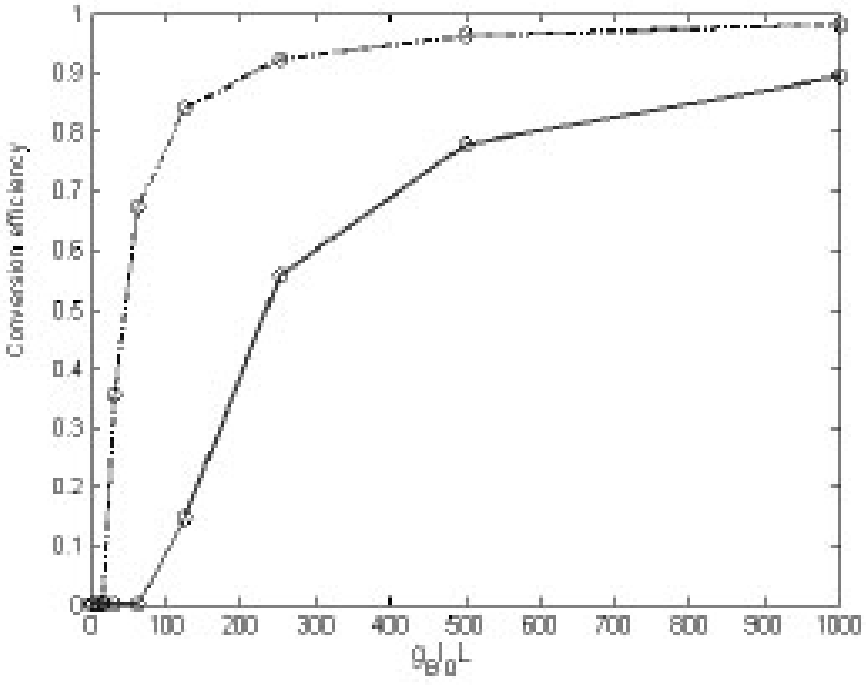

Figure 4.3: Conversion efficiency against pump intensity

CHAPTER 5

Distributed Stokes suppression in a circularly dichroic medium for suppression of Stimulated Brillouin scattering in an optic fiber

5.1 Introduction

We have thus far examined SBS suppression methods based on control of the acoustic environment. It was clear from the previous chapters that difficulties exist in obtaining a high threshold acoustic environment. In this chapter, we investigate the approach of SBS threshold enhancement by employing structures that affect the buildup and propagation of the Stokes wave. Lee et al. proposed recently a method of SBS suppression that aims to suppress SBS through control of the Stokes guidance properties [33]. They propose the use of fiber Bragg gratings tuned at the Stokes wavelength. This method has been criticized for the difficulty in writing a grating that can filter the Stokes but negligibly affect the pump (we remind the reader that the separation of the Stokes wavelength from the pump wavelength is quite small). We propose for the first time a novel method for achieving distributed Stokes suppression based on using circularly polarized light. A circularly polarized light of one handedness results in a scattered light of the other handedness. By designing a circularly dichroic medium we can thus increase the threshold. We estimate the suppression obtainable by such a scheme. We further discuss complications that can

arise due to residual birefringence effects.

In this chapter, we treat the general case of a distributed Stokes loss mechanism introduced in the fiber. In particular, we are interested in cases where the Stokes optical loss is considerably higher than the pump loss.

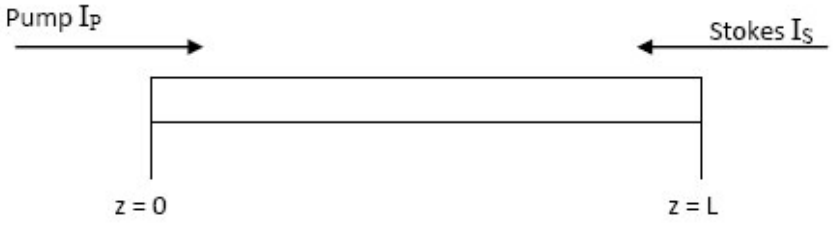

Figure 5.1: Schematic for the derivation

5.2 Polarization properties of SBS

In the case of linearly polarized pump and an isotropic medium, the acoustic wave is longitudinal and the density fluctuation is a scalar quantity. As a consequence, no coupling can occur between fields of orthogonal polarization states. Consider a pump field and the Stokes field with their polarization states included (as in [57])

$$\mathbf{E_P}(r) = E_P(r)e_P, \mathbf{E_S}(r) = E_S(r)e_S, \tag{5.1}$$

where $E_P(r)$ is the spatial form of the field and e_P is its polarization state. The acoustic field $Q(r)$ is scalar and has no polarization component. The interaction equations for the stokes field and the acoustic amplitude are [57],

$$\begin{aligned} &\frac{\delta}{\delta z}\mathbf{E_s} - \frac{\iota}{\mathbf{2k}}\nabla_{\mathbf{T}}^{\mathbf{2}}\mathbf{E_S} = \mathbf{E_L Q} * \\ &\left(\frac{\delta}{\delta t} + \frac{1}{2\tau_B}\right) Q = \gamma \mathbf{E_L} \cdot \mathbf{E_S^*}. \end{aligned} \tag{5.2}$$

We note that the laser and the Stokes field occur as a vector dot product $E_P \cdot E_S* = E_P E_S(e_S \cdot e_P*)$. If the laser and Stokes fields are parallel, they produce the acoustic

field with the maximum strength. For the case of plane wave interaction, we can conclude that the Stokes field will develop the same polarization state as the laser field. Extending this reasoning to circularly polarized basis states then, right-hand circularly polarized laser induces left-hand circularly polarized Stokes that is parallel to the laser field polarization. The change of handedness results because handedness is related to the rotation direction as perceived along the direction of propagation. This can be easily verified by expressing the circular polarized basis states in terms of linear basis states as:

$$e_P = \frac{(e_x + \iota e_y)}{\sqrt{2}},\ e_S = \frac{(e_x - \iota e_y)}{\sqrt{2}},$$

and subsequently performing a vector dot product.

With regard to polarization, SBS is identical to the reflection properties of a conventional mirror. We can clarify this concept even further by using the concept of angular momentum of a photon. This is described in figure 5.2.

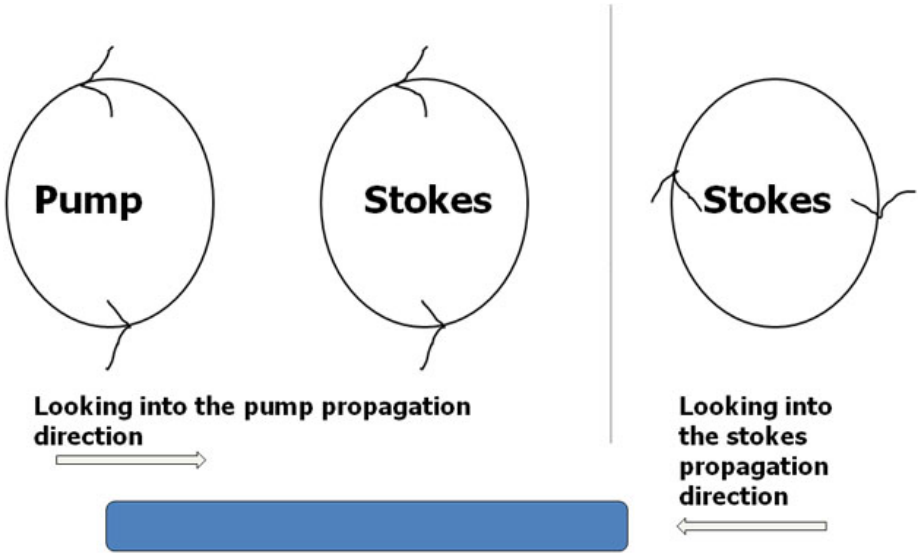

Figure 5.2: Visualizing SBS for circularly polarized pump light

Conservation of angular momentum results in the Pump and the Stokes photons rotating in the same sense when seeing the pump propagating away. But the Stokes

wave travels in the reverse direction. When seen from the other direction the Stokes wave now possesses the other circular handedness.

5.2.1 Theory

In this derivation, we revise the traditional Smith formula (see [16] for Brillouin threshold for the case of distributed Stokes loss and anti-guiding acoustic geometry. The starting point for our derivation is the equation for the evolution of the backward Brillouin Stokes wave power P_s [15] along the length of the fiber shown here in figure 5.1 .

$$\frac{dP_S(z)}{dz} - \alpha_s P_S(z) + \frac{g_B(\omega)}{A_{eff}} P_P(z) P_S(z) = 0,$$

where $P_S(z)$,$P_P(z)$ are the Stokes and Pump intensities at z, $g_B(\omega)$ is the Brillouin gain as a function of the frequency shift ω, $L(\omega)$ is the lorentzian lineshape and A_{eff} denotes the optical effective area and α_s denotes the loss for the Stokes wave. Upon making the pump no-depletion approximation, we can write

$$P_P(z) = P_P(0) exp(-\alpha_p z), \tag{5.3}$$

where α_p is the loss for the pump wave.

To determine the effect of amplified spontaneous Brillouin scattering, we consider the one photon approximation introduced by Smith [16]. This approximation assumes that the effect of amplified spontaneous Brillouin scattering is equivalent to the injection of one fictitious photon per longitudinal mode. The injected power must be scaled by the factor $kT/h\nu_B$ for the case of thermally generated acoustic phonons. Under the short fiber approximation ($L < 50km$, similar to ref [27] in [29]), this allows us to write for the Stokes power at the input end in terms of that at the

output end $z = L$ as

$$P_S(z=0) = P_S(z=L)exp(-\alpha_s L)exp(\frac{g_B(\omega)}{A_{eff}}P_P(0)L_{eff}), \tag{5.4}$$

where the effective length is defined as

$$L_{eff} = \frac{(1 - exp(-\alpha_p L))}{\alpha_P}. \tag{5.5}$$

Taking the power at the end ($z = L$) as a summation of one fictitious photon per longitudinal mode we get

$$P_S(z=0) = \frac{kT}{\nu_B}\exp(-\alpha_S L)\int_{\infty}^{-\infty} \omega\, exp(g_B(\omega)\frac{P_P(0)}{A_{eff}}L_{eff})\, d\omega. \tag{5.6}$$

For thresholds let us define

$$P_S(0) = \eta P_P(0). \tag{5.7}$$

This particular definition of threshold is motivated by the fact that the definition for SBS threshold by various authors can be arbitrary. The threshold is conventionally defined as the input pump power for which the Stokes power at the input becomes equal to the input pump power (We define $\eta = 1$ as in chapter 9. of [15]). However we note that reference [29] defines $\eta = 0.01$.

In order to solve equation 5.6, an exact functional form for $g_B(\omega)$ needs to be known. The integral in 5.6, can be evaluated approximately by using the method of steepest descent as the main contribution to the integral comes from a narrow region of ω near the peak gain $\omega = \omega_{sB}$ [15]. The result can be written as

$$P_s(0) = P_{sL}^{eff} exp\left(g_B(\omega_{sB})\frac{P_P(0)}{A_{eff}}L_{eff} - \alpha_s L\right), \tag{5.8}$$

where the effective Stokes seed power at $z = L$ is given by

$$P_{sL}^{eff} = kT\frac{\omega_{sB}}{\nu_B}B_{eff}, \tag{5.9}$$

with

$$\begin{aligned} B_{eff} &= \left[\frac{2\pi A_{eff}}{|g_B^{''}(\omega_{sB})P_P(0)P_P(0)L_{eff}|}\right]^{1/2} \\ g_B^{''}(\omega_{sB}) &= \left[\frac{\partial^2 g_B}{\partial\omega^2}\right]_{\omega=\omega_{sB}}. \end{aligned}$$

We will choose a lorentzian as the functional form of g_B as

$$g_B(\nu) = g_B(\omega_{sB})\frac{(w/2)^2}{(\nu-\nu_B)^2+(w/2)^2}, \tag{5.10}$$

where w is the FWHM.

After evaluating the derivative in 5.10, the threshold power P^{th} can finally be evaluated by the equation

$$P_{s0}^{eff} exp(g_B P^{th} L_{eff}) = \eta P^{th}. \tag{5.11}$$

Furthermore

$$B_{eff} = C\frac{1}{\sqrt{1-e^{-\alpha_p L}}}\frac{1}{\sqrt{P^{th}}}, \tag{5.12}$$

where

$$C = \left(\frac{\pi^2 w^4 A_{eff}\alpha_p}{2g_B(\omega_{sB})}\right)^{1/2}. \tag{5.13}$$

Thus

$$P_{s0}^{eff} = kTC\frac{2\pi}{\lambda_p\nu_B}\frac{1}{\sqrt{1-e^{-\alpha_p L}}}\frac{1}{\sqrt{P^{th}}}. \tag{5.14}$$

The transcendental equation for the threshold power P^{th} now becomes

$$P^{th\,3/2} = B\frac{e^{-\alpha_s L}}{\sqrt{1-e^{-\alpha_p L}}}\exp\left(g_B(\omega_{sB})\frac{P^{th}}{A_{eff}}L_{eff}\right), \tag{5.15}$$

where

$$B = \frac{\pi w kT}{\eta\lambda_p\nu_B}\left(\frac{2A_{eff}\alpha_p}{g_B(\omega_{sB})}\right)^{1/2}, \tag{5.16}$$

and λ_p is the wavelength of the pump light.

5.2.2 Results and discussion

We first examine threshold increase factor as a function of the distributed Stokes loss α_S. We take the following parameters for this simulation.

- $A_{eff} = 50\mu m^2$
- $L = 20m$
- $g_B = 5x10^{-11}m/W$
- $\nu_B = 11GHz$
- $w = 12MHz$
- $\eta = 1$
- $\lambda = 1.55\mu m$
- $T = 300K$
- $\alpha_p = 0.2dB/m.$

The threshold increase in dB defined by

$$10\log_{10}\left(\frac{P_{new}^{th}}{P_{old}^{th}}\right) \tag{5.17}$$

is plotted as a function of α_S in dB/m in figure 5.3. The gain for the Stokes wave is given by $exp(g_B I_0 L - \alpha_S L)$ under the no-pump depletion approximation. Thus, as α_S approaches $g_B I_0$, a larger increase in α_S is needed to achieve a proportional increase in the threshold. This behavior is seen in figure 5.3. A further confirmation of this behavior is observed when we next plot the threshold increase as a function of fiber length for a given α_S.

In figure 5.4 calculations are performed for the threshold values as a function of fiber length for two values of pump gain (10 dB/m and 20 dB/m) and values of 100 dB/m are assumed for the distributed stokes suppression scheme.

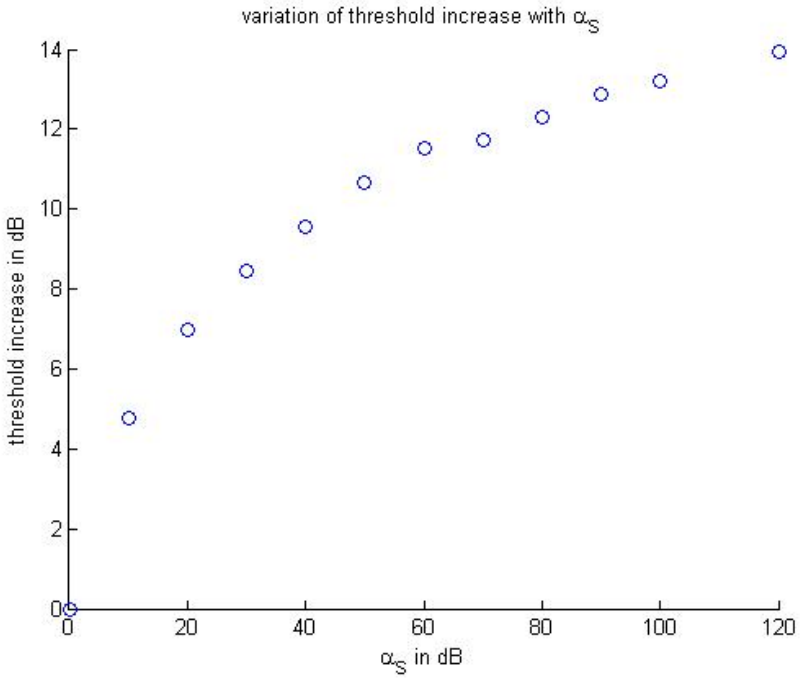

Figure 5.3: Threshold increase as a function of α_S

Several interesting features are observed from this figure

- Distributed stokes suppression mechanism is seen to be effective only for lengths greater than 10m or so.
- We observe a saturation-like behavior of the threshold values for lengths after the L = 25m or so.

The occurrence of the saturation like effect is not observed in the classical derivation of Smith and is a feature primarily linked to the Distributed Stokes suppression approach. The saturation of SBS threshold is important primarily from considerations of thermal design of a fiber laser system. The output power of a fiber laser is clamped at the value of the SBS threshold. For a given output power a longer length of the fiber can be used. This has advantages in that the heat generated from pump absorption is dissipated over a larger volume.

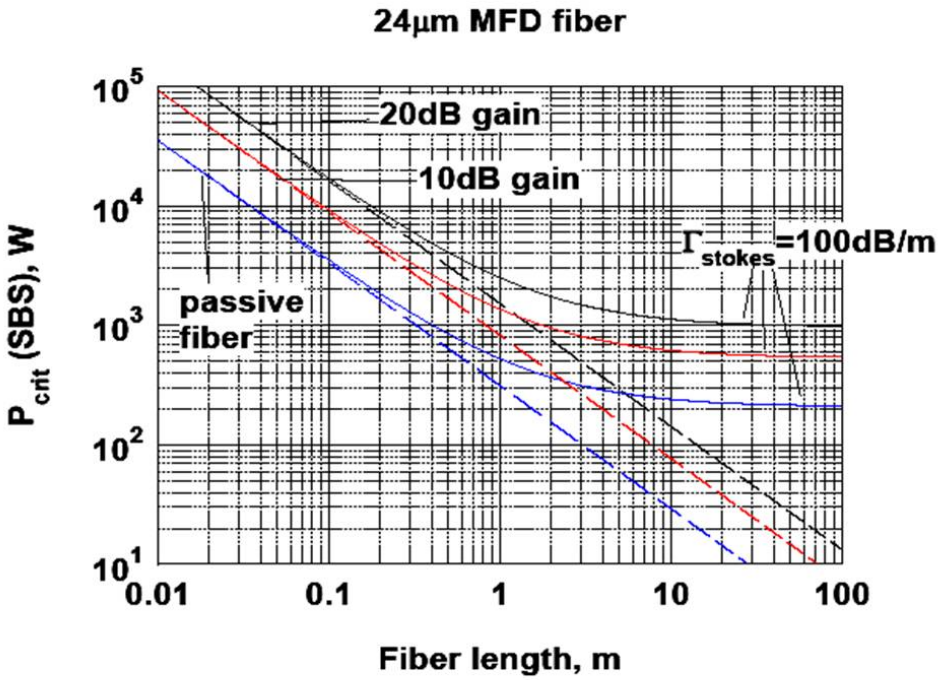

Figure 5.4: Plot of SBS threshold clearly showing saturation effects

5.3 Conclusions

In this chapter we quantified backward scattering thresholds in the presence of a distributed loss component that is markedly higher in comparison with the loss for the pump. A marked saturation like effect is seen to occur in the case of such a distributed Stokes loss component. This saturation effect is useful in designing thermal management systems. In particular, it decouples thermal management issues from design concerns regarding the fiber length.

We briefly remark on aspects related to the practical realization of this concept for SBS threshold increase. Chiral core fibers have been proposed which have circular birefringence and circular dichroism of the order of 30dB/m (see [58]). The fibers in [58] were short ($< 100cm$).

Incorporation of distributed Stokes loss in the CCC fiber

Distributed Stokes suppression using circular dichroism can be incorporated in the CCC architecture by using the concept of a helical stress rod. The idea of a helical stress rod for inducing circular birefringence was introduced by Huang [59]. The helical stress rod is composed of a material that has a different thermal expansion coefficient compared to the surrounding glass. The fiber drawn from such a composition will have residual stress effects due to the differing thermal expansion coefficients. Huang claims that this structure leads to a circularly birefringent fiber that has minimal residual linear birefringence. The stress rod can be integrated into the CCC architecture as shown in figure 5.5. The stress rod creates birefringence and the CCC side core can then be used to generate a differential absorption of the order of 100 dB/m between the two polarizations. Using the stress rod in a CCC setting thus results in a circularly dichroic medium with higher relative distributed

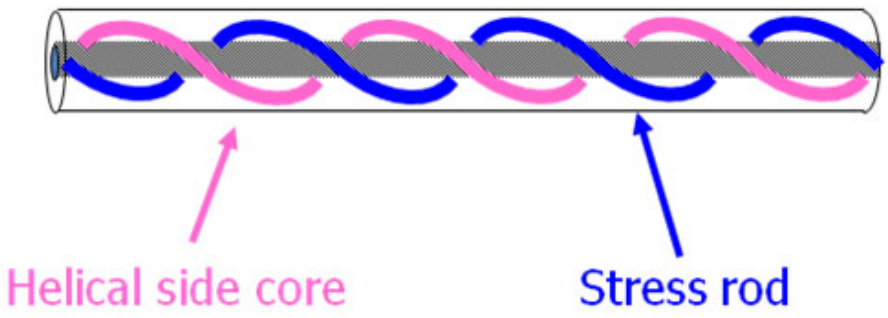

Figure 5.5: CCC distributed Stokes suppression scheme

loss for one polarization compared to the other. Using a right circular pump in this geometry will then result in a left circular Stokes with a higher relative loss. This results in increase in the SBS threshold for the configuration.

CHAPTER 6

Conclusions and future work

This dissertation addressed two interesting problems in the area of applied nonlinear optics. Specifically, we considered the problem of scattering in and by a nonlinear periodic medium.

First we considered the problem of extending the work on optical switching in nonlinear superlattices to the general case of a metamaterial superlattices. We established that a superlattice containing a combination of right handed and left handed slabs exhibit omnidirectional switching properties. We explained these anomalous properties by the presence of a gap soliton called the zero-n gap soliton.

Second, the problem of integrating nonlinearity suppression structures into high power large mode area fiber lasers was considered. Here we examined the approach of transverse acoustic velocity profile design in detail. We examined the core scaling issues that would be particularly relevant to large mode area fiber lasers. We find that a generalized ramp profile might be the most suitable design approach giving about 7dB in SBS threshold enhancement. Further work in designing has to carefully take into account the exact doping profile and the associated diffusing effects, the exact value of Brillouin gain for the particular acoustic environment. The approach established in this thesis can be generalized to serve as a design tool in the laboratory.

We considered extending the concept of acoustic control by considering the concept of phononic bandgap structure. A theory of SBS in a 1D elastic grating has been worked out in this thesis. The results relate the suppression metrics to the design of the bandgap structure. It is felt that this could be extended easily to the general case of SBS in a full phononic bandgap structure. This method has practical limitations due to the difficulty associated in fabricating a complicated microstructure fiber.

The search for further enhancements in SBS thresholds led finally to the simple and ingenious solution to SBS suppression that we present in this thesis. This method involved using a distributed loss component primarily selective of the Stokes component. We established the nonlinearity saturation effects that result purely as a byproduct of this technique.

6.1 Possible complications due to residual birefringence effects

We discuss next the possible complications that might occur due to the fact that a practical circular dichroic fiber system might have residual circular and/or linear birefringence effects. To this end, we lay the framework for describing the evolution of the fields in the presence of these residual effects.

Without loss of generality, consider a RCP pump which will generate LCP Stokes. As an additional concern, the residual linear birefringence in the implementation structure can result in the generation and copropagtion of a LCP pump wave resulting from the coupling of the RCP pump by the residual linear birefringence. Similarly, the LCP Stokes can result in the generation and copropagtion of an RCP Stokes wave. In the next section, we attempt a semi-qualitative description of this issue.

6.1.1 Analysis of SBS threshold increase in a circular dichroic medium with residual linear birefringence.

Let us initially consider two linearly polarized pump waves propagating in an SBS medium. These will generate Stokes waves of their corresponding polarizations. The acoustic wave is propagating forward.

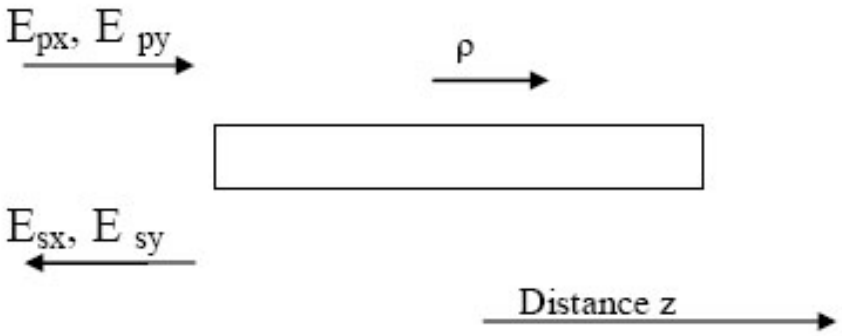

Figure 6.1: Schematic for the SBS equations.

The equation for the acousto-optic interaction in this structure is given (as in [29]) by

$$\frac{d^2\rho}{dt^2} - \Gamma\nabla^2\frac{d\rho}{dt} - v_l^2(r)\nabla^2\rho = -\frac{\gamma}{2}\nabla^2\mathbf{E^2}, \tag{6.1}$$

where ρ is the material density fluctuation around the mean value ρ_0, Γ is the damping factor, v_l is the longitudinal acoustic velocity and γ is the electrostrictive constant. The electric field E is expressed as a superposition

$$\begin{aligned}\bar{\mathbf{E}}(r,z,t) = \frac{1}{2}f(r)[E_{px}(z,t)e^{j(\omega_p t-\beta_p z)}\mathbf{u_x} &+ E_{py}(z,t)e^{j(\omega_p t-\beta_p z)}\mathbf{u_y} + \\ E_{sx}(z,t)e^{j(\omega_p t-\beta_p z)}\mathbf{u_x} &+ E_{sy}(z,t)e^{j(\omega_p t-\beta_p z)}\mathbf{u_y}] + c.c.,\end{aligned} \tag{6.2}$$

where $f(r)$ is the dimensionless fundamental optical modeprofile, $E_{px}, E_{py}, E_{sx}, E_{sy}$ are the slowly varying envelopes of the four waves (pump and the Stokes with the x

and y polarization respectively),u_x and u_y are the unit polarization vectors, the radial frequency and the wavevectors of the waves are given by $\omega_p, \omega_s, \beta_p, \beta_s$ respectively.

We seek for the solution of acoustic waves in equation (6.1) to be of the form

$$\rho(z,t,r,\theta) = \frac{1}{2}\sum_{m=1}^{M} \bar{\rho}_m(z,t)\zeta_m(r,\theta)e^{j(\Omega t - qz)} + c.c.,$$

where M is the number of acoustic modes $\zeta_m(r,\theta)$, while their frequencies Ω and wavevectors q satisfy the phase matching condition.

From Maxwell's equations we obtain the wave equation for the electric fields as

$$\nabla^2 \hat{E} = \frac{\epsilon_{tot}}{c^2}\frac{\delta^2 \hat{E}}{\delta t^2}, \tag{6.3}$$

where ϵ_{tot} is the dielectric function given by

$$\epsilon_{tot} = \epsilon_L + \epsilon_{NL} + \Delta\epsilon,$$

where ϵ_L is the permittivity of the unperturbed medium, ϵ_{NL} is the nonlinear perturbation resulting from SBS and $\Delta\epsilon$ is the perturbation that is induced to create the circular dichroism. The assumptions made in this equation are very similar to the ones made in the standard approach for deriving nonlinear pulse propagation problems in fiber optics. Most importantly we see that the perturbations are considered as small. The material parameters at the pump and stokes frequencies are assumed equal. To solve for the variation of the field amplitudes we evaluate the derivatives of the fields given in equation (6.2) and substitute in equation (6.3), we then make the slowly varying envelope approximation and finally use the fact that the optical modal profile has negligible dependence on the nonlinear effects. The optical modal equation is

$$\nabla_\perp^2 f(r) + \left[\frac{\omega^2 n^2(r)}{c^2} - \beta_j^2\right] f(r) = 0.$$

The terms are separated out according to the common exponential and the unit polarization vectors. The phase matching condition ensures that counter-propagating SBS waves are coupled while only the co-propagating fields are coupled via the linear perturbation term. The coupling matrix

$$\kappa = \begin{bmatrix} \kappa_{11} & \kappa_{12} \\ \\ \kappa_{21} & \kappa_{22} \end{bmatrix}$$

is obtained when we use the normalization relation for the modes

$$\int u_m \cdot u_n \, dxdy \; = \; N_n \delta_{mn}. \tag{6.4}$$

Its elements are given by

$$\kappa_{mn} = \frac{k_0}{2n_0 N_0} \int u_n^* \cdot \Delta\epsilon \cdot u_m \, dxdy. \tag{6.5}$$

We then write for the evolution of the linearly polarized fields thus

$$\begin{aligned}
\frac{dE_{px}}{dz} &= -\frac{1}{2}\alpha_x E_{px} - \iota\sigma E_{px} \left|E_{sx}\right|^2 + \iota\kappa_{11} E_{px} + \iota\kappa_{12} E_{py} \\
\frac{dE_{py}}{dz} &= -\frac{1}{2}\alpha_y E_{py} - \iota\sigma E_{py} \left|E_{sy}\right|^2 + \iota\kappa_{21} E_{py} + \iota\kappa_{22} E_{px} \\
\frac{dE_{sx}}{dz} &= +\frac{1}{2}\alpha_x E_{sx} - \iota\sigma^* E_{sx} \left|E_{px}\right|^2 - \iota\kappa_{11} E_{sx} - \iota\kappa_{12} E_{sy} \\
\frac{dE_{sy}}{dz} &= +\frac{1}{2}\alpha_y E_{sy} - \iota\sigma^* E_{sy} \left|E_{py}\right|^2 - \iota\kappa_{21} E_{sy} - \iota\kappa_{22} E_{sx},
\end{aligned} \tag{6.6}$$

(6.7)

where

$$\sigma = \frac{n^9 \epsilon_0 p_{12}^2 \omega^3}{2\rho_0 c^3 (\Omega_m^2 - \Omega^2 + \iota\Omega\Gamma q^2)} \frac{\langle \zeta_m f^2 \rangle^2}{\langle \zeta_m^2 \rangle \langle f^2 \rangle},$$

and is similar to reference [29]. We next seek to convert these fields into a circular basis representation. First, note that the direction of propagation of the Stokes wave

is opposite and the handedness has to be properly considered. We write down next the equations after the fields have been converted to a circular basis

$$\begin{aligned}
\frac{dE_{PR}}{dz} &= -\frac{1}{2}\alpha_R E_{PR} - \frac{1}{2}g_B(\nu)I_{SL}E_{PR} + \frac{\iota}{2}\delta E_{PR} + \frac{\iota}{2}\Delta\beta E_{PL}. \qquad (6.8)\\
\frac{dE_{SL}}{dz} &= +\frac{1}{2}\alpha_L E_{SL} - \frac{1}{2}g_B(\nu)I_{PR}E_{SL} - \frac{\iota}{2}\delta E_{SL} + \frac{\iota}{2}\Delta\beta E_{SR}.\\
\frac{dE_{PL}}{dz} &= -\frac{1}{2}\alpha_L E_{PL} - \frac{1}{2}g_B(\nu)I_{SR}E_{PL} - \frac{\iota}{2}\delta E_{PL} + \frac{\iota}{2}\Delta\beta E_{PR}.\\
\frac{dE_{SR}}{dz} &= +\frac{1}{2}\alpha_R E_{SR} - \frac{1}{2}g_B(\nu)I_{PL}E_{SR} + \frac{\iota}{2}\delta E_{SR} + \frac{\iota}{2}\Delta\beta E_{SL},
\end{aligned}$$

(6.9)

where α_R, α_L denote the optical losses for the right and cleft circular handedness and the I terms the corresponding intensities of the fields. This dichroism is assumed to be included in the medium by specific design and for now we assume that it is independent of optical frequency. The four wave model in circular basis can be shown by the following schematic. The coupling constants matrix expressed in the circular

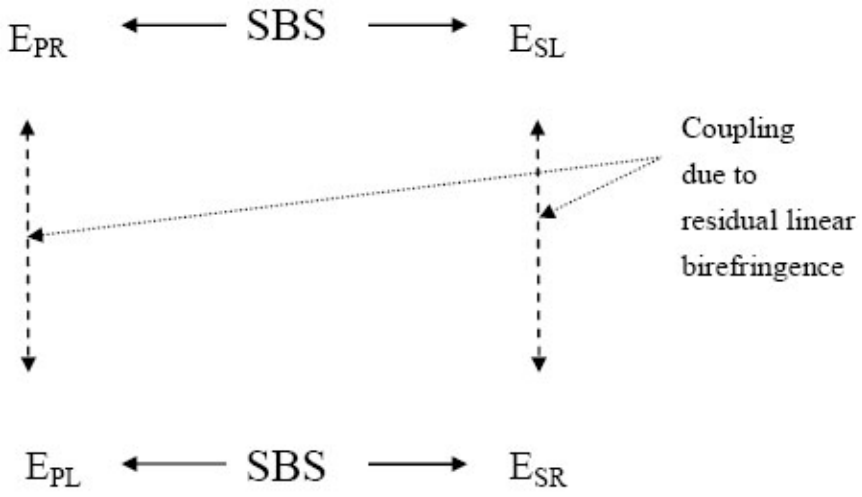

Figure 6.2: The four wave model for SBS in a circularly dichroic medium.

basis for a circular dichroic medium is

$$\kappa = \frac{1}{2}\begin{bmatrix} \delta & \Delta\beta e^{\iota 2\alpha_0 z} \\ \Delta\beta e^{-\iota 2\alpha_0 z} & -\delta \end{bmatrix},$$

where δ is the circular birefringence expressed in rad/m and $\Delta\beta$ is the residual linear birefringence. It is easy to see that any medium possessing circular birefringence must have a helical symmetry of some kind. One way to achieve this is through spinning the fiber and this effect can be included in the coupling matrix by the alpha term. However for simplicity we will ignore this additional complication and treat the coupling matrix in the following simplified form.

$$\kappa = \frac{1}{2}\begin{bmatrix} \delta & \Delta\beta \\ \Delta\beta & -\delta \end{bmatrix}.$$

The first simplification we introduce to solve the above system is to ignore pump depletion and thus write for the pump fields

$$\frac{dE_{PR}}{dz} = -\frac{1}{2}\alpha_R E_{PR} + \frac{\iota}{2}\delta E_{PR} + \frac{\iota}{2}\Delta\beta E_{PL}.$$
$$\frac{dE_{PL}}{dz} = -\frac{1}{2}\alpha_L E_{PL} - \frac{\iota}{2}\delta E_{PL} + \frac{\iota}{2}\Delta\beta E_{PR}.$$

This lead to the following equation for E_{PR}

$$\frac{d^2E_{PR}}{dz^2} = C_1\frac{dE_{PR}}{dz} + C_2 E_{PR},$$

where the constants are

$$C_1 = \frac{-(\alpha_L + \alpha_R)}{2}$$
$$C_2 = \frac{\Delta\beta^2 - \alpha_R\alpha_L + \iota\delta(\alpha_R + \alpha_L) - \delta^2}{4}.$$

Without loss of generality, let us consider that the structure is designed to primarily attenuate LCP light. An RCP pump will then bleed into an LCP pump. In order to

qualitatively understand the impact of residual linear birefringence, we next make some assumptions

- The relative loss for the Stokes is significantly higher than that for the pump. $\alpha_R >> \alpha_L$.
- The residual linear birefringence is weak. The SBS interaction resulting from the LCP pump give a RCP Stokes. However because of the weak nature of the residual linear birefringence and the high loss for LCP light, this SBS interaction has threshold much higher than that of the RCP pump related SBS interaction. We will thus drop these SBS terms.
- The LCP Stokes has high loss and thus the effect of the residual linear birefringence in generating an RCP Stokes wave is negligible.

The assumptions above help to reduce the systems of equations further to a three wave model described in 6.3 The corresponding equations are thus,

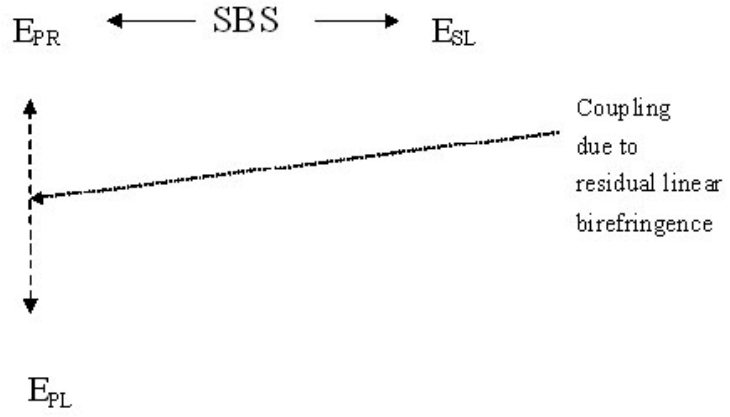

Figure 6.3: Simplified three wave model

$$\begin{aligned} \frac{dE_{PR}}{dz} &= -\frac{1}{2}\alpha_R E_{PR} - \frac{1}{2}g_B(\nu)I_{SL}E_{PR} + \frac{\iota}{2}\delta E_{PR} + \frac{\iota}{2}\Delta\beta E_{PL}. \qquad (6.10) \\ \frac{dE_{SL}}{dz} &= +\frac{1}{2}\alpha_L E_{SL} - \frac{1}{2}g_B(\nu)I_{PR}E_{SL} - \frac{\iota}{2}\delta E_{SL}. \end{aligned}$$

$$\frac{dE_{PL}}{dz} = -\frac{1}{2}\alpha_L E_{PL} - \frac{\iota}{2}\delta E_{PL} + \frac{\iota}{2}\Delta\beta E_{PR}.$$

6.2 Distributed Stokes suppression for mitigation of forward scattering

The concept of distributed Stokes suppression for mitigation of self-induced scattering also holds in the case when the Stokes wave is scattered in the forward direction. This method has implications for suppression of stimulated Raman scattering. We discuss next the theory of distributed Stokes suppression for forward scattering.

The starting point for our derivation is again the equation for the evolution of the forward scattered Stokes wave power $P_s(z)$ along the length of the fiber

$$\frac{dP_S(z)}{dz} = -\alpha_s P_S(z) + \gamma P_P(z) P_S(z),$$

where, $P_S(z)$,$P_P(z)$ are the Stokes and Pump powers at z. Upon making the pump no-depletion approximation, we can write

$$P_P(z) = P_P(0) exp(-\alpha_P z). \tag{6.11}$$

To determine the effect of amplified spontaneous forward scattering, we again revert to the photon approximation introduced by Smith. This approximation assumes that the effect of amplified spontaneous forward scattering is equivalent to the injection of one fictitious photon per mode. Under the short fiber approximation (similar to [29]), this allows us to write for the Stokes power at the output end in terms of that at the input end as

$$P_S(z = L) = P_S(z = 0) exp(-\alpha_S L) exp(\gamma P_P(0) L_{eff}), \tag{6.12}$$

where the effective length defined as

$$L_{eff} = \frac{(1 - exp(-\alpha_P L))}{\alpha_P}. \tag{6.13}$$

After the one-photon approximation mentioned earlier we get

$$P_S(z = L) = \exp(-\alpha_S L) \int_{\infty}^{-\infty} \nu \, exp(\gamma P_P(0) L_{eff}) \, d\nu. \tag{6.14}$$

For thresholds let us define

$$P_S(L) = \eta P_P(0). \tag{6.15}$$

If we assume a lorentzian function for the dependence of γ on frequency a transcendental equation of the following form results

$$x^{3/2} B = \frac{e^{-\alpha_S L}}{\sqrt{1 - e^{-\alpha_P L}}} \times exp(x(1 - e^{-\alpha_p L})), \tag{6.16}$$

where

$$B = \frac{\eta \alpha_P \nu_R \lambda_{pump}}{\sqrt{\pi} \gamma(\nu_R) c w},$$

where ν_R and w are the frequency downshift and the FWHM of the lorentzian forward scattering process. And the threshold power will be obtained by using the equation

$$P^{th} = \frac{x \alpha_P}{\gamma(\nu_R)}. \tag{6.17}$$

We strongly suspect that the saturation like behavior will also hold for this case.

APPENDIX

.1 Chapter 2

.1.1 calculate the transmission in a linear mixed superlattice

```
%Calculates reflectivity and transmitance of a mixed type NIM-PIM
%superlattice.

%general constants

er1 = 4;%2.673;  % PIM dielectric constant
ur1 = 1;  % permeability constant
d1 = 12e-3;%100e-9;
alp1 = 0;  % kerr nonlinearity
er2 = -4.0;%2.465;  % nIM dielectric constant
ur2 = 1.0;   % permeability constant
alp1 = 0;   % kerr nonlinearity
c1 = 100;    %
c2 = 100;    % dieprsion relation constants
d2 = 6e-3;%85e-9;

%run constants
N = 16; % number of unit cells
angsweep = 100;
global beta2;
global erur;
```

```
%frequency loop


for a = 1:100
     w(a) = 2*pi*(a*9e-2)*1e9


     for ac = 1%:100
 theta(1) = 0; %1.0996;
 %theta(ac) =  0.890*ac *pi/180;
 %w(1) = 2*pi*3*1e9;


 %er2(a) = 1 +  25/(0.81 - (2.3)^2) + 100/(11.5^2 - (2.3)^2);
 %ur2(a) = 1 + 9/(0.902^2 - (2.3)^2);



%er2(a) = 1 +  25/(0.81 - (1 + a*9e-3)^2) + 100/(11.5^2
- (1 + a*9e-3)^2);
 %ur2(a) = 1 + 9/(0.902^2 - (1 + a*9e-3)^2);


er2(a) = -50 + a ;%1.2 - 100/(2 +a*9e-3)^2;% +  25/(0.81
- (1 + 9e-2*a)^2) + 50/(11.5^2 - (1+ 9e-2*a)^2);
ur2(a) = -1;%1 - 100/(2+ a*9e-3)^2;% +  9/(0.902^2
- (1 + 9e-2*a)^2);



    ko = w(a)*(1.2566e-6*8.8542e-12)^0.5;
```

```
    %ko = 2*pi/488e-9;%w(a)*(1.2566e-6*8.8542e-12)^0.5;
    b2n = sqrt(er2(a)*ur2(a) - (sin(theta(ac)))^2)/ur2(a);
    b2p = sqrt(er1*ur1 - (sin(theta(ac)))^2)/ur1;


      kn = ko*b2n;
    if er2(a) < 0 & ur2(a) < 0
 kn = -ko*b2n;
end


       kp = ko*b2p;


    Tp = [ cos(-kp*d1),  -sin(-kp*d1)/b2p;
           b2p*sin(-kp*d1),   cos(-kp*d1) ];
% %
     Tn = [ cos(-kn*d2),  -sin(-kn*d2)/b2n;
           b2n*sin(-kn*d2),   cos(-kn*d2) ];



    T = (Tn*Tp)^16
%
%
%     %defining the permitivity variations
%
Inten = 1;
E = Inten*[1 ; 1/(120*pi)*cos(theta(ac))]
```

```
  %for  hf = 1:16




  %end

%

% %

%  Er = 0.5* (E(1) + i*E(2)*sec(theta(ac)));
%  Ei = 0.5* (E(1) - i*E(2)*sec(theta(ac)));
%
 Tr(a) = 2*cos(theta(ac))/( (T(1,1)+T(2,2))*
 cos(theta(ac)) + i* (T(1,2)*cos(theta(ac))^2 - T(2,1)));
%  Re(a) = abs(Er/Ei)^2;

Tr(a) = abs(Tr(a))^2;
```

```
end

end

%semilogy(w/(2*pi),Tr);

%     plot(theta*180/pi, Tr);

    %semilogy(a,Tr);



subplot(1,2,1);

plot(er2,w/(2*pi));

hold on;

plot(ur2,w/(2*pi));


subplot(1,2,2);

semilogx(Tr, w/(2*pi))
```

.1.2 calculates the transmission in a mixed type superlattice with added nonlinearity

```
%trial 2


%general constants

er1 = 1.0;  % PIM dielectric constant

ur1 = 1.0;  % permeability constant

d1 = 1e-6;

alp1 = 0;  % kerr nonlinearity

er2 = -1.0;%2.465;  % nIM dielectric constant

ur2 = -1;   % permeability constant

alp2 = 0;   % kerr nonlinearity

d2 = 1e-6;

N = 16; % number of unit cells


%substrate and cladding RI

ns = 1.5;

nc = 1.5;




global beta2;

global erur;


%output intensity loop
```

```
for m = 1: 100
Inten = m*.2;

%frequency loop

for a = 1%:1000

   %w(a) = 2*pi*(2.4 + 1e-3*a)*1e9;

     for ac = 1
 theta(ac) = 50*pi/180; %1.0996;
%theta(ac) = (40 + 0.3*ac) *pi/180;

pc = nc*cos(theta(ac));
ps = sqrt(ns^2 - (nc*sin(theta(ac)))^2);



 %ko = w(a)*(1.2566e-6*8.8542e-12)^0.5;
 ko = 2*pi/(488e-9);


%er2(a) =  1 +  25/(0.81 - (1.8+ 1e-3*a)^2) +
100/(11.5^2 - (1.8+ 1e-3*a)^2);
```

```
%ur2(a) =  1 +   9/(0.902^2 - (1.8 + 1e-3*a)^2);




E = Inten*[1 ; i*ps];

du = d1+d2;



options = odeset('Refine', 4 );



for  hf = 1:N


%negative layer

beta2 = (nc*sin(theta(ac)))^2;

erur = er2(a)*ur2(a);

%

E(2) = ur2(a)*E(2)/ur1;

[xg,FE]  = ode45('nlon',[((N-hf)*du + du)*ko,


((N-hf)*du + d1)*ko], E,options);

%plot(xg/ko, abs(FE(:,1).^2));

E =  conj(FE(max(size(FE)),:)');

E(2) = ur1*E(2)/ur2(a);
```

```
%hold on;


%positive layer
beta2 = (nc*sin(theta(ac)))^2;
erur = er1*ur1;
[xg,FE]  = ode45('nlop',[((N-hf)*du + d1)*ko,
((N-hf)*du)*ko], E, options);
%plot(xg/ko, abs(FE(:,1).^2));
E =  conj(FE(max(size(FE)),:)');
%hold on;
end



 Er =       0.5* (E(1) + (1/pc)*i*E(2));
 Ei(m,ac) = 0.5* (E(1) - (1/pc)*i*E(2));


  Tr(m,ac) = (ps/pc)*abs(Inten/Ei(m,ac))^2;
 Re(a) = abs(Er/Ei(m,ac))^2;



end
end


end
incint = abs(Ei.^2);
```

```
figure(2);

plot(incint, Tr);

%plot(theta*180/pi, Tr(1,:));


%

% subplot(1,2,1);

% plot(er2,w/(2*pi));

% hold on;

% plot(ur2,w/(2*pi));

%

% subplot(1,2,2);

% semilogx(Tr, w/(2*pi))
```

.1.3 Draws the bistability curves

```
%trial 2


%general constants

er1 = 1.0;  % PIM dielectric constant

ur1 = 1.0;  % permeability constant

d1 = 1e-6;

alp1 = 0;  % kerr nonlinearity

er2 = -1.0;%2.465;  % nIM dielectric constant

ur2 = -1;   % permeability constant

alp2 = 0;   % kerr nonlinearity
```

```
d2 = 1e-6;

N = 16; % number of unit cells


%substrate and cladding RI

ns = 1.5;

nc = 1.5;




global beta2;

global erur;


%output intensity loop


for m = 1: 100

Inten = m*.2;


%frequency loop


for a = 1%:1000


   %w(a) = 2*pi*(2.4 + 1e-3*a)*1e9;


     for ac = 1

 theta(ac) = 50*pi/180; %1.0996;
```

```
%theta(ac) = (40 + 0.3*ac) *pi/180;


pc = nc*cos(theta(ac));
ps = sqrt(ns^2 - (nc*sin(theta(ac)))^2);




 %ko = w(a)*(1.2566e-6*8.8542e-12)^0.5;
 ko = 2*pi/(488e-9);



%er2(a) =  1 +  25/(0.81 - (1.8+ 1e-3*a)^2) +
 100/(11.5^2 - (1.8+ 1e-3*a)^2);
%ur2(a) =  1 +   9/(0.902^2 - (1.8 + 1e-3*a)^2);






E = Inten*[1 ; i*ps];
du = d1+d2;



options = odeset('Refine', 4 );
```

```
for  hf = 1:N


%negative layer

beta2 = (nc*sin(theta(ac)))^2;

erur = er2(a)*ur2(a);

%

E(2) = ur2(a)*E(2)/ur1;

[xg,FE]  = ode45('nlon',[((N-hf)*du + du)*ko,

((N-hf)*du + d1)*ko], E,options);

%plot(xg/ko, abs(FE(:,1).^2));

E =  conj(FE(max(size(FE)),:)');

E(2) = ur1*E(2)/ur2(a);

%hold on;


%positive layer

beta2 = (nc*sin(theta(ac)))^2;

erur = er1*ur1;

[xg,FE]  = ode45('nlop',[((N-hf)*du + d1)*ko,

((N-hf)*du)*ko], E, options);

%plot(xg/ko, abs(FE(:,1).^2));

E =  conj(FE(max(size(FE)),:)');

%hold on;

end
```

```
 Er =       0.5* (E(1) + (1/pc)*i*E(2));

 Ei(m,ac) = 0.5* (E(1) - (1/pc)*i*E(2));


  Tr(m,ac) = (ps/pc)*abs(Inten/Ei(m,ac))^2;

 Re(a) = abs(Er/Ei(m,ac))^2;



end

end


end

incint = abs(Ei.^2);


figure(2);

plot(incint, Tr);

%plot(theta*180/pi, Tr(1,:));


%

% subplot(1,2,1);

% plot(er2,w/(2*pi));

% hold on;

% plot(ur2,w/(2*pi));

%

% subplot(1,2,2);

% semilogx(Tr, w/(2*pi))
```

.1.4 propagates the electric field through a nonlinear slab through direct integration of the nonlinear wave equation

```
function efield = propagate(E,a)


options = odeset ('Refine', 10);

global er1;

global ur1;

global d1;

global d2;

global N;

global er2;

global ur2;

global theta;

global w;

global Ei;


%

% hf = 1;du = d1+d2;

% %beta2 = sin(theta)^2;

% erur = er2(a)*ur2(a);

% efield = nlon(1,2);


%[xg,FE]  = ode45('nlon',[((N-hf)*du + du)*ko,
```

```
((N-hf)*du + d1)*ko], E,options);


ko = w(a)*(1.2566e-6*8.8542e-12)^0.5;




for  hf = 1:N

%     d1 = d1 + 3e-3*rand;
%     d2 = d2 + 3e-3*rand;
    du = d1+d2;



    %negative layer
beta2 = sin(theta)^2;
erur = er2(a)*ur2(a);


E(2) = ur2(a)*E(2)/ur1;
[xg,FE]  = ode45('nlon',[((N-hf)*du + du)*ko,
((N-hf)*du + d1)*ko], E,options, erur, beta2);
E =  conj(FE(max(size(FE)),:)');
E(2) = ur1*E(2)/ur2(a);


% %positive layer
beta2 = sin(theta)^2;
```

```
erur = er1*ur1;

[xg,FE]  = ode45('nlop',[((N-hf)*du + d1)*ko,

((N-hf)*du)*ko], E);

E =  conj(FE(max(size(FE)),:)');

end


efield =  0.5* (E(1) - i*E(2)*sec(theta));
```

.2 Chapter 3

```
% % five layer guiding

%

% % 5 layered structure ...

% %  get the Brillouin spectrum of a 5 layered structure.

% %  for the case of an anti-guiding fiber

% %

%

% % IN DOING ANY NUMERICAL THING ..... PLEASE MAKE SURE THAT

% % YOU HAVE NORMALIZED EVERY DAMN THING MAN !

% % IT IS VERY ESSENTIAL

% %ELSE THINGS ARE RELATIVELY OUT OF PROPORTION AND IT

% %WILL START KILLING YOU

% %

%
```

```
% %global constants
global n1;
global n2;


global a1;
global b;
global ao;


global Vl1;
global Vl2;


global betaac;
global lambda;
global intfsq;


global Ao;
global Bo;
global ko1;
global ko2;







% Enter profile information -- in terms of thickness of the
% 5 layers and the respective index and velocity values
```

```
doping_5L_G(1);


% Solve for the optical mode
lambda = 1.064; %lambda in microns
ko = (2*pi)/lambda;
for sc = 1: 1000
     x(sc) = n2+ sc*(n1 - n2)/1000;%1.0 + (.449/120)*i;
     y(sc) = optcharec(x(sc));
 end;
% % %
figure(2);
  plot(x,log(y));
neff = x(755);
optmodep(755);



  %     neff = x(633);%633,1.4578for50um
    33um,248 1.4578,  456for40um1.4578
% % % 315for33um,,,,633for50um
% optmodep(neff);
% %
% % %   % Calculate integral of f^2
betaopt = 2*pi*neff/lambda;
betaac = 2*betaopt;
```

```
p1 = quadl(@intIsq,0,ao);

p2 = quadl(@intIsq,ao,b);


 Isq =2*pi* (p1+p2); % integral of filed ^4


 p3 = quadl(@intfsqua,0,ao);

p4 = quadl(@intfsqua,ao,b);


 fsq = 2*pi*(p3+p4); % integral of filed ^2


 Aeff = fsq^2/Isq;

% %

% % % MODES Guided  in layer 1

% %characteristic equation and


%identification of eigenmodes

% for sc = 1: 1000

%      x(sc) = Vl1 + sc*(5900 - Vl1)/1000;

%      y(sc) = fiveL_G_modes_1_charec(x(sc));

%  end;

%

%

%   figure(2);

%    plot(x,log(y));

%   hold on;
```

```
%
% %pick and count modes
%
% modind = 0;
% for sc = 2: 999
%      if (log(y(sc)) < log(y(sc-1)) )
& (log(y(sc)) < log(y(sc+1)))
%          modind = modind +1;
%          modeV(modind) = x(sc);
%          freq(modind) = (2*neff/lambda)*modeV(modind);
%      end
% end
%
% mod2a = modind;
% clear x;
% clear y;
%
% % % % determine modeprofile and overlap integral for eigenmodes
% % % figure(3)
% for t = 1:mod2a
%    gain(t) =  fiveL_G_eigenmodes_1(modeV(t));
%    amao(t) = fsq^2/gain(t)^2;
% end
%
% % %
```

```
% % %
% %
% % % % MODES Guided layer 1,2
% % % % characteristic equation and identification of eigenmodes
%
% for sc = 1: 1000
%    x(sc) = Vl2 + sc*(6000 - Vl2)/1000;%1.0 + (.449/120)*i;
%      y(sc) = fiveL_G_modes_12_charec(x(sc));
% end;
% for sc = 1001: 3000
%    x(sc) = 6000 + (sc-1001)*(6400- 6000)/2999;%1.0
+ (.449/120)*i;
%      y(sc) = fiveL_G_modes_12_charec(x(sc));
% end;
%
%
% %    figure(2);
% %    plot(x,log(y));
% %   hold on;
% % % %
% % % %pick and count modes
% % %
% modind = mod2a;
% for sc = 2: 999
%      if (log(y(sc)) < log(y(sc-1)) )
```

```
& (log(y(sc)) < log(y(sc+1)))
%          modind = modind +1;
%          modeV(modind) = x(sc);
%          freq(modind) = (2*neff/lambda)*modeV(modind);
%      end
% end
%
% mod2b = modind;
% clear x;
% clear y;
% % %
% % % % % determine modeprofile and overlap integral
for eigenmodes
%  for t = mod2a+1:mod2b
%  %  subplot(mod2b-mod2a,1,t-mod2a);
%      gain(t) = fiveL_G_eigenmodes_12(modeV(t));
%      amao(t) = fsq^2/gain(t)^2;
%  end
% % %
% % % %
% % %
% % % %
% % %
% % %
% % normalizing the gain so that ..
```

```
% % free space gain = 1; as the mode shapes are identical
%
% %gain = gain./sqrt(Isq);
%
% %
% % %
% % % % %
% % % %Construct the spectrum and threshold calculations
% % %
%
% n = neff;    %refractive index
% p12 = 0.286;  %lasto-optic coeff
% lamp = 1.06e-6; %1.55e-6; %1.08e-6; %1.06e-6;
%1.55e-6; %wavelength
% rho0 = 2204; %density
% c = 3e8; %light speed
% vb = 16.25e9;%11.25e9; %16e9; %16.5e9;%11e9;
%average shift of modes
% vel_a = 2250;
% delvb = 17.5e6;%12e6; % broadening of each mode, inv lifetim
% alph = 2.78*0.2301e-3;% loss per m
% gb = (4*pi*n^8*p12^2)/ (c*lamp^3*rho0*vb*delvb);
%
%   Tau = (17.5);
%
```

```
%     for gfd = 1: 1000
%
%          f(gfd) = 14e3 + (5)*(gfd-1);
%          Spec(gfd) = 0;
%
%          for t = 1:mod2b
%    Spec(gfd) = Spec(gfd) +
gb*Aeff./amao(t)*(Tau)^2 /( (f(gfd) - freq(t))^2 + Tau^2);
% end
%
% end
%
%  figure(9);
% hold on;
%
%  semilogy(f/1000,Spec);
%
%  specG=[f;Spec];
%
%  fid = fopen('50um_Gspec','w');
% fprintf(fid,'%f  %1.15f\n',specG);
% fclose(fid);
%
%
%
```

```
%
%  %save 30um_xaxis_spec f -ascii
%  %save 30um_G_spec Spec -ascii
% % %
% %
% %  %
% % %
% % %
% % %
% % %
% % %
% % % % %
% % % % % %
% % % % % %
% % % % % %


%expression to evaluate the mode power
%uz*uz


function optsq = Intfsqua(x)


global Ao;
global Bo;


global ko1;
```

```
global ko2;


global ao;
global b;


 if (x <= b)
   optmo = (Bo*besselk(0,ko2*x)).^2;
     optsq = x.*(optmo);
end


if (x <= ao)
  optmo = (Ao*besselj(0,ko1*x)).^2;
  optsq = x.*(optmo);
end


function doping_5L_G(t)


global n1;
global n2;


global a;
global b;
global ao;


global Vl1;
```

```
global Vl2;



% distance
a = 4.3;%17.5;        % acoustic core
ao =4.3;% 17.5;
b = 65.12;   %cladding

%velocities
Vl1 =  5890; %6040;%5890;
Vl2 = 5933;

n1 = 1.458 ;
NA = 0.15;%0.06;
n2 = sqrt(n1^2 - NA^2);



%plotting out these profiles and properties

for m = 1:300

    h(m) = -a - 10 + ((2*a + 20)/299)*(m-1);

    %acoustic mode and velocity profile.
    if (abs(h(m)) <= a)
```

```
    n(m) = n1;
        vl(m) = Vl1;
    end

     if (abs(h(m)) > a)
     n(m) = n2;
        vl(m) = Vl2;
    end

 end

figure(1);

subplot(2,1,1);
plot(h,n);
xlabel('distance (\mum)');
ylabel('refractive index');

subplot(2,1,2);
plot(h,vl);
ylabel('longitudinal acoustic velocity m/s');
xlabel('distance (\mum)');
%
% refind=[h;n];
% accvelG=[h;vl];
```

```
%
% fid = fopen('50um_ref_ind','w');
% fprintf(fid,'%f  %f\n',refind);
% fclose(fid);
%
% fid = fopen('50um_acc_vel_G','w');
% fprintf(fid,'%f  %f\n',accvelG);
% fclose(fid);



%
%
%save 30um_ref_index n -ascii
%save 30um_acc_vel_G vl -ascii
%



%charecteristic equation
%CLADDING MODES

% CHARECTERISTIC EQUATION

function f = fiveL_AG_modes_4_charec(V)

%define all the fiber constants, later we can pass
```

```
%these as parameters

global n1;

global n2;


global a1;

global a2;

global a3;

global a4;

global b;

global ao;


global Vl1;

global Vl2;

global Vl3;

global Vl4;

global Vl5;


global lambda;

global betaac;


%Define the propagation constants

h1t  = betaac*( sqrt(Vl1^2-V^2)/ Vl1);

h2t = betaac*( sqrt(Vl2^2-V^2)/ Vl2);

h3t = betaac*( sqrt(Vl3^2-V^2)/ Vl3);

h4 = betaac*( sqrt(V^2-Vl4^2)/ Vl4);
```

```
h5t = betaac*( sqrt(Vl5^2--V^2)/ Vl5);


%Define the ABCD terms
A1 = besseli(0,h1t*a1);
A2 = -besseli(1,h1t*a1);
A3 = besseli(0,h2t*a1);
A4 = -besseli(1,h2t*a1);
A5 = besselk(0,h2t*a1);
A6 = besselk(1,h2t*a1);


B1 = besseli(0,h2t*a2);
B2 = -besseli(1,h2t*a2);
B3 = besselk(0,h2t*a2);
B4 = besselk(1,h2t*a2);
B5 = besseli(0,h3t*a2);
B6 = -besseli(1,h3t*a2);
B7 = besselk(0,h3t*a2);
B8 = besselk(1,h3t*a2);


C1 = besseli(0,h3t*a3);
C2 = -besseli(1,h3t*a3);
C3 = besselk(0,h3t*a3);
C4 = besselk(1,h3t*a3);
C5 = besselj(0,h4*a3);
C6 = besselj(1,h4*a3);
```

```
C7 = bessely(0,h4*a3);

C8 = bessely(1,h4*a3);


D1 = besselj(0,h4*a4);

D2 = besselj(1,h4*a4);

D3 = bessely(0,h4*a4);

D4 = bessely(1,h4*a4);


D7 = besselk(0,h5t*a4);

D8 = besselk(1,h5t*a4);



%form the characteristic determinannt

%




  C = [    0                B1/(h2t*B2)

          -B5/(h2t*B2)      0  0    0       ;

       0               -h2t*B2/ (h2t*B2)

         h3t*B6/(h2t*B2)   0   0   0    ;

        0    0                C1/ (h3t*C2)

             -C5/ (h3t*C2)  -C7/ (h3t*C2)    0  ;

       0     0          -h3t*C2/ (h3t*C2)
```

```
       h4*C6/ (h3t*C2)  h4*C8/ (h3t*C2) 0 ;
      0    0      0          D1      D3      -D7;
      0    0      0      -h4*D2  -h4*D4   h5t*D8]


  f = abs(det(C));

%
%
%
%
%
% this will solve the SBS equations

function gbatv = gb_at_v(v)
alph = 0.2*0.2301e-3; %loss per m
L      =      20e3;

rho_0 = 2204  ;%kg/m3
p12 = 0.286;
n = 1.45;
wb = 12e6;
vb = 11e9;
lambda = 1.55e-6;
c = 3e8;
```

```
ama01 = 91.5 e-12;

amao2 = 3928e-12;

amao3 = 4921e-12;


gb = (4*pi*n^8*p12^2)/(lambda^3*rho_0*c*wb*vb);


Latv = ((wb/2)^2)/((wb/2)^2 + (vb - v)^2);


gbatv = gb*Latv;


% 5 layered structure ...

%  get the Brillouin spectrum of a 5 layered structure.

%  for the case of an anti-guiding fiber

%


% IN DOING ANY NUMERICAL THING ..... PLEASE MAKE SURE THAT

% YOU HAVE NORMALIZED EVERY DAMN THING MAN !

% IT IS VERY ESSENTIAL

%ELSE THINGS ARE RELATIVELY OUT OF PROPORTION AND IT

%WILL START KILLING YOU

%


%global constants

global n1;
```

```
global n2;


global a1;

global a2;

global a3;

global a4;

global b;

global ao;


global Vl1;

global Vl2;

global Vl3;

global Vl4;

global Vl5;

global betaac;

global lambda;

global intfsq;

% Enter profile information -- in terms of thickness of the

% 5 layers and the respective index and velocity values

doping_5L_AG(1);


% Solve for the optical mode

lambda = 1.064; %lambda in microns

ko = (2*pi)/lambda;

for sc = 1: 1000
```

```
     x(sc) = 1.4578 + sc*(n1 - 1.4578)/1000;%1.0
     + (.449/120)*i;
     y(sc) = optcharec(x(sc));
 end;
% % %
 %plot(x,log(y));
 neff = x(633);
% % % clear x; clear y;
optmodep(neff);
%
% %   % Calculate integral of f^2
betaopt = 2*pi*neff/lambda;
betaac = 2*betaopt;

p1 = quad8(@intIsq,0,ao);
p2 = quad8(@intIsq,ao,b);

 Isq =2*pi* (p1+p2); % integral of filed ^4

 p3 = quad8(@intfsq,0,ao);
p4 = quad8(@intfsq,ao,b);

 fsq = 2*pi*(p3+p4); % integral of filed ^2

 Aeff = fsq^2/Isq;
```

```
%MODES Guided everywhere except in layer 1,2,3 (guides in 4 5)
%characteristic equation and identification of eigenmodes
 for sc = 1: 1000
     x(sc) = Vl5 + sc*(Vl3 - Vl5)/1000;
     y(sc) = fiveL_AG_modes_45_charec(x(sc));
 end;

%   figure(2);
%    plot(x,log(y));
%   hold on;%

%pick and count modes

modind = 0;
for sc = 2: 999
     if (log(y(sc)) < log(y(sc-1)) ) & (log(y(sc))
      < log(y(sc+1)))
         modind = modind +1;
         modeV(modind) = x(sc);
         freq(modind) = (2*neff/lambda)*modeV(modind);
     end
end

mod2a = modind;
clear x;
```

```
clear y;
% determine modeprofile and overlap integral for eigenmodes
figure(3)
for t = 1:mod2a
   %subplot(mod2a,1,t);
   gain(t) =  fiveL_AG_eigenmodes_45(modeV(t));
    amao(t) = fsq^2/gain(t)^2;
end


%
%
% %
%
% % % MODES Guided everywhere except in layer
1,2 (guides in 3 4 5)
% % % characteristic equation and identification
of eigenmodes
 for sc = 1: 1000
      x(sc) = Vl3 + sc*(Vl2 - Vl3)/1000;
      y(sc) = fiveL_AG_modes_345_charec(x(sc));
  end;
% % %
%    figure(4);
%   plot(x,log(y));
%  hold on;
```

```
% %
% % %pick and count modes
% %
modind = mod2a;
for sc = 2: 999
     if (log(y(sc)) < log(y(sc-1)) )
     & (log(y(sc)) < log(y(sc+1)))
          modind = modind +1;
          modeV(modind) = x(sc);
          freq(modind) = (2*neff/lambda)*modeV(modind);
     end
end


mod2b = modind;
clear x;
clear y;
%
% % % determine modeprofile and overlap integral for eigenmodes
 for t = mod2a+1:mod2b
 %  subplot(mod2b-mod2a,1,t-mod2a);
     gain(t) = fiveL_AG_eigenmodes_345(modeV(t));
  amao(t) = fsq^2/gain(t)^2;
 end
% %
% %
```

```
%
% %
%
% MODES Guided everywhere except in layer 1 (guides in 2 3 4 5)
% characteristic equation and identification of eigenmodes
for sc = 1: 1000
       x(sc) = Vl2 + sc*(Vl1 - Vl2)/1000;
       y(sc) = fiveL_AG_modes_2345_charec(x(sc));
   end;
% % % %
%     figure(2);
%     plot(x,log(y));
%  hold on;

%pick and count modes

modind = mod2b;
for sc = 2: 999
     if (log(y(sc)) < log(y(sc-1)) ) & (log(y(sc)) < log(y(sc+1)))
         modind = modind +1;
         modeV(modind) = x(sc);
         freq(modind) = (2*neff/lambda)*modeV(modind);
     end
end
```

```
mod2c = modind;

clear x;

clear y;

%

% % determine modeprofile and overlap integral for eigenmodes

%

% %  figure(5);

for t = mod2b+1:mod2c

   %  subplot(10,1,t-mod2b)

          gain(t) = fiveL_AG_eigenmodes_2345(modeV(t));

        amao(t) = fsq^2/gain(t)^2;

       end

% % %


%

% % %CLADDING MODES

% %characteristic equation and identification of eigenmodes

for sc = 1: 1000

   x(sc) = Vl1 + sc*(6310 - Vl1)/1000;

   y(sc) = fiveL_AG_clad_modes_charec(x(sc));

end;

for sc = 1001:1500

   x(sc) = 6310 + (sc-1000)*(6400- 6375 )/500;

   y(sc) = fiveL_AG_clad_modes_charec(x(sc));

end;
```

```
%
figure(3);
   plot(x,log(y));
% % hold on;
% %pick and count modes
%
modind = mod2c;
for sc = 2: 999
     if (log(y(sc)) < log(y(sc-1)) ) & (log(y(sc)) < log(y(sc+1)))
         modind = modind +1;
         modeV(modind) = x(sc);
         freq(modind) = (2*neff/lambda)*modeV(modind);
     end
end

mod2d = modind;
clear x;
clear y;

% %
% % % determine modeprofile and overlap integral for eigenmodes
for t = mod2c+1:mod2d
     % subplot(4,1,t-mod2c);
   gain(t) = fiveL_AG_eigenmodes_cladding(modeV(t));
 amao(t) = fsq^2/gain(t)^2;
```

```
end



n = neff;   % refractive index

p12 = 0.286;  %lasto-optic coeff

lamp = 1.06e-6; 1.55e-6; %1.08e-6;

%1.06e-6; %1.55e-6; %wavelength

rho0 = 2204; %density

c = 3e8; %light speed

vb = 16.85e9;%11.25e9; 16e9;

%16.5e9;%11e9; %average shift of modes

vel_a = 2250;

delvb = 17.5e6;%12e6; broadening of each mode, inv lifetim

alph = 2.78*0.2301e-3;%loss per m

gb = (4*pi*n^8*p12^2)/ (c*lamp^3*rho0*vb*delvb);



%Construct the spectrum and threshold calculations


  Tau = (17.5);


    for gfd = 1: 1000


        f(gfd) = 14e3 + (5)*(gfd-1);

        Spec(gfd) = 0;
```

```
        for t = 1:mod2d
   Spec(gfd) =
   Spec(gfd)+ gb*(Aeff/amao(t))*(Tau)^2
   /( (f(gfd) - freq(t))^2 + Tau^2);
end

end

 figure(9);
hold on;

%Spec=Spec./2;

 plot(f/1000,Spec,'k');
xlabel('frequency shift(GHz)');
ylabel('g_B m/W');
title('50um');

specG=[f;Spec];

 fid = fopen('30um_AGspec','w');
fprintf(fid,'%f  %1.15f\n',specG);
fclose(fid);
```

```
%
%



function doping_5L_AG(t)


global n1;
global n2;


global a1;
global a2;
global a3;
global a4;
global b;
global ao;


global Vl1;
global Vl2;
global Vl3;
global Vl4;
```

```
global Vl5;


% distance
a1 = (50/33)*(17.5/25)*6;%(15.4/2);
%           15.4;        % acoustic core
a2 = (50/33)*(17.5/25)*15.4;%(25.5/2);
%          25.5;
a3 = (50/33)*(1/2)*32.8;
a4 = (50/33)*(1/2)*33;
ao = a4;
b = 65.12;   %cladding


%velocities
Vl1 =  6300; %6040;%5890;
Vl2 = 6180;
Vl3 = 6010;
Vl4 = 5900;
Vl5 = 5933;%5954;


n1 = 1.458 ;
NA = 0.06;
n2 = sqrt(n1^2 - NA^2);



%plotting out these profiles and properties
```

```
for m = 1:300

    h(m) = -a4 - 10 + ((2*a4 + 20)/299)*(m-1);

    %acoustic mode and velocity profile.
      if (abs(h(m)) < b)
    n(m) = n2;
        vl(m) = Vl5;
    end

     if (abs(h(m)) <a4 )
      n(m) = n1;
        vl(m) = Vl4;
  end

  if (abs(h(m)) <a3 )
       vl(m) = Vl3;
        n(m) = n1;
   end

    if (abs(h(m)) <a2)
     n(m) = n1;
       vl(m) = Vl2;
    end
```

```
      if (abs(h(m)) <a1)
     n(m) = n1;
       vl(m) = Vl1;
    end

end

figure(1);

subplot(2,1,1);
plot(h,n);
title('refractive index');
subplot(2,1,2);
plot(h,vl);
title('longitudinal acoustic velocity');

refind=[h;n];
accvelAG=[h;vl];

fid = fopen('50um_acc_vel_AG','w');
fprintf(fid,'%f  %f\n',accvelAG);
fclose(fid);
```

```
 %save 30um_xaxis_nvl  h -ascii
 %save 30um_ref_index n -ascii
 %save 30um_acc_vel_AG vl -ascii
%
```

```
%calculates the eigenmodes given the eigenfrequency
function overlap = fiveL_AG_eigenmodes_cladding(V)

% define global constants
global n1;
global n2;

global a1;
global a2;
global a3;
global a4;
global b;
global ao;

global Vl1;
```

```
global Vl2;

global Vl3;

global Vl4;

global Vl5;

global betaac;

global lambda;


global acnorm;

global Ao;

global Bo;


global ko1;

global ko2;


global h1;

global h2;

global h3;

global h4;

global h5;


global A_1;

global A_2;

global B_2;

global A_3;

global B_3;
```

```
global A_4;

global B_4;

global A_5;

global B_5;


%define all the bessel quantities to form

the charecteristic matrix

%Define the propagation constants

h1  = betaac*( sqrt(V^2 - Vl1^2)/ Vl1);

h2 = betaac*( sqrt(V^2 - Vl2^2)/ Vl2);

h3 = betaac*( sqrt(V^2 - Vl3^2)/ Vl3);

h4 = betaac*( sqrt(V^2 - Vl4^2)/ Vl4);

h5 = betaac*( sqrt(V^2 - Vl5^2)/ Vl5);


%Define the ABCD terms

A1 = besselj(0,h1*a1);

A2 = besselj(1,h1*a1);

A3 = besselj(0,h2*a1);

A4 = besselj(1,h2*a1);

A5 = bessely(0,h2*a1);

A6 = bessely(1,h2*a1);


B1 = besselj(0,h2*a2);

B2 = besselj(1,h2*a2);

B3 = bessely(0,h2*a2);
```

```
B4 = bessely(1,h2*a2);

B5 = besselj(0,h3*a2);

B6 = besselj(1,h3*a2);

B7 = bessely(0,h3*a2);

B8 = bessely(1,h3*a2);


C1 = besselj(0,h3*a3);

C2 = besselj(1,h3*a3);

C3 = bessely(0,h3*a3);

C4 = bessely(1,h3*a3);

C5 = besselj(0,h4*a3);

C6 = besselj(1,h4*a3);

C7 = bessely(0,h4*a3);

C8 = bessely(1,h4*a3);


D1 = besselj(0,h4*a4);

D2 = besselj(1,h4*a4);

D3 = bessely(0,h4*a4);

D4 = bessely(1,h4*a4);

D5 = besselj(0,h5*a4);

D6 = besselj(1,h5*a4);

D7 = bessely(0,h5*a4);

D8 = bessely(1,h5*a4);


E2 = besselj(1,h5*b);
```

```
E4 = bessely(1,h5*b);



%form the matrix that will be inverted
C = [         -A3/A1        -A5/A1
 0    0      0    0    0     0 ;
         h2*A4/(-h1*A2)     h2*A6/(-h1*A2)


          0    0      0    0    0      0  ;
B1/(-h2*B2)       B3/(-h2*B2)      -B5/(-h2*B2)    -B7/(-h2*B2)
    0  0    0     0  ;
 -h2*B2/(-h2*B2)   -h2*B4/(-h2*B2)    h3*B6/(-h2*B2)
  h3*B8/(-h2*B2)   0   0   0     0;
          0   0             C1/(-h3*C2)
  C3/(-h3*C2)     -C5/(-h3*C2)  -C7/(-h3*C2)    0  0;
 0   0       -h3*C2/(-h3*C2)  -h3*C4/(-h3*C2)
  h4*C6/(-h3*C2)  h4*C8/(-h3*C2) 0 0;
          0   0   0     0      D1      D3     -D5  -D7;
         0   0   0     0   -h4*D2  -h4*D4   h5*D6  h5*D8];


% solve for the coefficients
sol = inv(C)*[-1;-1;0;0;0;0;0;0];
A_1 = 1;
A_2 = sol(1);
B_2 = sol(2);
```

```
A_3 = sol(3);

B_3 = sol(4);

A_4 = sol(5);

B_4 = sol(6);

A_5 = sol(7);

B_5 = sol(8);


%integrate the eigenmodes to get the normalizing constant

pow1 = quad8(@accpow_5L_AG_clad,0,a1);

pow2 = quad8(@accpow_5L_AG_clad,a1,a2);

pow3 = quad8(@accpow_5L_AG_clad,a2,a3);

pow4 = quad8(@accpow_5L_AG_clad,a3,a4);

pow5 = quad8(@accpow_5L_AG_clad,a4,b);


  accpower = 2*pi*(pow1+pow2+pow3 +pow4+pow5) ;


A_1 = A_1/sqrt(accpower);

A_2 = A_2/sqrt(accpower);

B_2 = B_2/sqrt(accpower);

A_3 = A_3/sqrt(accpower);

B_3 = B_3/sqrt(accpower);

A_4 = A_4/sqrt(accpower);

B_4 = B_4/sqrt(accpower);

A_5 = A_5/sqrt(accpower);

B_5 = B_5/sqrt(accpower);
```

```
% display the modes with the optical ones as well
for m = 1:3000
       h(m) = -a4 - 4  + ((2*a4 + 8 )/2999)*(m-1);
  %optmode(m) = exp( -(h(m)/wopt)^2);
   if (abs(h(m)) <= b)
    optm(m) = (Bo*besselk(0,ko2*abs(h(m)))).^2;
phi(m) = (A_5*besselj(0,h5*abs(h(m)))+
B_5*bessely(0,h5*abs(h(m))));
end
  if (abs(h(m)) <= a4)
optm(m) = (Ao*besselj(0,ko1*abs(h(m)))).^2;
phi(m) = (A_4*besselj(0,h4*abs(h(m)))+
B_4*bessely(0,h4*abs(h(m))));
end
if (abs(h(m)) <= a3)
optm(m) = (Ao*besselj(0,ko1*abs(h(m)))).^2;
phi(m) = (A_3*besselj(0,h3*abs(h(m)))+
B_3*bessely(0,h3*abs(h(m))));
end
if (abs(h(m)) <= a2)
optm(m) = (Ao*besselj(0,ko1*abs(h(m)))).^2;
phi(m) = (A_2*besselj(0,h2*abs(h(m)))+
B_2*bessely(0,h2*abs(h(m))));
end
```

```
if (abs(h(m)) <= a1)
optm(m) = (Ao*besselj(0,ko1*abs(h(m)))).^2;
phi(m) = (A_1*besselj(0,h1*abs(h(m))));
end

end

p3 = quad8(@intfsq,0,ao);
p4 = quad8(@intfsq,ao,b);

 fsq = 2*pi*(p3+p4); % integral of filed ^2

%figure(3);
plot(h,phi,'b');
 hold on;
plot(h,optm/fsq, 'k');


% calculate the overlap with the optical mode

olap1 = quad8(@olaparg_5L_AG_clad,0,a1);
olap2 = quad8(@olaparg_5L_AG_clad,a1,a2);
olap3 = quad8(@olaparg_5L_AG_clad,a2,a3);
olap4 = quad8(@olaparg_5L_AG_clad,a3,a4);
```

```
olap5 = quad8(@olaparg_5L_AG_clad,a4,b);
%
overlap = 2*pi*(olap1+olap2+olap3+olap4+olap5);
%




%calculates the eigenmodes given the eigenfrequency
function overlap = fiveL_G_eigenmodes_1(V)

% define global constants
global n1;
global n2;
global a;
global b;

global Vl1;
global Vl2;

global lambda;
global betaac;
global A_1;
global A_2;
```

```
%implemented for a dual layer fiber for the acoustic mode.



global acnorm;

global Ao;

global Bo;


global ko1;

global ko2;


global h1;

global h2t;


%Define the propagation constants

h1 = betaac*( sqrt(V^2 - Vl1^2)/ Vl1);

h2t = betaac*( sqrt(Vl2^2 - V^2)/ Vl2);


%Define the ABCD terms

A1 = besselj(0,h1*a);

A2 = besselj(1,h1*a);


B1 = besselk(0,h2t*a);

B2 = besselk(1,h2t*a);


A_2 = 1;
```

```
A_1 = B1/A1;

%integrate the eigenmodes to get the normalizing constant

pow1 = quad8(@accpow_5L_G_1,0,a);
pow2 = quad8(@accpow_5L_G_1,a,b);

  accpower = 2*pi*(pow1+pow2) ;

A_1 = A_1/sqrt(accpower);
A_2 = A_2/sqrt(accpower);



for m = 1:3000
       h(m) = -a-4 + ((2*a+8 )/2999)*(m-1);
  %optmode(m) = exp( -(h(m)/wopt)^2);
   if (abs(h(m)) <= b)
    optm(m) = (Bo*besselk(0,ko2*abs(h(m)))).^2;
phi(m) = (A_2*besselk(0,h2t*abs(h(m))));
end

   if (abs(h(m)) < a)
optm(m) = (Ao*besselj(0,ko1*abs(h(m)))).^2;
phi(m) = (A_1*besselj(0,h1*abs(h(m))));
end
```

```
end



% display the modes with the optical ones as well



figure(3);

hold on;

plot(h,phi,'k');

% hold on;

% plot(h,optm/max(optm), 'k');


% calculate the overlap with the optical mode


olap1 = quad8(@olaparg_5L_G_1,0,a);

olap2 = quad8(@olaparg_5L_G_1,a,b);


%

overlap =2*pi*( olap1+olap2);

%



% PLOTS MODE PROFILE
```

```
function overlap = modeprofile_B_woacl(V)


global modind;

global ao;

global a;

global b;


global Vl1;

global Vl2;


global lambda;

global betaac;

global A_1;

global A_2;

global B_2;




global lam1;

global mu1;

global lam2;

global mu2;


%implemented for a dual layer fiber for the acoustic mode.
```

```
global acnorm;

global Ao;

global Bo;



global ko1;

global ko2;



global h1;

global h2;



%Define the propagation constants

h1 = betaac*( sqrt(V^2 - Vl1^2)/ Vl1);

h2 = betaac*( sqrt(V^2 - Vl2^2)/ Vl2);



%Define the propagation constants

A1 = besselj(0,h1*a);

A2 = besselj(1,h1*a);

B1 = besselj(0,h2*a);

B2 = besselj(1,h2*a);
```

```
B3 = bessely(0,h2*a);

B4 = bessely(1,h2*a);


C2 = besselj(1,h2*b);

C4 = bessely(1,h2*b);


%form the determinannt to solve for ABC,  D =1;


A_2 = -C4/C2;

B_2 = 1;

A_1 = A_2*B1/A1+  B3/A1;


%acoustic power calculations

pow1 = quad8(@accpow_B_woacl,0,a);

pow2 = quad8(@accpow_B_woacl,a,b);


  accpower = 2*pi*(pow1+pow2);


A_1 = A_1/sqrt(accpower);

A_2 = A_2/sqrt(accpower);

B_2 = B_2/sqrt(accpower);



% %construct the mode profile

for m = 1:3000
```

```
      h(m) = -a - 4  + ((2*a + 8 )/2999)*(m-1);
  %optmode(m) = exp( -(h(m)/wopt)^2);

  if (abs(h(m)) <= b)
optm(m) = (Bo*besselk(0,ko2*abs(h(m)))).^2;
phi(m) = (A_2*besselj(0,h2*abs(h(m)))+
B_2*bessely(0,h2*abs(h(m))));
end
%    if (abs(h(m)) <= ao)
% optm(m) = (Ao*besselj(0,ko1*abs(h(m)))).^2;
% phi(m) = (A_2*besselj(0,h2*abs(h(m)))+
B_2*bessely(0,h2*abs(h(m))));
% end
   if (abs(h(m)) <= a)
optm(m) = (Ao*besselj(0,ko1*abs(h(m)))).^2;
phi(m) = (A_1*besselj(0,h1*abs(h(m))));
end
end
%determine mode acoustic power and then normalize
%better to determine lambda and mu

% acnorm = max(abs(phi));
%
% A = A/acnorm;
% B = B/acnorm;
```

```
% plot(h,phi/max(abs(phi)),'b');
% hold on;
% plot(h,optm/max(optm), 'k');

olap1 = quad8(@olaparg_B_woacl,0,a);
olap2 = quad8(@olaparg_B_woacl,a,b);

%
overlap = 2*pi*(olap1+olap2);
%
%
% olap1 = quadl(@olaparg1A,0,a);
% olap2 = quad8(@olaparg1A,a,b);
% %   olap3 = quadl(@olaparg,25.12,65);
% %
% overlap = (olap1+olap2);
% %

%square of the acoustic wave function

function uzstuz = accpow_5L_AG_345(x)
global h1t;
global h2t;
```

```
global h3;

global h4;

global h5;


global A_1;

global A_2;

global B_2;

global A_3;

global B_3;

global A_4;

global B_4;

global A_5;

global B_5;


global a1;

global a2;

global a3;

global a4;

global b;

global ao;


 if (x <= b)

  mod = (A_5*besselj(0,h5*x)+ B_5*bessely(0,h5*x));

  uzstuz = x.*mod.^2;

end
```

```
  if (x <= a4)
mod = (A_4*besselj(0,h4*x)+ B_4*bessely(0,h4*x));
uzstuz = x.*mod.^2;
end
if (x <= a3)
mod = (A_3*besselj(0,h3*x)+ B_3*bessely(0,h3*x));
uzstuz = x.*mod.^2;
end
if (x <= a2)
mod = (A_2*besseli(0,h2t*x)+ B_2*besselk(0,h2t*x));
uzstuz = x.*mod.^2;
end
if (x <= a1)
mod = (A_1*besseli(0,h1t*x));
uzstuz = x.*mod.^2;
end



function val = corning(x)

%threshold computation
global Aao1;
global alph;
global gb;
global amao;
```

```
global mod2b;


n = 1.458;    %refractive index

p12 = 0.286;  %lasto-optic coeff

lamp = 1.06e-6; %1.55e-6; %1.08e-6;

%1.06e-6; %1.55e-6; %wavelength

rho0 = 2204; %density

c = 3e8; %light speed

vb = 16.5e9;%11.25e9; %16e9;

%16.5e9;%11e9; %average shift of modes

vel_a = 2250;

delvb = 17.5e6;%12e6;

% broadening of each mode, inv lifetim

alph = 2.78*0.2301e-3;% loss per m

eta = 0.01; %threshold defn fraction

k = 1.3866e-23; %boltzmans

T = 300; %temp

L = 80; %meters


gb = (4*pi*n^8*p12^2)/ (c*lamp^3*rho0*vb*delvb);


Aao1=  min(amao)*1e-12;%24.0402e-12;

%276.7764e-12; %8.1805e-12; % 120.5481e-12;

%12.8347e-12;%45.2563e-12; %80.2815e-12;%21.7247e-12;

%80.2815e-12; %43.4269e-12; %51.5968e-12;
```

```
%91.5e-12; %91.5e-12;


%amao = 1e-12*[9,41,2.5485e4,1.2925e4,3.3244e4, 630,1967,3319,
4461,5360,6114,6904,8151,1.08e4,1.87e4,6.5151e4];


%amao = 1e-12*[ 10,490, 2.745e5,1.4e5,2.7e5,12.2e5];
% Aao1_1 = 91.5e-12;
% Aao2_1 = 3928e-12;
% Aao3_1 = 4921e-12;
% gb = gb/3.26;
B = (Aao1*eta*alph*vb*lamp)/(sqrt(pi)*k*T*gb*c*delvb);
%r = [ Aao1/Aao1_1 , Aao1/Aao2_1, Aao1/Aao3_1];
r = Aao1./(1e-12*amao);


cons = exp(-alph*L)/sqrt(1 - exp(-alph*L));
series = 0;
for k =85:90
    series = series +
    exp( r(k)*x*(1-exp(-alph*L))) /sqrt(r(k));
end


% for k = 79:89
%     series = series +
 exp( r(k)*x*(1-exp(-alph*L))) /sqrt(r(k));
% end
```

```
val = cons*series- B*x.^1.5;

%val =   B*x.^1.5;


%charecteristic equation

%CLADDING MODES


% CHARECTERISTIC EQUATION


function f = fiveL_AG_clad_modes_charec(V)


%define all the fiber constants, later we can pass

%these as parameters

global n1;

global n2;


global a1;

global a2;

global a3;

global a4;

global b;

global ao;


global Vl1;

global Vl2;
```

```
global Vl3;

global Vl4;

global Vl5;


global lambda;

global betaac;


%Define the propagation constants

h1  = betaac*( sqrt(V^2 - Vl1^2)/ Vl1);

h2 = betaac*( sqrt(V^2 - Vl2^2)/ Vl2);

h3 = betaac*( sqrt(V^2 - Vl3^2)/ Vl3);

h4 = betaac*( sqrt(V^2 - Vl4^2)/ Vl4);

h5 = betaac*( sqrt(V^2 - Vl5^2)/ Vl5);


%Define the ABCD terms

A1 = besselj(0,h1*a1);

A2 = besselj(1,h1*a1);

A3 = besselj(0,h2*a1);

A4 = besselj(1,h2*a1);

A5 = bessely(0,h2*a1);

A6 = bessely(1,h2*a1);


B1 = besselj(0,h2*a2);

B2 = besselj(1,h2*a2);

B3 = bessely(0,h2*a2);
```

```
B4 = bessely(1,h2*a2);

B5 = besselj(0,h3*a2);

B6 = besselj(1,h3*a2);

B7 = bessely(0,h3*a2);

B8 = bessely(1,h3*a2);


C1 = besselj(0,h3*a3);

C2 = besselj(1,h3*a3);

C3 = bessely(0,h3*a3);

C4 = bessely(1,h3*a3);

C5 = besselj(0,h4*a3);

C6 = besselj(1,h4*a3);

C7 = bessely(0,h4*a3);

C8 = bessely(1,h4*a3);


D1 = besselj(0,h4*a4);

D2 = besselj(1,h4*a4);

D3 = bessely(0,h4*a4);

D4 = bessely(1,h4*a4);

D5 = besselj(0,h5*a4);

D6 = besselj(1,h5*a4);

D7 = bessely(0,h5*a4);

D8 = bessely(1,h5*a4);


E2 = besselj(1,h5*b);
```

```
E4 = bessely(1,h5*b);


%form the characteristic determinannt
%
C = [ A1          -A3       -A5     0
  0      0    0    0     0 ;
       -h1*A2    h2*A4    h2*A6 0    0
            0    0    0      0  ;
       0                B1       B3     -B5
        -B7    0  0    0     0  ;
       0               -h2*B2  -h2*B4
        h3*B6  h3*B8 0   0   0     0;
        0    0   0             C1
           C3     -C5  -C7    0  0;
       0     0   0       -h3*C2
        -h3*C4   h4*C6  h4*C8 0 0;
       0    0   0   0     0
         D1      D3     -D5  -D7;
       0    0   0   0     0
        -h3*D2  -h3*D4   h4*D6  h4*D8;
       0   0   0   0     0
          0                  0       -E2    -E4];


 f = abs(det(C));
```

```
%expression to evaluate the mode power


function optsquz = olaparg_5L_AG_clad(x)


global Ao;

global Bo;


global ko1;

global ko2;


global h1;

global h2;

global h3;

global h4;

global h5;


global A_1;

global A_2;

global B_2;

global A_3;

global B_3;

global A_4;

global B_4;

global A_5;
```

```
global B_5;


global a1;

global a2;

global a3;

global a4;

global b;

global ao;



  if (x <= b)

    optmo = (Bo*besselk(0,ko2*x)).^2;

mod = (A_5*besselj(0,h5*x)+ B_5*bessely(0,h5*x));

 optsquz = x.*(optmo).*mod;

end


if (x <= a4)

optmo = (Ao*besselj(0,ko1*x)).^2;

mod = (A_4*besselj(0,h4*x)+ B_4*bessely(0,h4*x));

 optsquz = x.*(optmo).*mod;

end


if (x <= a3)

optmo = (Ao*besselj(0,ko1*x)).^2;

mod = (A_3*besselj(0,h3*x)+ B_3*bessely(0,h3*x));
```

```
 optsquz = x.*(optmo).*mod;
end


if (x <= a2)
optmo = (Ao*besselj(0,ko1*x)).^2;
mod = (A_2*besselj(0,h2*x)+ B_2*bessely(0,h2*x));
 optsquz = x.*(optmo).*mod;
end


if (x <= a1)
optmo = (Ao*besselj(0,ko1*x)).^2;
mod = (A_1*besselj(0,h1*x));
 optsquz = x.*(optmo).*mod;
end
```

.3 Chapter 4

```
% %
global gbiol;
global alphL;
global R;
global lzl;
global kapL;
global deloL;
```

```
rho_0 = 2204  ;%kg/m3

p12 = 0.286;

n = 1.45;

wb = 12e6;

vb = 11e9;

lambda = 1.55e-6;

c = 3e8;

gb = (4*pi*n^8*p12^2)/(lambda^3*rho_0*c*wb*vb);


alpha = 0.2/(4.343e3);

L = 20000;

alphL = alpha*L



% velocity grating things

v1 = 5944;

v2 = 5944*(1- .5*7.2e-3); %1.5 wt% geo2


vlo = sqrt (( v1^2 + v2^2 )/2)

vlosq = vlo^2;

delvlosq = v2^2 - v1^2;

grate = abs(delvlosq/vlosq)


lz = vlo / (pi*wb)

lzl = lz/L
```

```
R = (grate /pi )*vb/wb


(1+R^2)


R = 2.1;
kapL = 2.0;
deloL = 0;


%
%
% %
%
% %
% %


%
%   for swp = 1
% %
%  gb(swp) = 10^(3*swp/25);
 % gbiol = 10^(3*swp/25);
gbiol = 120;
alphL = .1;


il = fsolve(@integ, 1e-6, optimset('fsolve'));
```

```
%[z,I] = ode45(@deriv, [1,0], [il,1e-9]);


%[z,A] = ode45(@deriv, [1,0], [sqrt(0.1470),3.162e-5]);
[z,A] = ode45(@deriv, [1,0], [il,3.162e-5]);
%[z,A] = ode45(@deriv, [1,0], [il,1,0]);
[rz,cz] = size(z);
I = A.*conj(A);
% so(swp) = I(rz,2);
% end;


%
% subplot(1,2,1);
% hold on;
plot(z,I(:,1));
grid on;
%
% subplot(1,2,2);
% hold on;
% plot(z, I(:,2));
% grid on;
% semilogx(gb,so);
% hold on;
%scatter(gb,so);
%
```

```
%



%decide_on_a_suitable_gridresolution

RES = 51;

%obtain all the relevant fields
%data_input;
filedgen;

%optical_parameters
lambda = 1.06e-6;
k0 = 2*pi/lambda;
neff = 1.459065;
k1 = k0*neff;
k2 = k1;

%get_the_deltaeps_matrix
p11 = 0.121;
p12 = 0.270;
p44 = 0.5*(p11 - p12);
```

```
for ind = 1:RES*RES
   ep11(ind) = (p11*ex(ind) + p12*ey(ind)
   + p12*ez(ind));
   ep22(ind) = (p12*ex(ind) + p11*ey(ind)
   + p12*ez(ind));
   ep33(ind) = (p12*ex(ind) + p12*ey(ind)
   + p11*ez(ind));
   ep23(ind) = p44*(eyz(ind));
   ep32(ind) = ep23(ind);
   ep13(ind) = p44*(exz(ind));
   ep31(ind) = ep13(ind);
   ep12(ind) = p44*(exy(ind));
   ep21(ind) = ep12(ind);
end

%obtain the epE2

epE2 = zeros(RES*RES, 3);
E1t = zeros(RES*RES, 3);
H1t = zeros(RES*RES, 3);
epE2t = zeros(RES*RES, 3);

for ind = 1:RES*RES
   epE2(ind,1) = ep11(ind)*Ex2(ind)
```

```
   + ep12(ind)*Ey2(ind) + ep13(ind)*Ez2(ind);
   epE2(ind,2) = ep21(ind)*Ex2(ind)
   + ep22(ind)*Ey2(ind) + ep23(ind)*Ez2(ind);
   epE2(ind,3) = ep31(ind)*Ex2(ind)
   + ep32(ind)*Ey2(ind) + ep33(ind)*Ez2(ind);
      E1t(ind,:) = [Ex1(ind), Ey1(ind), 0];
      E2t(ind,:) = [Ex2(ind), Ey2(ind), 0];
      H1t(ind,:) = [Hx1(ind), Hy1(ind), 0];
      epE2t(ind,:) = [epE2(ind,1), epE2(ind,2), 0];
end

%

%implement Q1, Q2
Q1 = 0;
Q2 = 0;
I12_1 = 0;
I12_2 = 0;
I12_3 = 0;
Inew = 0;
for ind = 1: RES*RES
       cr1 = cross (E1t(ind,:), conj(H1t(ind,:)));
       cr2 = cross (epE2t(ind,:), conj(H1t(ind,:)));
       Q1 = Q1 + 2*k1*cr1(3)*dx*dy;
       I12_1 = I12_1 +  (k0^2)*cr2(3)*dx*dy;
```

```
        I12_2 = I12_2 +
         (k0*k1)*conj(Ez1(ind))*epE2(ind,3)*dx*dy;
        Evec = [Ex1(ind), Ey1(ind), Ez1(ind)];
        dot1 = dot(conj(Evec), epE2(ind,:)) ;
        Inew = Inew + (k0*k1)*dot1;
end




%the coupling constants
ref_kap = -i*2*neff^2*p44/2
kap_new = -neff^4*Inew/Q1
kap = -neff^4*(I12_1 + I12_2)/Q1


% delepEm = zeros(RES,RES);
% for ind = 1: RE
%    for jnd = 1:RES
%        t1 = 0;%(epEmx(ind+2, jnd+1)
- epEmx(ind,jnd+1))/(2*dx);
%        t2 = 0;%(epEmy(ind+1, jnd+2)
- epEmy(ind+1,jnd))/(2*dy);
%        t3 = 0;
%        delepEm(ind,jnd)=t1+t2+t3;  end
% end
%convert delepsEm back to a vector
```

```
DepE2 = zeros(RES*RES,1);
%
% for ind = 1: RES
%    for jnd = 1:RES
%       DepE2((ind-1)*RES+jnd) =  delepEm(ind,jnd);
%    end
% end
  %  I12_1 = I12_1 +  (k0^2)*cr3(3)*dx*dy;
     %  I12_2 = I12_2 +
     (k0*k1)*conj(Ez1(ind))*epE2(ind,3)*dx*dy;
     %  I12_3 = I12_3 -
     i*k0*conj(Ez1(ind))*DepE2(ind)*dx*dy;



 %convert epsE to matrix form
% tmpx = zeros(RES, RES);
% tmpy = zeros(RES, RES);
% tmpz = zeros(RES, RES);
%
% for ind = 1: RES
%    for jnd = 1:RES
%     tmpx(ind,jnd) = epE2((ind-1)*RES+jnd, 1);
%     tmpy(ind,jnd) = epE2((ind-1)*RES+jnd, 2);
%     tmpz(ind,jnd) = epE2((ind-1)*RES+jnd, 3);
%     end
```

```
% end
%
% epEmx = zeros(RES+2, RES+2);
% epEmx(2:RES+1, 2:RES+1) = tmpx;
% epEmy = zeros(RES+2, RES+2);
% epEmy(2:RES+1, 2:RES+1) = tmpy;
% epEmz = zeros(RES+2, RES+2);
% epEmz(2:RES+1, 2:RES+1) = tmpz;
%
% clear tmpx;
% clear tmpy;
% clear tmpz;
%


% this will generate the LP01 modes in a 2d grid of choosing
%decide_on_a_suitable_gridresolution


RES = 11;
LIM = 20;
dx = 2*LIM*1e-6/(RES-1);
dy = 2*LIM*1e-6/(RES-1);
a = 17.5e-6; %core radius


%optical_parameters
lambda = 1.06e-6;
```

```
k0 = 2*pi/lambda;

n1 = 1.4592;

n2 = 1.458;

neff = 1.459065;

k1 = k0*neff;

k2 = k1;

u = k0*sqrt(n1^2 - neff^2);

w = k0*sqrt(neff^2 - n2^2);


for gh = 1: 1000

    n(gh) = 1.459 + (gh-1)*(n1-1.459)/999;

    u = k0*sqrt(n1^2 - n(gh).^2);

    w = k0*sqrt(n(gh).^2 - n2^2);


    C = [besselj(0,u*a), besselk(0,w*a);

     -u*besselj(0,u*a), -w*besselk(0,w*a)];

    detn(gh) = det(C);

end


%plot(n,log10(detn));

neff = n(76);

%generate the grid

x = linspace(-LIM, LIM, RES)*1e-6;

Ex1 = zeros(RES*RES,1);

Ey1 = zeros(RES*RES,1);
```

```
Ez1 = zeros(RES*RES,1);

Ex2 = zeros(RES*RES,1);

Ey2 = zeros(RES*RES,1);

Ez2 = zeros(RES*RES,1);

Hx1 = zeros(RES*RES,1);

Hy1 = zeros(RES*RES,1);

Hz1 = zeros(RES*RES,1);


%generate the electric fields

for ind = 1: RES

    for jnd = 1 : RES

        X = x(ind);

        Y = x(jnd);

        R = sqrt(X^2 + Y^2);

        phi = atan(Y/X);


       xpl (((ind-1)*RES + jnd)) = x(ind);

        ypl (((ind-1)*RES + jnd)) = x(jnd);


        if (R <= a)

          Ex1 (((ind-1)*RES + jnd))

          = besselj(0,u*R);

          Ez1 (((ind-1)*RES + jnd))

          = (i/k1)*cos(phi)*(-u*besselj(1,u*R));

          Ey2 (((ind-1)*RES + jnd))
```

```
  = besselj(0,u*R);
  Ez2 (((ind-1)*RES + jnd))
  = (i/k1)*sin(phi)*(-u*besselj(1,u*R));
  Hy1 (((ind-1)*RES + jnd))
  = neff*besselj(0,u*R);
  Hz1 (((ind-1)*RES + jnd))
  = neff*(i/k1)*sin(phi)*(-u*besselj(1,u*R));
end

if (R > a)
  Ex1 (((ind-1)*RES + jnd))
  = besselk(0,w*R);
  Ez1 (((ind-1)*RES + jnd))
  = (i/k1)*cos(phi)*(-w*besselk(1,w*R));
  Ey2 (((ind-1)*RES + jnd))
  = besselk(0,w*R);
  Ez2 (((ind-1)*RES + jnd))
  = (i/k1)*sin(phi)*(-w*besselk(1,w*R));
  Hy1 (((ind-1)*RES + jnd))
  = neff*besselk(0,w*R);
  Hz1 (((ind-1)*RES + jnd))
   = neff*(i/k1)*sin(phi)*(-w*besselj(1,w*R));
end

if(Y == 0 && X == 0)
```

```
            Ez1 (((ind-1)*RES + jnd)) = 0;
            Ez2 (((ind-1)*RES + jnd)) = 0;
            Hz1 (((ind-1)*RES + jnd)) = 0;
        end



    end
end

%generate the elastic fields

ex = zeros(RES*RES,1);
ey = zeros(RES*RES,1);
ez = zeros(RES*RES,1);
exy = zeros(RES*RES,1);
exz = zeros(RES*RES,1);
eyz = zeros(RES*RES,1);

for ind = 1: RES
    for jnd = 1 : RES
        eyz (((ind-1)*RES + jnd)) = x(ind);
        exz (((ind-1)*RES + jnd)) = -x(jnd);
    end
end
```

```
%data input


% %load all the filed values
% load mode1_ex.txt mode1_ex -ascii;
% load mode1_ey.txt mode1_ey -ascii;
% load mode1_ez.txt mode1_ez -ascii;
% load mode1_hx.txt mode1_hx -ascii;
% load mode1_hy.txt mode1_hy -ascii;
% load mode1_hz.txt mode1_hz -ascii;
%
% load mode2_ex.txt mode2_ex -ascii;
% load mode2_ey.txt mode2_ey -ascii;
% load mode2_ez.txt mode2_ez -ascii;
% %load mode2_hx.txt mode2_hx -ascii;
% %load mode2_hy.txt mode2_hy -ascii;
% %load mode2_hz.txt mode2_hz -ascii;
%
% clear tmp;
% tmp = mode1_ex;
% clear mode1_ex;
% Ex1 = tmp(:,3);
%
% tmp = mode1_ey;
% clear mode1_ey;
```

```
% Ey1 = tmp(:,3);
%
% tmp = mode1_ez;
% clear mode1_ez;
% Ez1 = i*tmp(:,3);
%
% tmp = mode1_hx;
% clear mode1_hx;
% Hx1 = tmp(:,3);
%
% tmp = mode1_hy;
% clear mode1_hy;
% Hy1 = tmp(:,3);
%
% tmp = mode1_hz;
% clear mode1_hz;
% Hz1 = i*tmp(:,3);
%
% tmp = mode2_ex;
% clear mode2_ex;
% Ex2 = tmp(:,3);
%
% tmp = mode2_ey;
% clear mode2_ey;
% Ey2 = tmp(:,3);
```

```
%
% tmp = mode2_ez;
% clear mode2_ez;
% Ez2 = i*tmp(:,3);
%
% % tmp = mode2_hx;
% % clear mode2_hx;
% % Hx2 = tmp(:,3);
% %
% % tmp = mode2_hy;
% % clear mode2_hy;
% % Hy2 = tmp(:,3);
% %
% % tmp = mode2_hz;
% % clear mode2_hz;
% % Hz2 = i*tmp(:,3);



%load the stresses


load ex.txt ex -ascii;
load ey.txt ey -ascii;
load ez.txt ez -ascii;
load exy.txt exy -ascii;
load exz.txt exz -ascii;
```

```
load eyz.txt eyz -ascii;


tmp = ex;

clear ex;

ex = tmp(:,4);


tmp = ey;

clear ey;

ey = tmp(:,4);


tmp = ez;

clear ez;

ez = tmp(:,4);


tmp = exy;

clear exy;

exy = tmp(:,4);


tmp = exz;

clear exz;

exz = tmp(:,4);


tmp = eyz;

clear eyz;

eyz = tmp(:,4);
```

```
%we will now create the twist strain fields.


%
%
% RES = 51;
% x = linspace(-50, 50, RES)*1e-6;
% ex = zeros(RES*RES);
% ey = zeros(RES*RES);
% ez = zeros(RES*RES);
% exy = zeros(RES*RES);
% exz = zeros(RES*RES);
% eyz = zeros(RES*RES);
% y_el = zeros(RES*RES,2);
%
% for ind = 1: RES
%     for jnd = 1 : RES
%         eyz (((ind-1)*RES + jnd)) = x(ind);
%         exz (((ind-1)*RES + jnd)) = -x(jnd);
%     end
% end
%
```

BIBLIOGRAPHY

BIBLIOGRAPHY

[1] Pochi Yeh. Yariv A. *Optical waves in crystals*. John Wiley and sons., 1984.

[2] Winful HG. *PhD dissertation*. University of Southern California, Los Angeles, CA, 1981.

[3] W Chen and DL Mills. "Gap solitons and the nonlinear optical response of superlattices". *Physical Review Letters*, 58(2):160–163, Jan 12 1987.

[4] W.S. Weiglhofer and A. Lakhtakia (Eds.). *Introduction to Complex Mediums for Electromagnetics and Optics*. SPIE Press,, Bellingham, WA, USA,, 2003.

[5] Veselago V. G. "Electrodynamics of substances with simulataneous negative values of sigma and mu". *Soviet Physics Uspekhi-USSR*, 10(4):509–&, 1968.

[6] Pendry, J. B. . "Negative refraction makes a perfect lens". *Phys. Rev. Lett.*, 85(3966), 2000.

[7] Papen GC Dragic PD, Liu CH. "Optical Fiber With an Acoustic Guiding Layer for Stimulated Brillouin Scattering Suppression". *Conference on Lasers and Electro-Optics (CLEO), MAY 22-27, 2005, Baltimore, MD*, 1-3:1984–1986, 2005.

[8] A Galvanauskas. "High power fiber lasers". *optics and photonics news*, 15(7):42–47, 2004.

[9] Jens Limpert, Fabian Roeser, Sandro Klingebiel, Thomas Schreiber, Christian Wirth, Thomas Peschel, Ramona Eberhardt, and Andreas Tuennermann. "The rising power of fiber lasers and amplifiers". *IEEE Journal of selected topics in Quantum Electronics*, 13(3):537–545, May-Jun 2007.

[10] R Paschotta, J Nilsson, AC Tropper, and DC Hanna. "Ytterbium-doped fiber amplifiers". *IEEE Journal of Quantum Electronics*, 33(7):1049–1056, Jul 1997.

[11] Liu CH. *PhD dissertation*. The University of Michigan, Ann Arbor, MI, 2007.

[12] CH Liu, B Ehlers, F Doerfel, S Heinemann, A Carter, K Tankala, J Farroni, and A Galvanauskas. "810 W continuous-wave and singletransverse-mode fibre laser using 201 mu m core Yb-doped double-clad fibre". *Electronics Letters*, 40(23):1471–1472, Nov 11 2004.

[13] Steven J. Augst, Jinendra K. Ranka, T. Y. Fan, and Antonio Sanchez. "Beam combining of ytterbium fiber amplifiers (Invited)". *Journal of the Optical Society of America B-Optical Physics*, 24(8):1707–1715, Aug 2007.

[14] Boyd R. W. *Nonlinear Optics*. Academic Press; 2 edition, 2002.

[15] Agrawal G. P. *Nonlinear Fiber Optics*. Academic Press; 4 edition, 2006.

[16] RG Smith. "Optical power handling capacity of low loss optical fibers as determined by stimulated Raman and Brillouin-scattering". *Applied Optics*, 11(11):2489–&, 1972.

[17] V. I. Kovalev and R. G. Harrison. "Threshold for stimulated Brillouin scattering in optical fiber". *Optics Express*, 15(26):17625–17630, Dec 24 2007.

[18] S Le Floch and P Cambon. "Theoretical evaluation of the Brillouin threshold and the steady-state Brillouin equations in standard single-mode optical fibers". *Journal of the Optical Society of America A-Optics Image Science and Vision*, 20(6):1132–1137, Jun 2003.

[19] A Hadjifotiou and GA Hill. "Suppression of stimulated Brillouin backscattering by PSK modulation for high-power optical-transmission". *IEE Proceedings-J Optoelectronics*, 133(4):256–258, Aug 1986.

[20] L Eskildsen, PB Hansen, U Koren, BI Miller, MG Young, and KF Dreyer. "Stimulated Brillouin scattering suppression with low residual AM using a novel temperature wavelength-dithered DFB laser diode". *Electronics Letters*, 32(15):1387–1389, Jul 18 1996.

[21] YK Chen, YL Liu, and CC Lee. "Directly modulated 1.55 mu m AM-VSB video EDFA-repeatered supertrunking system over 110km standard singlemode fibre using split-band and wavelength division multiplexing techniques". *Electronics Letters*, 33(16):1400–1401, Jul 31 1997.

[22] K Shiraki, M Ohashi, and M Tateda. "Suppression of stimulated Brilllouin-scattering in a fiber by changing the core radius". *Electronics Letters*, 31(8):668–669, Apr 13 1995.

[23] J Hansryd, F Dross, M Westlund, PA Andrekson, and SN Knudsen. "Increase of the SBS threshold in a short highly nonlinear fiber by applying a temperature distribution". *Journal of Lightwave Technology*, 19(11):1691–1697, Nov 2001.

[24] Weiwen Zou, Zuyuan He, Masato Kishi, and Kazuo Hotate. "Stimulated Brillouin scattering and its dependences on strain and temperature in a high-delta optical fiber with F-doped depressed inner cladding". *Optics Letters*, 32(6):600–602, Mar 15 2007.

[25] Anping Liu. "Suppressing stimulated Brillouin scattering in fiber amplifiers using nonuniform fiber and temperature gradient". *Optics Express*, 15(3):977–984, Feb 5 2007.

[26] VI Kovalev and RG Harrison. "Suppression of stimulated Brillouin scattering in high-power single-frequency fiber amplifiers". *Optics Letters*, 31(2):161–163, Jan 15 2006.

[27] JMC Boggio, JD Marconi, and HL Fragnito. "Experimental and numerical investigation of the SBS-threshold increase in an optical fiber by applying strain distributions". *Journal of Lightwave Technology*, 23(11):3808–3814, Nov 2005.

[28] Papen GC Galvanauskas A Dragic PD, Liu CH. "optical fiber with an acoustic guiding layer for stimulated brillouin scattering suppression". *2005 Conference on Lasers and Electro-optics(CLEO)*, 1-3:1984–1986, 2005.

[29] A Kobyakov, S Kumar, DQ Chowdhury, AB Ruffin, M Sauer, SR Bickham, and R Mishra. "Design concept for optical fibers with enhanced SBS threshold". *Optics Express*, 13(14):5338–5346, Jul 11 2005.

[30] P Dainese, PSJ Russell, N Joly, JC Knight, GS Wiederhecker, HL Fragnito, V Laude, and A Khelif. "Stimulated Brillouin scattering from multi-GHz-guided acoustic phonons in nanostructured photonic crystal fibres". *Nature Physics*, 2(6):388–392, Jun 2006.

[31] V Laude, A Khelif, S Benchabane, M Wilm, T Sylvestre, B Kibler, A Mussot, JM Dudley, and H Maillotte. "Phononic band-gap guidance of acoustic modes in photonic crystal fibers". *Physical Review B*, 71(4), Jan 2005.

[32] P Dainese, PSJ Russell, GS Wiederhecker, N Joly, HL Fragnito, V Laude, and A Khelif. "Raman-like light scattering from acoustic phonons in photonic crystal fiber". *Optics Express*, 14(9):4141–4150, May 1 2006.

[33] H Lee and GP Agrawal. "Suppression of stimulated Brillouin scattering in optical fibers using fiber Bragg gratings". *Optics Express*, 11(25):3467–3472, Dec 15 2003.

[34] HG Winful, JH Marburger, and E Garmire. "Theory of bistability in non-linear distributed feedback structures". *Journal of the Optical society of America*, 69(10):1421, 1979.

[35] HG Winful, JH Marburger, and E Garmire. "Theory of bistability in non-linear distributed feedback structures" . *Applied Physics Letters"*, 35(5):379–381, 1979.

[36] B. J. Eggleton (Editor) R. E. Slusher (Editor). *Nonlinear Photonic Crystals*. Springer; 1 edition, 2004.

[37] L Wu, SL He, and LF Shen. "Band structure for a one-dimensional photonic crystal containing left-handed materials". *Physical Review B*, 67(23), Jun 15 2003.

[38] HT Jiang, H Chen, HQ Li, YW Zhang, J Zi, and SY Zhu. "Properties of one-dimensional photonic crystals containing single-negative materials". *Physical Review E*, 69(6, Part 2), Jun 2004.

[39] LG Wang, H Chen, and SY Zhu. "Omnidirectional gap and defect mode of one-dimensional photonic crystals with single-negative materials". *Physical Review B*, 70(24), Dec 2004.

[40] HT Jiang, H Chen, HQ Li, and YW Zhang. "Omnidirectional gaps of one-dimensional photonic crystals containing single-negative materials". *Chinese Physics Letters*, 22(4):884–886, Apr 2005.

[41] MW Feise, IV Shadrivov, and YS Kivshar. "Tunable transmission and bistability in left-handed band-gap structures". *Applied Physics Letters*, 85(9):1451–1453, Aug 30 2004.

[42] KY Xu, XG Zheng, and WL She. "Properties of defect modes in one-dimensional photonic crystals containing a defect layer with a negative refractive index". *Applied Physics Letters*, 85(25):6089–6091, Dec 20 2004.

[43] IV Shadrivov, NA Zharova, AA Zharov, and YS Kivshar. "Defect modes and transmission properties of left-handed bandgap structures". *Physical Review E*, 70(4, Part 2), Oct 2004.

[44] J Li, L Zhou, CT Chan, and P Sheng. "Photonic band gap from a stack of positive and negative index materials". *Physical Review Letters*, 90(8), Feb 28 2003.

[45] F; Langevin U Trutschel, U; Lederer. "optical-response of nonlinear absorbing and saturable multilayer systems". *Physica Status Solidi B-Basic Research*, 150(2):805–810, 1988.

[46] R Shih, HR Fetterman, W W Ho, R McGraw, D Rogovin, and B Bobbs. "Microwave phase conjugation in a liquid suspension of elongated microparticles". *Physical Review Letters*, 65(5):579–582, Jul 30 1990.

[47] B Bobbs, R Shih, HR Fetterman, and WW Ho. "Nonlinear microwave susceptibility measurement of an artificial Kerr medium". *Applied Physics Letters*, 52(1):4–6, Jan 4 1988.

[48] M Ohashi and M Tateda. "Design of strain-free-fiber with nonuniform dopant concentratiom for stimulated Brillouin-scattering suppression". *Journal of Lightwave Technology*, 11(12):1941–1945, Dec 1993.

[49] N Yoshizawa and T Imai. "Stimulated Brillouin-scattering suppression by means of applying strain distribution to fiber with cabling". *Journal of Lightwave Technology*, 11(10):1518–1522, Oct 1993.

[50] PJ Thomas, NL Rowell, HM Vandriel, and GI Stegeman. "Normal acoustic modes and Brillouin-scattering in single-mode optical fibers". *Physical Review B*, 19(10):4986–4998, 1979.

[51] C K Jen and N Goto. "Backward collinear guided-wave-acousto-optic interactions in single-mode fibers". *Journal of Lightwave Technology*, 7(12):2018–2023, Dec 1989.

[52] N Shibata, RG Waarts, and RP Braun. "Brillouin-Gain spectra for single-mode fibers having pure-silica GeO2-doped and P2O5-doped cores". *Optics Letters*, 12(4):269–271, Apr 1987.

[53] N Shibata, Y Azuma, T Horiguchi, and M Tateda. "Identification of longitudinal acoustic modes guided in the core region of a single-mode optical fiber by Brillouin gain spectra measurements" . *Optics Letters*, 13(7):595–597, Jul 1988.

[54] Y Koyamada, S Sato, S Nakamura, H Sotobayashi, and W Chujo. "Simulating and designing brillouin gain spectrum in single-mode fibers". *Journal of Lightwave Technology*, 22(2):631–639, Feb 2004.

[55] J. C. Beugnot, T. Sylvestre, D. Alasia, H. Maillotte, V. Laude, A. Monteville, L. Provino, N. Traynor, S. Foaleng Mafang, and L. Thevenaz. "Complete experimental characterization of stimulated Brillouin scattering in photonic crystal fiber". *Optics Express*, 15(23):15517–15522, Nov 12 2007.

[56] P Bayvel and P M Radmore. "Solutions of the SBS equations in single-mode optical fibers and implications for fiber transmission-systems". *Electronics Letters*, 26(7):434–436, Mar 29 1990.

[57] A Mocofanescu V Babin M J Damzen, V Vlad. *Stimulated Brillouin Scattering: Fundamentals and Applications*. Taylor & Francis, (September 1, 2003).

[58] Singer J Chao N Neugroschl D Genack AZ Kopp VI, Churikov VM. "chiral fiber gratings". *SCIENCE*, 305(5680):74–75, 2004.

[59] Huang HC. "practical circular-polarization-maintaining optical fiber". *Applied Optics*, 36(27):6968–6975, Sep 20 1997.